

Dissertation for the Doctor's degree
submitted to the Faculty of Chemistry and Pharmacy
at the Ludwig-Maximilians-University Munich

**Investigation of UVC Induced DNA Damage Formation
and Photolyase Catalyzed Repair of Cyclobutane
Pyrimidine Dimers**



Lal Mohan Kundu

Hooghly, West Bengal, India

2005

Erklärung

Diese Dissertation wurde im Sinne von § 13 Abs. 3 bzw. 4 der Promotionsordnung vom 29. Januar 1998 von *Herrn Prof. Dr. Thomas Carell* betreut.

Ehrenwörtliche Versicherung

Diese Dissertation wurde selbständig, ohne unerlaubte Hilfe erarbeitet.

München, am 01.02. 2005

Lal Mohan Kundu

Dissertation eingereicht am 01.02. 2005

Gutachter: Prof. Dr. Thomas Carell

Gutachter: Prof. Dr. Hendrik Zipse

Mündliche Prüfung am 18.02. 2005

The present work was performed from September 2000 to February 2004, under the supervision of Prof. Dr. Thomas Carell in the Department of Chemistry, Philipps-University Marburg and Department of Chemistry and Pharmacy, Ludwig-Maximilians University Munich.

Dedicated to

*my dear parents, my beloved brother, affectionate uncles and adorable
grandparents*

"Our duty is to encourage every one in his struggle to live up to his own highest idea, and strive at the same time to make the ideal as near as possible to the Truth" -----**Swami Vivekananda**

सत्यमेव जयते

*Asato Ma Sadgamaya
Tamaso Ma Jyotir-Gamaya*

"Science seldom proceeds in the straightforward logical manner imagined by outsiders" -----**James D. Watson**

Acknowledgement

First of all, my heartiest thanks goes to *Prof. Dr. Thomas Carell* for offering me an interesting and important research topic; for his sincere supervision, guidance and valuable suggestions throughout this work; for his time and care in correcting the thesis and also for the personal care and affection, which I received from him and his wife *Birgit*.

I am very thankful to *Prof. Dr. Hendrik Zipse* for taking responsibility as the co-referee and also for his time to correct the thesis.

I thank *Prof. Dr. Ingo-Peter Lorenz*, *Prof. Dr. Heinz Langhals*, *Prof. Dr. Heinrich Leonhardt* and *Prof. Dr. Thomas Lindel* for their acceptance to take charge as examiners.

I'm very thankful to *Dr. Uwe Linne*, for his constant cooperation and effective collaboration. I also thank *Prof. Dr. Alfred Batschauer* for his generous help and valuable collaboration through-out this work.

My sincere thanks to the mass spectrometry and NMR section of *Phillips-University Marburg* and *Ludwig-Maximilians-University Munich* for providing me the necessary help and instrumental facilities.

I'm grateful to all of my colleagues in the *Carell* group, both in Marburg and in Munich, for their cooperation and helping hands in all directions. My heartiest

thanks to *Ms. Alexandra Mees*, for her warm friendship and extensive help in correcting the thesis. I thank *Ms. Simone Arnold*, *Mr. Sascha Breeger* and *Ms. Friederike Grolle* for their affection and friendship. My special thanks to *Dr. David Hammond* and *Mr. Ulrich Hennecke* for their time and care in correcting the thesis. Many thanks to *Mr. Johannes Gierlich* and *Mr. Martin von Meltzer* for their essential help in solving computer related problems. I'm also thankful to *Ms. Ina Pinnschmidt*, *Ms. Katja Kraeling*, *Mrs. Slava Gaertner* and *Mrs. Sabine Voss* for their help and cooperation.

My sincere thanks to my dearest friends *Judith*, *Srinivasa* and *Roopa*, for their unforgettable help, company and suggestions. My heartiest thanks to dear *Sukanya*. Thanks to *Kiran*, *Sabyashachi*, *Shyama* and *Subhashisda* for their friendship and help.

Above all, I owe to my parents *Sabita* and *Krishna Chandra Kundu*, brother *Pintu*, uncle *Bishnu Pada Mondal* and *Harisankar Kundu* and all of my well wishers for their love and blessings.

Table of Contents

SUMMARY.....	1
ZUSAMMENFASSUNG	4
1. INTRODUCTION.....	8
1.1. <i>Consequence of ozone layer destruction.....</i>	<i>8</i>
1.2. <i>Effect of UV exposure.....</i>	<i>10</i>
1.3. <i>Photoproducts</i>	<i>11</i>
1.3.1. DNA, mutagenesis and cancer.....	16
1.3.2. Photolesions and mutagenesis.....	19
1.3.3. Structure-activity relationships of the photoproducts	23
1.4. <i>Repair of DNA photoproducts.....</i>	<i>26</i>
1.5. <i>DNA photolyases.....</i>	<i>30</i>
1.5.1. The mechanism of action of CPD photolyase.....	31
1.5.2. Electron transfer mechanism between CPD and photolyase.....	35
1.5.3. Energy transfer between the cofactors.....	37
1.5.4. The photoactivation of FAD	40
1.5.5. Photolyase-substrate co-crystal study	42
1.5.6. (6-4) photolyases.....	43
1.6. <i>Molecular Beacons</i>	<i>45</i>
1.6.1. Principles of MBs.....	46
1.6.2. Designing molecular beacons:	49
1.6.3. Kinetics and thermodynamics of MBs.....	51
1.6.4. Surface immobilized MBs	52
1.6.5. Applications of MBs	54
1.7. <i>Mass spectrometry for biomolecular analysis.....</i>	<i>56</i>
2. AIMS OF RESEARCH.....	60
3. UV INDUCED DAMAGE FORMATION EVENT	62
3.1. <i>HPLC methodology</i>	<i>65</i>
3.2. <i>Lesion formation on the different of nucleobases</i>	<i>66</i>
3.3. <i>Stability of photoproducts under various pH conditions</i>	<i>72</i>
3.4. <i>Enzymatic digestion and lesion analysis.....</i>	<i>74</i>
3.5. <i>HPLC-ESI-MS for damage detection.....</i>	<i>75</i>

3.6.	<i>Characterization of photoproducts by HPLC-ESI-MS/MS</i>	79
3.7.	<i>Dose-dependence study</i>	86
3.8.	<i>Sequence context</i>	87
3.9.	<i>Conformation-dependence on photoproduct formation</i>	98
3.9.1.	CD spectral analysis.....	100
3.10.	<i>Summary and conclusion</i>	107
4.	PHOTOLYASE CATALYZED CPD-LESION REPAIR STUDY	110
4.1.	<i>Activities of CPD-photolyase</i>	110
4.2.	<i>Molecular beacon based photolyase-substrate DNA</i>	111
4.2.1.	Synthesis of the molecular beacon.....	115
4.2.2.	Characterization of the molecular beacon	117
4.3.	<i>Activity profiling of Type-II photolyase with molecular beacon substrate</i>	121
4.3.1.	HPLC profiling of photolyase activity	123
4.4.	<i>Repair study with Class-II photolyase from A. thaliana</i>	126
4.5.	<i>Activity profiling of Class-II photolyase in crude cell extracts</i>	128
4.6.	<i>Study with living cell: single cell detection</i>	131
4.7.	<i>Stability of the MB-probe in cell extract</i>	133
4.8.	<i>Summary and conclusion</i>	136
5.	EXPERIMENTAL SECTION	138
5.1.	<i>Materials and Methods</i>	138
5.1.1.	Equipments used in this study.....	138
5.1.2.	Materials and Reagents.....	143
5.2.	<i>Methods</i>	145
5.2.1.	DNA damage study	145
5.2.2.	DNA repair.....	154
6.	ABBREVIATIONS	160
7.	LITERATURE	162

Summary

Gradual depletion of the ozone layer and consequently, increased ultraviolet (UV) radiation on the Earth's surface induces DNA-lesions inside the genome, thereby causing mutations. Three kinds of photoproducts are mainly formed, namely: cyclobutane pyrimidine dimers (CPD), pyrimidine-(6-4)-pyrimidone dimer [(6-4)PP] and the Dewar valence isomer of (6-4)PP lesion. The formation of these photolesions is a major cause of cell death (aging) and fatal disease like skin cancer.

A part of this research was performed to investigate the formation and characterization of DNA-lesions under UVC radiation. Small, fluorescent labeled oligonucleotide hairpins (DNA, RNA and mixed DNA-RNA) were employed to this purpose. The amount of damage was quantified using HPLC. Here, a new method was developed, using ion-exchange SAX-column which works at pH = 13, to measure the lesion formation in a direct way. In order to know which lesions are formed, the irradiated hairpins were enzymatically digested. The lesions were separated by HPLC followed by their characterization using MS/MS fragmentation analysis.

Investigation was performed to understand the impact of the neighboring nucleobases on the photo-reactivity of a dTpdT-dinucleotide. For this, hairpins were prepared in various sequential contexts. Analysis of these irradiated hairpins revealed the surprising result that the reactivity is strongly reduced when a dTpdT dinucleotide is locked between two neighboring 2'-deoxyguanosines, strongly implying that genomic DNA will be inhomogeneously damaged and hence mutated under UVC radiation.

In order to account for the effect of oligonucleotide conformations (A versus B) on the photolesions formation, DNA, RNA and mixed DNA-RNA hairpins were irradiated. The most surprising observation is that the oligonucleotide hairpins, possessing more A-like conformations were found to be very much resistant to UVC degradation. RNA hairpins containing UpU dinucleotides were found to be fully protected from being damaged. A short, dTpdT-containing DNA stretch, embedded in an A-like RNA environment, was also found to be highly stable under UVC light.

In the second part of this study, investigation was performed to assay the activities of CPD-photolyase enzyme isolated from different organisms. A synthetic *cis-syn* thymidine dimer with an open backbone was incorporated into DNA (Figure 1). CPD-photolyases were found to recognize and split this CPD-lesion, *via* a $[2\pi + 2\pi]$ cycloreversion process, into two 2'-deoxythymidine monomers.

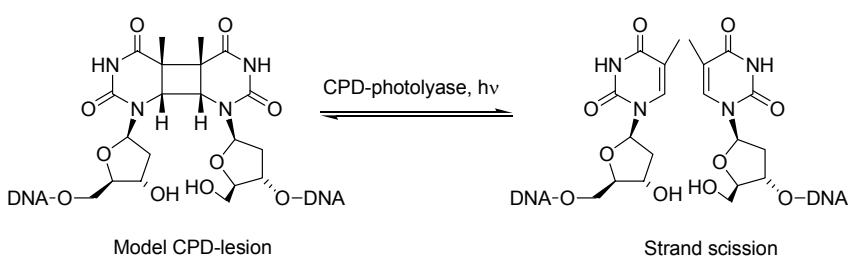


Figure 1: Schematic presentation of a DNA containing the model CPD-lesion with open backbone structure.

In order to profile the activities of photolyases and also to study photolyase activity inside living cell, a sensitive DNA-probe, known as molecular beacon

(Figure 2) was synthesized. The hairpin probe, which features a loop and stem structure contains the model CPD-lesion in its loop region. The molecular beacon (MB 1) in its closed form, is non-fluorescent due to efficient energy transfer (FRET) from the 5'-FAM to 3'-Dabsyl.

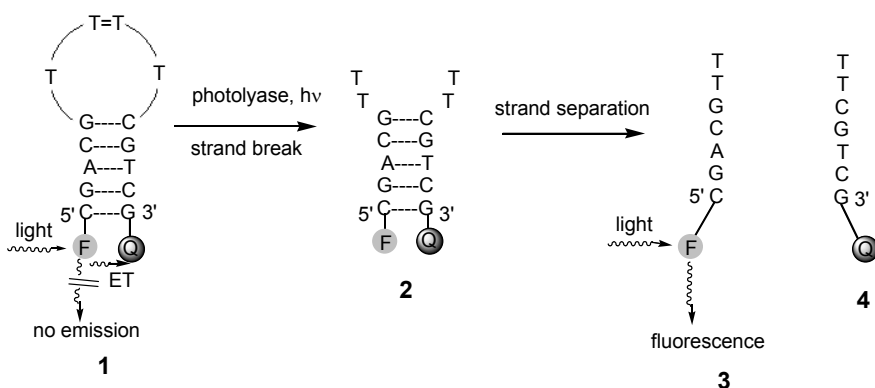


Figure 2: Depiction of the molecular beacon strategy to quantify DNA-repair activity.

The MB 1 was designed to undergo strand break on reaction with photolyase in presence of light, thus separating the FAM and the Dabsyl and causing the fluorescence of FAM to be restored (see Figure 2). The activities of the photolyase can be studied by monitoring the fluorescence change. Activities of CPD-photolyase isolated from *A. nidulans* and *A. thaliana* were studied using this MB-probe.

The sensitivity of this probe was tested with wild-type cell-extract from *A. thaliana*. The fishing-out of photolyase activity from this wild-type extract was possible. Effort was made to investigate the repair process within a living cell, using laser scanning fluorescence microscopy. The insertion of this artificial, chemically modified DNA-substrate in the cell nucleus was achieved.

Zusammenfassung

Die graduelle Zerstörung der Ozonschicht und die folglich erhöhte ultraviolette (UV) Strahlung auf der Erdoberfläche induzieren DNA-Schäden innerhalb des Genoms, die Mutationen verursachen.

Drei Arten von Photoschäden werden hauptsächlich gebildet: Cyclobutan-Pyrimidin-Dimer (CPD), Pyrimidin-(6-4)-Pyrimidon-Dimer [(6-4)PP] und das Dewar-Valenzisomer des (6-4)PP-Schaden. Die Bildung dieser Photoschäden ist eine Hauptursache für Zelltod (Alterung) und gefährliche Krankheiten wie Hautkrebs.

Ein Teil dieser Forschung wurde durchgeführt, um Bildung und Charakterisierung von DNA-Schäden unter UVC-Belichtung zu untersuchen. Hierfür wurden kurze, fluoreszenz-markierte Oligonukleotid-Haarnadeln (DNA, RNA und gemischte DNA-RNA) eingesetzt. Die Schadensmenge wurde mittels HPLC quantifiziert. Hierbei wurde eine neue Methode entwickelt, in der eine Ionenaustauscher-SAX-Säule bei $\text{pH} = 13$ verwendet wird und die Schadensbildung auf direktem Weg mißt. Diese sensitive analytische Methode erlaubt die Trennung von den Schäden enthaltenden Haarnadeln von ihren ungeschädigten Gegen stücken. Um zu wissen, welche Schäden gebildet wurden, wurden die belichteten Haarnadeln enzymatisch verdaut. Die Schäden wurden mittels HPLC getrennt und anschließend mit MS/MS-Fragmentierungsanalyse charakterisiert.

Der Einfluß der Nachbarbasen auf die Reaktivität eines dTpdT-Dinukleotids wurde untersucht. Zu diesem Zweck wurden Hairpins verschiedener Sequenz

hergestellt. Die Analyse belichteter Hairpins lieferte das überraschende Ergebnis, daß die Reaktivität eines dTpdT-Dinukleotids, welches zwischen zwei 2'-Desoxyguanosinen liegt, stark reduziert ist. Dies läßt den Schluß zu, daß genomische DNA von UVC-Strahlung in inhomogener Weise geschädigt wird, was zu Mutationen führt.

Um den Effekt der Oligonukleotidkonformation (A vs. B) auf die Entstehung von Photoschäden aufzuklären, wurden DNA-, RNA- und gemischte DNA-RNA-Hairpins belichtet. Die überraschendste Beobachtung war, daß Hairpins mit überwiegend A-ähnlicher Konformation äußerst resistent gegen UVC-Abbau waren. RNA-Hairpins, die ein UpU-Dinukleotid enthielten, waren sogar völlig vor Schäden geschützt. Ein kurzer, ein dTpdT enthaltender DNA-Abschnitt, welcher in eine A-ähnliche RNA-Konformation eingebettet war, zeigte sich ebenfalls als sehr stabil gegenüber UVC-Licht.

Im zweiten Teil dieser Arbeit wurde ein Assay entwickelt, um die Enzymaktivität von CPD-Photolyasen aus verschiedenen Organismen zu testen. Hierzu wurde ein synthetisches *cis,syn*-Thymidindimer mit einem offenen Rückgrat in DNA eingebaut. Man konnte zeigen, daß die CPD-Photolyase den Schaden erkennt und über eine $[2\pi + 2\pi]$ -Cycloreversion in die zwei 2'-Desoxythymidinmonomere spaltet (Abbildung 1).

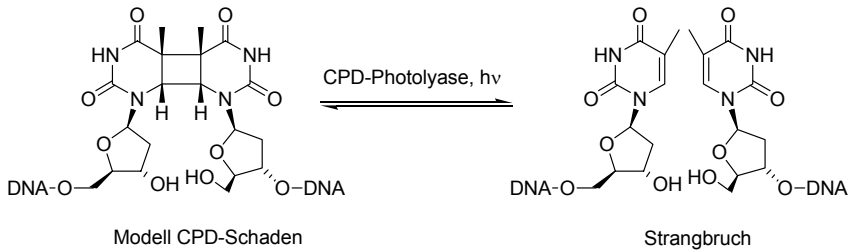


Abbildung 1: Schematische Darstellung von DNA, welche die CPD-Modellverbindung mit offenem Rückgrat enthält.

Um die Photolyaseaktivität auch in lebenden Zellen zu verfolgen, wurde eine sehr empfindliche DNA-Sonde, der *molecular beacon* 1 (Abbildung 2), synthetisiert. Die Hairpinsonde, bestehend aus einem *loop* und dem Schaft, enthält die CPD-Schadenmodellverbindung im *loop*. Der *molecular beacon* (MB 1) enthält ein Fluorophor (FAM) am 5'-Ende und einen Fluoreszenzlöcher (Dabsyl) am 3'-Ende. In geschlossener Form ist der *molecular beacon* nicht fluoreszent aufgrund von effizientem Energietransfer (FRET) vom FAM zum Dabsyl.

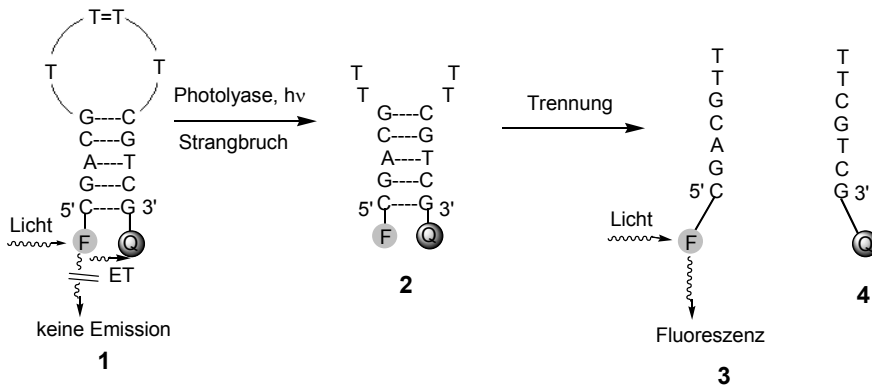


Abbildung 2: Darstellung der *molecular beacon*-Strategie zur Quantifizierung der DNA-Reparaturaktivität.

MB 1 wurde so gestaltet, daß durch die Photolyasereaktion in Anwesenheit von Licht ein Strangbruch entsteht, durch den das FAM und das Dabsyl voneinander getrennt werden, was zum Wiederauftreten der Fluoreszenz des FAMs führt (siehe Abbildung 2). Die Aktivität der Photolyase kann so anhand der Änderung der Fluoreszenz verfolgt werden. Unter Verwendung der MB-Sonde konnte die Aktivität von Photolyasen aus *A. nidulans* und *A. thaliana* untersucht werden.

Die Empfindlichkeit der Sonde wurde mit einem Wildtyp-Extrakt aus *A. thaliana* getestet. Es war möglich, die Photolyaseaktivität selektiv aus dem Wildtyp-Extrakt „herauszufischen“. Es wurden Anstrengungen unternommen, um den Reparaturprozess in lebenden Zellen unter Verwendung von Fluoreszenzmikroskopie zu untersuchen. Das künstliche, chemisch modifizierte DNA-Substrat konnte erfolgreich in den Zellkern eingebracht werden.

1. Introduction

1.1. *Consequence of ozone layer destruction*

The sun, at the center of our solar system, provides us with the light and energy necessary for life. Along with essential rays, sunlight also contains very harmful ultraviolet (UV) radiation which ranges from 200-400 nm. Light of this wavelength range causes damage to DNA and proteins of living organisms. The ozone layer, situated in the stratosphere about 15 to 30 km above the earth's surface, shields the harmful UV radiation from reaching the planet Earth,^[1, 2] and thereby acts as a 'space suit' to protect the living world.^[3-5] Over the past decades, however, anthropogenous factors have caused a severe reduction of ozone in the ozone layer.^[6-11] The growing concentration of chlorofluorocarbons (CFC's) is a major cause of ozone layer destruction.^[12, 13] The increasing production of greenhouse gases^[14, 15] (such as gases used for aerosols) also play a role in ozone layer depletion. It was observed that chemical reactions responsible for ozone depletion are extremely sensitive to temperature.^[16] Relatively low temperatures favor the reactivities of the singlet oxygen radicals that are involved in the process. Hence, even small amounts of stratospheric cooling can greatly increase ozone depletion. When sunlight strikes the Earth's surface, a part of the radiation is reflected back towards space as infra-red radiation (heat). Greenhouse gases absorb this infra-red radiation and trap the heat in the atmosphere which warms the Earth's atmosphere but cools the stratosphere radiatively. As a result the ozone degradation rate increases.^[17-19] The rate of destruction of the ozone layer is higher in high-latitude areas. In the Antarctic circle, a large ozone hole has been

observed from 1989 through 1996.^[3, 8, 20] It is the most prominent example of how anthropogenic emissions of nitric oxides and other ozone-degrading gases cause ozone layer degradation. The depletion of the ozone layer, in turn, leads to an increase in UV-B/C radiation, which now reaches the surface of our planet.^[21]

An estimated 10% increase in UV radiation in Western Europe has been reported.^[22] One of the proposed mechanisms of ozone degradation by CFC's is presented in Figure 1.1. The mechanism is believed to proceed *via* several radical steps involving singlet oxygen.^[2, 7, 14, 15, 23]

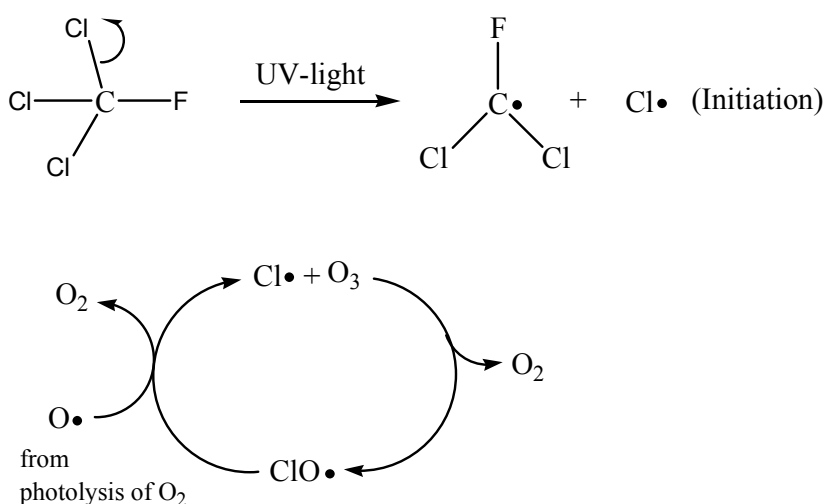


Figure 1.1: Mechanism of degradation of ozone by Chlorofluorocarbons.

Exposure to UV radiation is the major cause of skin cancer^[24-27]. The DNA/RNA in sunlight-exposed skin suffers formation of photo dimers between the neighboring nucleobases (see section 1.3), thereby causing mutations in the genome. One consequence of this is the generation of cancerous cells.^[28-33]

1.2. Effect of UV exposure

Sunlight consists of three types of UV radiation termed as UVA, UVB and UVC.

UVA, ranging from 320-400 nm, is responsible for skin aging and cancers such as melanoma. Since UVA passes successfully through the ozone layer, it accounts for the majority of UV exposure. ^[34]

UVB radiation (290-320 nm) causes sunburns, cataracts, immune-system damage and skin cancer. The most prevalent form is melanoma. Although most UVB rays are absorbed by the ozone layer, a considerable amounts still pass through, to cause severe damage.

UVC contains rays within a range of 230-290 nm and is most fetal to exposed skin (malignant melanoma). Most of these rays are however absorbed by the ozone layer and normally do not reach the Earth. ^[35]

The super-most layer of our skin (epidermis, 100 μm thick) contains three different types of cell: flat cells on the surface called squamous cells, round shaped cells called basal cells and melanocytes, which give skin it's color. ^[35]

Basal cells carcinoma (500,000 cases/yr, 500 deaths/yr) and squamous cells carcinoma (120,000 cases/yr, 1,500 deaths/yr) are the most common types of skin cancer whereas malignant melanoma (32,000 new cases/yr, 6,500 deaths/yr) is the most dangerous form of skin cancer due to damage caused to melanocytes. ^[36-38]

Melanocytes possess a highly UV-absorbing pigment called melanin (responsible for color of the skin), and therefore are more susceptible to UV damage. Figure 1.2 shows the development of different types of skin cancers. ^[35]

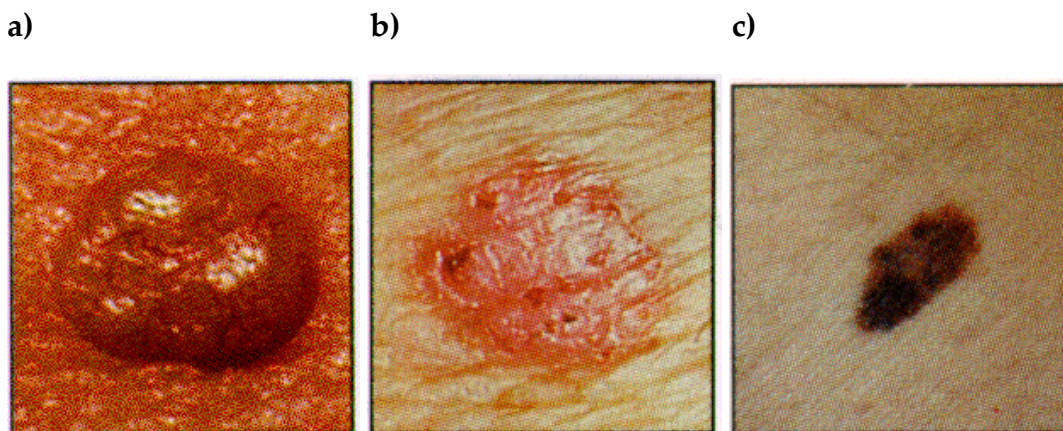


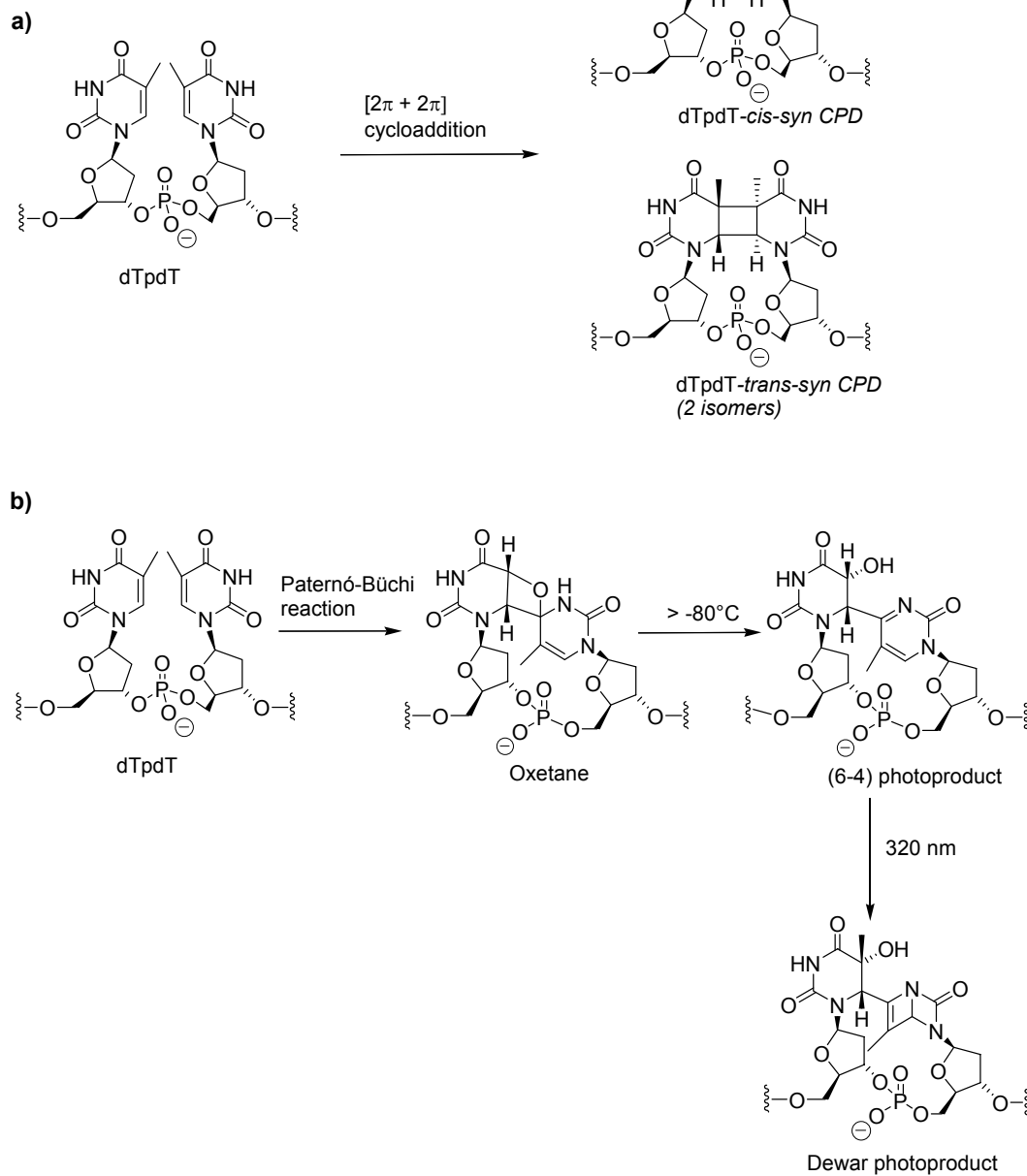
Figure 1.2: Depiction of three kinds of skin cancer: **a)** Basal cell carcinoma, **b)** Squamous cell carcinoma and **c)** Malignant melanoma

1.3. Photoproducts

The heterocyclic bases in DNA/RNA exhibit UV absorption in the range of 260 to 280 nm. Radiation in this wavelength region raises the bases to their excited singlet or triplet state which then undergo various photochemical reactions.^[39, 40] Generally, the nucleobases react with their immediate neighboring counterparts present in the same DNA/RNA strand,^[41, 42] although the formation of inter-strand photoproducts have also been reported.^[43-47] Intra-strand dimers are favorable over the inter-strand crosslink photoproducts due to the well-organized B-duplex structure of DNA and partially due to intra-strand stacking between the neighboring bases. Pyrimidine nucleobases were found to be the most vulnerable sites for such photochemical reactions when exposed to UV-B/C light, leading to formation of photolesions.^[32, 40, 48, 49] As DNA nucleobases absorb light between 260 nm and 280 nm, cells are most vulnerable to UVC (230-290 nm) radiation. The commonly occurring photoproducts from UVC radiation are: TT-

dimers, TC/CT-dimers and CC-dimers.^[37, 41, 49-51] The best-known photoproducts are the cyclobutane pyrimidine dimers (CPD), the (6-4) pyrimidine-pyrimidone dimers [(6-4)PP] and their Dewar valence isomeric lesions.^[39, 52] The CPD-lesions are formed by $[2\pi + 2\pi]$ cycloaddition reaction between the adjacent pyrimidines, as shown in Figure 1.3. The (6-4)PP photoproducts are formed due to Paternó-Büchi reaction which proceeds *via* an oxetane or azetidine intermediate. These intermediate products are unstable above -80 °C and undergo rapid ring opening to the (6-4)PP photolesions (Figure 1.3).^[37, 53, 54] The structures of well-known photoproducts are given in Figure 1.3 to Figure 1.5. The (6-4)PP photolesions undergo photo-isomerization to their Dewar valence counterparts when irradiated with UVB light (around 320 nm). A less frequently observed photolesion, known as spore-photoproduct, has been identified in recent years. Spore photoproducts are found as the major photolesions in bacterial spores.^[55, 56] These lesions are produced by addition of the methyl group of a thymine to the C5 position of another neighboring thymidine (Figure 1.6) and are conceived only in compact, dry, DNA under UVC light.^[57-61]

dTpdT photoproducts



dCpdC photoproducts

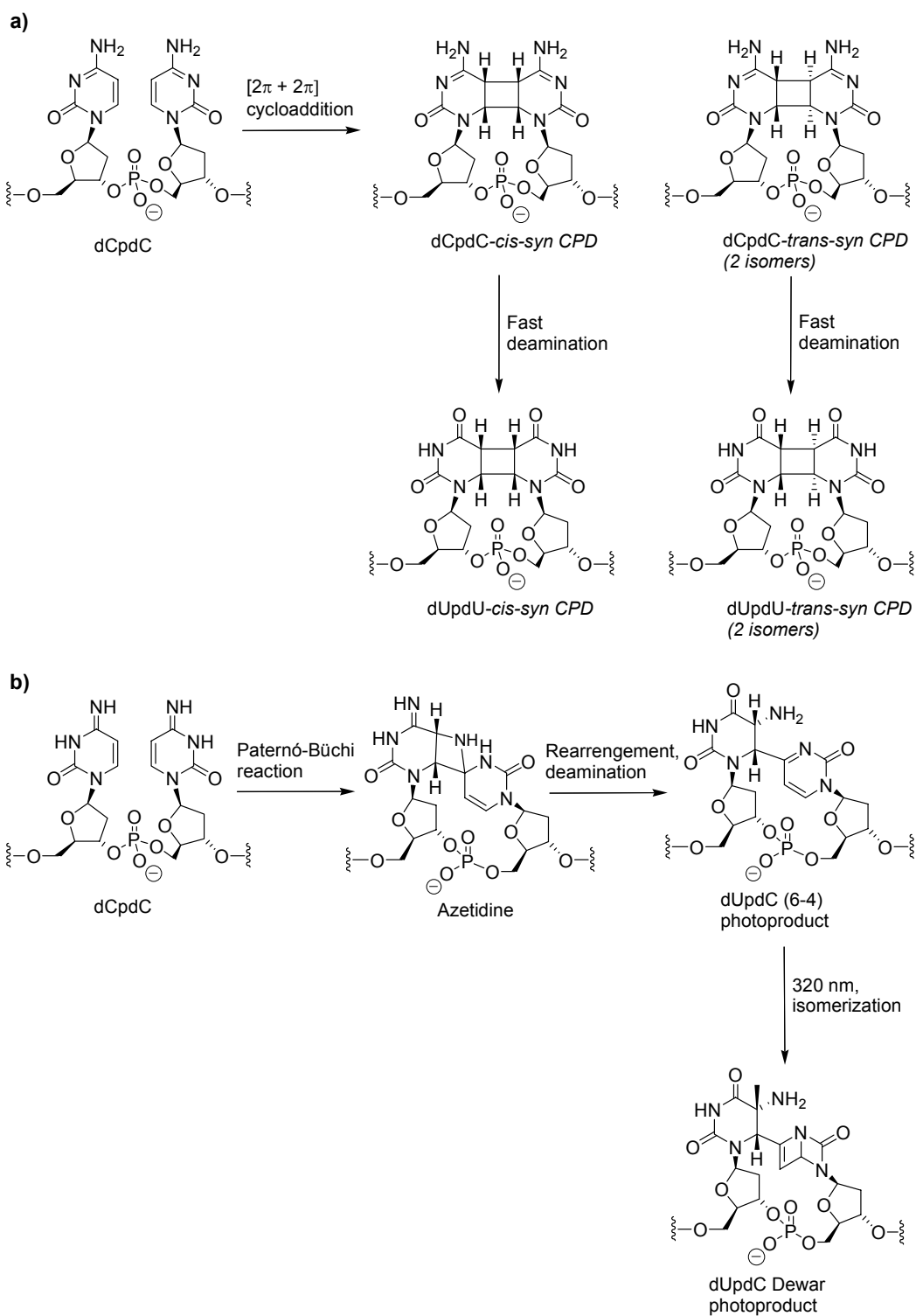
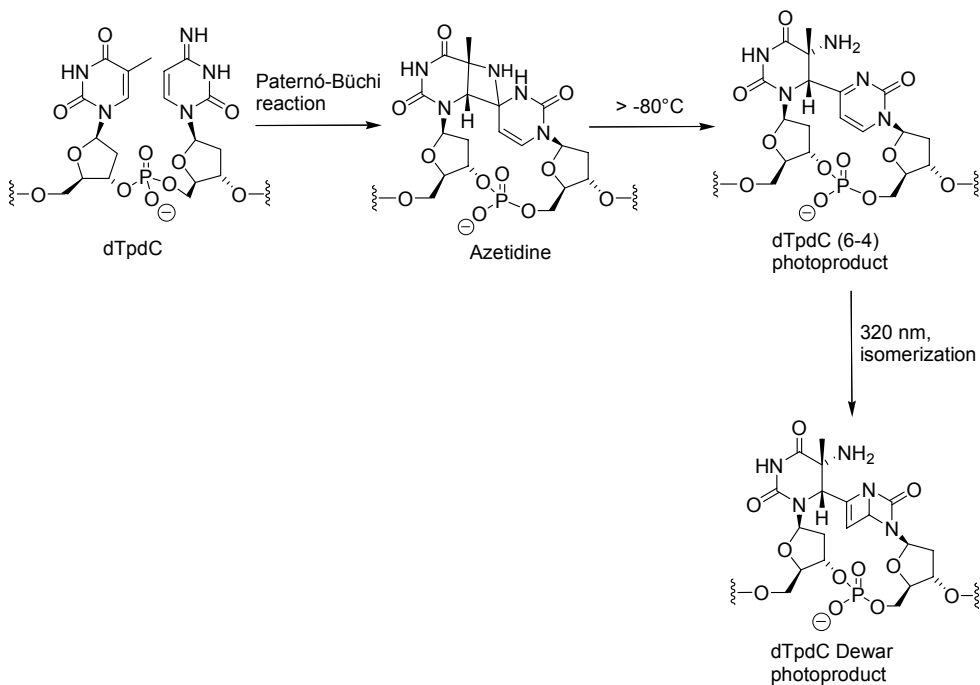
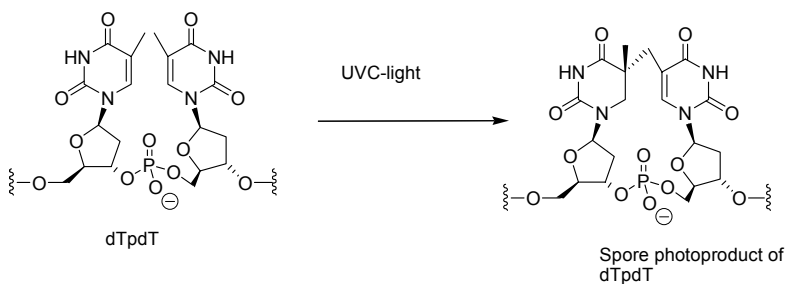


Figure 1.4: Formation of cytosine-cytidine (dCpdC) photolesions and their deaminated products by **a)** $[2\pi + 2\pi]$ cycloaddition reaction, **b)** Paternó-Büchi reaction

dTpdC photoproduct**Figure 1.5:** Photo-induced reaction of dTpdC dinucleotides**Figure 1.6:** Formation of dTpdT spore photoproduct in bacterial spore.

1.3.1. DNA, mutagenesis and cancer

The biomolecule that masters the function and properties of cell is deoxyribonucleic acid, in short, DNA. It stores the genetic information which passes on through generations. The building units of DNA are four nucleosides, constituted from four heterocyclic nucleobases A, T, G and C.^[62] The permutations and combinations of these nucleobases manufacture the 46 chromosomes of a nucleus in a human cell. The novel A:T and G:C base-pairing (Watson-Crick) and the double-helix structure make DNA a unique biomolecule,^[63] capable of replicating and thereby enabling DNA to storing informations.^[62] A set of three nucleobases, known as a codon, directs amino acid synthesis and hence DNA governs the synthesis of a protein molecule to carry out the cell's requirements.^[62, 64, 65] Another important biomolecule, similar to DNA, is RNA. RNA plays an important role in translating the genetic information, stored in DNA, into protein synthesis. It has been proposed that RNA were the very first molecules that started the life on Earth from the primordial soup.^[66]

A single base mutation within the genome can stop or misdirect protein synthesis, causing either cell death or uncontrolled cell division.^[67] All living cells are constantly undergoing mitotic or meiotic divisions, regulated e.g. by two kinds of genes: proto-oncogenes and tumor suppressor genes. The former encourages cell division whilst tumor suppressor genes (e.g. p53 gene) prevent excessive cell division (apoptosis). The product of these two polar functions balances the frequency of cell division. When mutated in its mutational hotspot, a proto-oncogene becomes an oncogene and functions differently. Likewise, if a tumor suppressor gene is damaged or mutated, it might also promote cell

division instead of suppressing it. Either of these cases results in excessive cell division, known as tumor cell growth. After a first mutation, multiple mutations are highly feasible which finally causes formation of cancer cells (Figure 1.7). A general overview of how cancer cells are formed is demonstrated in Figure 1.8.

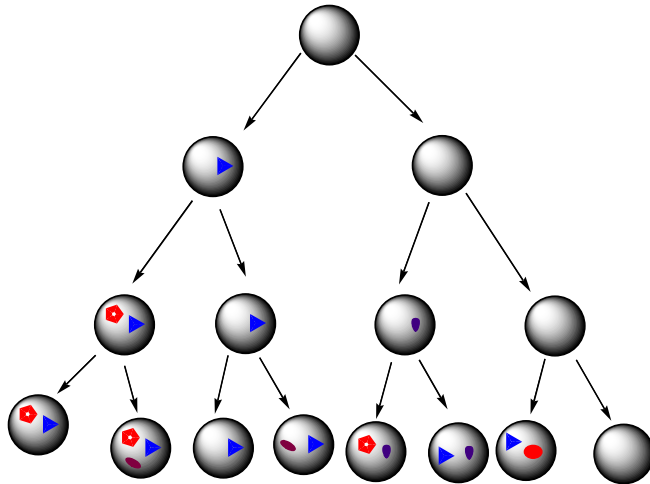


Figure 1.7: Propagation of DNA-mutation during cell divisions. The spots of various shapes indicate multiple type mutations.

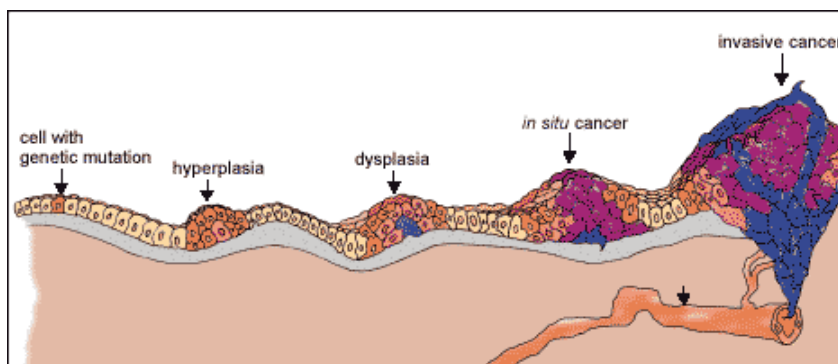


Figure 1.8: Depiction of various stages for advancement of invasive tumor from a single-point genetic mutation.

Mutations occur due to damage of the genomic DNA (human genome contains about 10^9 nucleotides^[62]). The DNA in cells are constantly exposed to many internal and external chemical agents such as highly reactive radicals and other reactive oxygen species that are produced during aerobic respiration.^[68, 69] Exposure to UV light can also affect the DNA in exposed skin.^[36] These chemical agents or the ultraviolet radiation can cause severe damage to the DNA/RNA nucleotides, thereby inducing mutations in the genome. The unstable hydroxyl radicals react with guanine or adenine bases in DNA to produce 8-oxo-guanines or 8-oxo-adenines which alter the Watson-Crick base-pairing properties: hence DNA is more vulnerable to mutations.^[70] A schematic presentation of possible consequences of DNA damage is shown in Figure 1.9. ^[71,72]

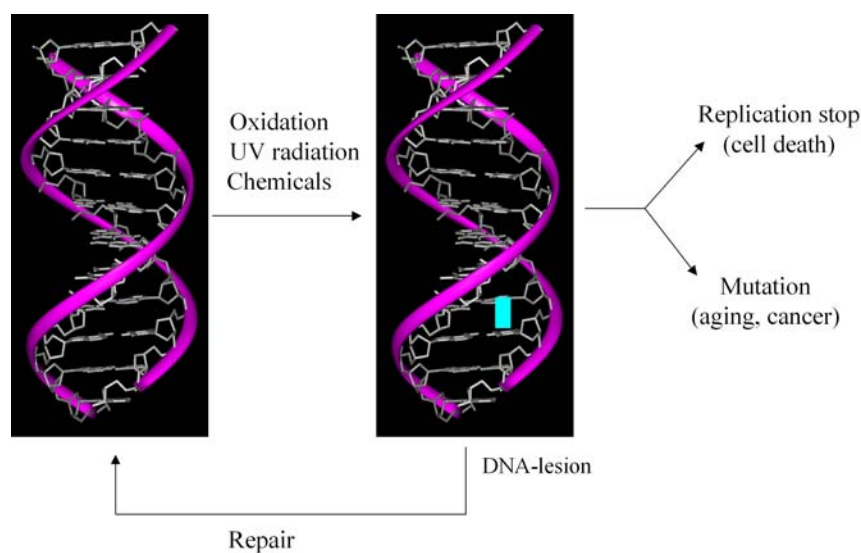


Figure 1.9: Demonstration of possible consequences of DNA damage and photoproducts.

1.3.2. *Photolesions and mutagenesis*

During cell division, DNA makes a copy of itself for the new cell. This procedure, called replication, is carried out by a set of specialized enzymes known as polymerases. The single-stranded DNA, after denaturation of the double helix, serves as a template for replication. The presence of any damage inside DNA is usually detected by the polymerase before replication, and is immediately being repaired/replaced with correct nucleotides by repair enzymes. There are, however, lesions that are not detected by the polymerase and are therefore bypassed during replication. There also exist some polymerases (e.g. pol η , pol ι and pol κ) which can bypass the lesions. During bypass, the lesions, due to different base-pairing properties than their undamaged precursors, lead to mutations of the genomic DNA and thereby alter the amino acid sequence it encodes. DNA photoproducts, when bypassed by the polymerases or unsuccessfully repaired, induce various mutations into the genome.^[39, 73, 74] This section will describe the mechanisms of mutations, induced by different photoproducts.

Cyclobutane pyrimidine dimer lesions (CPD) induced mutations

The cytosine-derived CPD-lesion, formed upon UVB/C exposure, undergoes CC \rightarrow TT double point mutations *via* a fast deamination into UU CPD-lesion, described in Figure 1.10. ^[41, 73]

The deamination of the dCpdC CPD-lesion is a fast process, with a half-life of only about 5-6 hours, *in vivo*.^[75, 76] The resulting dUpdU dinucleotide serves as a DNA template for polymerase and directs incorporation of 2'-deoxyadenosines in the counter-strand, which on further replication yields C → T transformation.^[77] The p53 tumor suppressor gene of most common types of skin cancers has been found to possess C → T mutations including CC → TT double mutations.^[32, 74, 77, 78]

The dTpdT cyclobutane pyrimidine dimer (CPD) lesions are in general not mutagenic. Although dT[c,s]pdT lesion is efficiently bypassed by the polymerase, it is not mutagenic due its inability to alter the Watson-Crick base pairing properties compared to the undamaged dTpdT dinucleotide.^[32, 79, 80] The 5'-dT of 5'-dT[t,s]pdT-3' lesion act as a mismatch as the methyl group (*syn* conformation) stays at the interface of Watson-Crick base pairing.^[81]

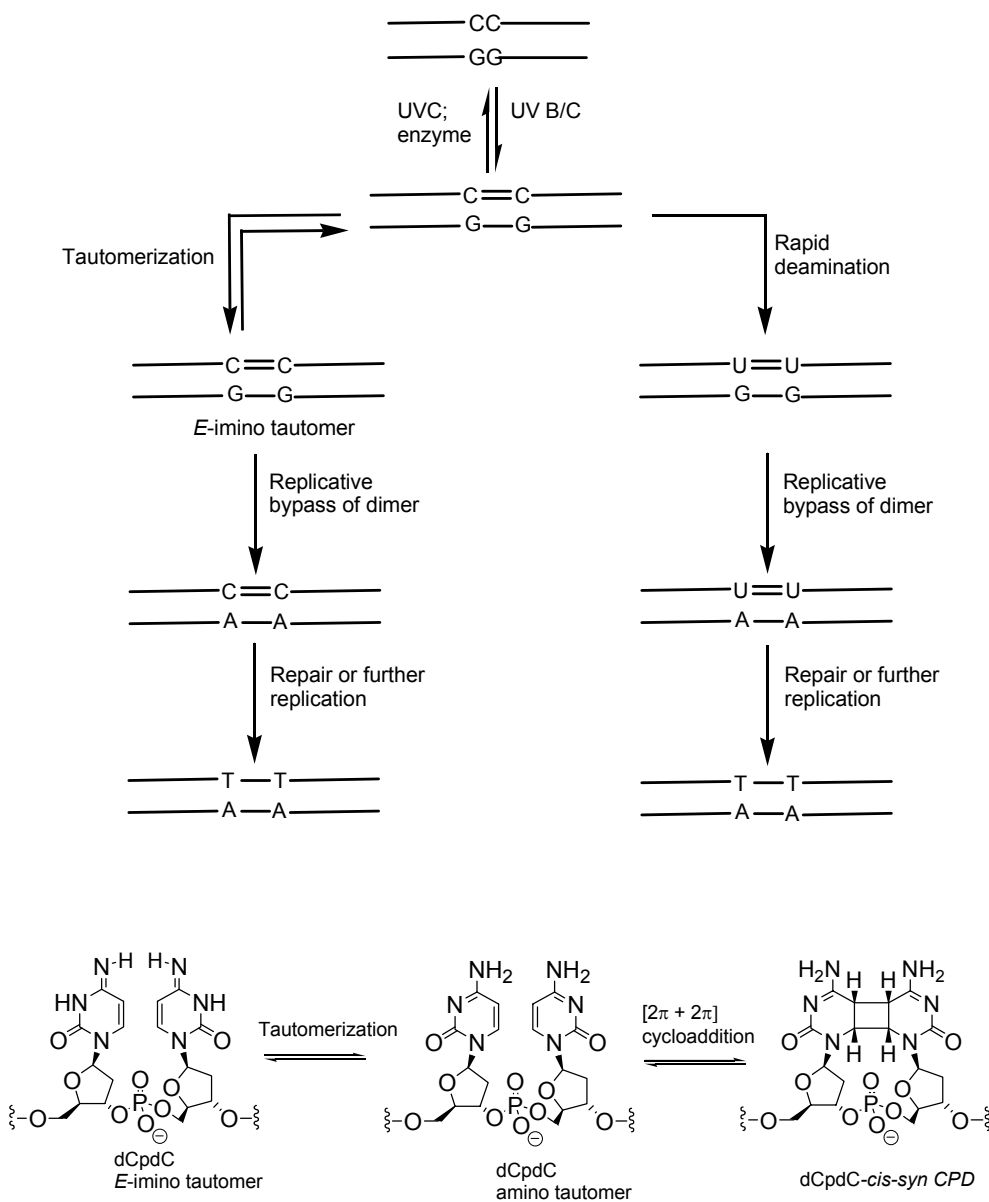


Figure 1.10: Mutagenic potential of the cyclobutane-pyrimidine photolesion from dCpdC dinucleotide which causes CC → TT double point mutation. The structures below demonstrate formation of two possible isomers with similar mutagenic threat, the dCpdC-CPD photolesion and the E-imino tautomer of the dCpdC dinucleotide.

Mutation of (6-4)PP lesions

The (6-4)PP photoproducts of dTpdT, dTpdC/dCpdT and dCpdC are highly mutagenic. The dTpdT-(6-4)PP lesion induces a T → C mutation in the genome. Studies showed that the 3'-dT of this lesion preferentially pairs with a 2'-deoxyguanosine while the 5'-dT remains well-paired with a 2'-deoxyadenosine in the opposite strand as shown in Figure 1.11.^[82-84]

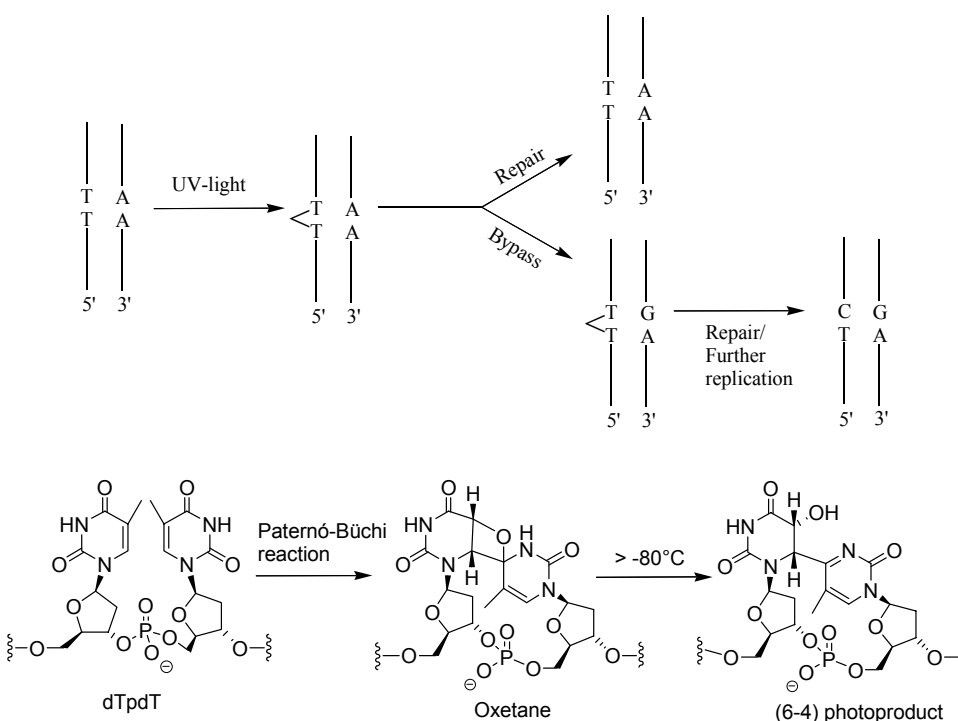


Figure 1.11: Mechanistic pathway of T → C mutation induced by dTpdT-(6-4)PP photolesion due to mispairing of 3'-dT of the (6-4)PP lesion. The structures demonstrate the course of formation of the (6-4)PP lesion.

The (6-4)PP lesions of dCpdC and dTpdC photoproducts probably induce a C → T mutation at the cytosine site due to its fast deamination into uracil.

Mutagenicity of Dewar valence lesions

Dewar valence photoproduct of a dTpdT-dinucleotide is also highly mutagenic. The exact kind of mutation by Dewar lesion is not very well-understood.^[85] As like (6-4)PP lesion, the 3'-T of the Dewar-dTpdT lesion was also found to induce T → C mutation, although occurrence of double point mutation may not be ruled out.^[52]

1.3.3. Structure-activity relationships of the photoproducts

The efficiency with which a photoproduct induces mutation does not only depend on its base-pairing property but also on several other important factors:^[36]

Lesion recognition and repair: the higher the distortion of the B-duplex DNA by a photoproduct, the less mutagenic it is. A lesion which induces a large local distortion or bend in the double helix will be easily identified by the repair system and will be repaired or replaced by the correct nucleotide(s) immediately. Among dTpdT derived photoproducts, the *cis-syn* cyclobutane dimer bends the DNA only by 7°^[86] and in accord with *Kaptein et al.* and *Taylor et al.*, does not strongly perturb the thermodynamics of the DNA^[87]: hence this CPD-lesion is not

easily recognized by polymerases and repair enzymes. However, as it does not alter the Watson-Crick base-pairing properties compared to its undamaged counterpart, this lesion is unlikely to induce a mutation.^[81] The *trans-syn* CPD-lesion of dTpdT, due to its rigid stereochemical orientation, bends DNA by a large amount up to 22°, thereby increasing the thermodynamic energy of the duplex significantly. ^[81, 86, 87] As a result, this lesion possesses only a little mutagenic potential, being recognized easily by the repair enzymes. The surprising fact that the Dewar valence isomer is more mutagenic than (6-4)PP lesion was explained by molecular modeling. *Taylor et al.* showed that photoisomerization of the planar pyrimidone ring of the (6-4)PP product into the Dewar structure results in a more compact photoproduct which fits better in B-DNA. Thus, the Dewar structure perturbs the local DNA structure to a lesser extent than the (6-4)PP lesion.^[85]

Rate at which photoproducts are formed: the higher the rate of production of a lesion, the greater the chance that it will lead to a mutation. It has been found that in general cyclobutane dimers are formed at much higher amounts than (6-4)PP or Dewar valence photoproducts. *Taylor et al.* have demonstrated that sunlight-exposed dTpdT-derived *cis-syn*, *trans-syn* and (6-4)PP photolesions are formed at a ratio of 1: 0.1: 0.01 in duplex DNA.^[36, 88]

Rate of further chemical transformation: among the three dTpdT derived photoproducts only the (6-4)PP lesion undergoes photoisomerization into its Dewar product, with a half life of about 4 hrs in sunlight.^[36] The Dewar product is quite stable at neutral pH despite its strained structure.

Rate of repair of a photoproduct: the repair of an individual lesion largely depends on the ease of recognition by the repair enzymes. It was shown, *in vivo*, that the *cis-syn* dimers are repaired much slower (half life 24 hrs) than corresponding (6-4)PP or Dewar photoproducts (half life 3-4 hr).^[89] Site-specific incorporations of dTpdT photoproducts and their enzymatic repair by *E. coli uvr* BC excinuclease showed relative repair rates of *cis-syn*, *trans-syn*, (6-4)PP and Dewar dTpdT photoproduct as 1:7:9:9.^[90] The rate of incision can be approximately regarded as the rate of recognition by the *uvrA* subunit, which bound with relative affinities of 1:10:9:4. ^[91]

Rate of bypass by polymerase: the ability of a lesion not to be detected and hence bypassed by polymerases play a very important role in determining its mutagenic potential.^[36] As the *cis-syn* CPD-lesion induces less disorder into the B-DNA, it has the highest capability to be overlooked and hence bypassed by polymerases during replication. The relative bypassing rates of *cis-syn*, *trans-syn*, (6-4)PP and Dewar photolesion of dTpdT by an exonuclease deficient polymerase from T7 bacteriophage, have been found to be 1: 0.3: 0.006: 0.1. Noteworthy is the fact that the (6-4)PP lesion is much less bypassed than its Dewar isomer, again demonstrating the better compatibility of the latter lesion into duplex DNA.^[88]

1.4. Repair of DNA photoproducts

Our cells are continuously damaged due to many external and internal affairs (approximately 10^4 - 10^6 DNA damage events per cell per day). Hence an adult human (10^{12} cells) needs about 10^{16} - 10^{18} DNA damage repair everyday.^[92]

The DNA photoproducts, discussed in section 1.3, formed upon UV-light exposure, are highly lethal and carcinogenic unless otherwise repaired from the genome. Cells have developed various methodologies to repair or replace such harmful lesions. Some of the important and well-studied repair mechanisms are described below.

Nucleotide Excision Repair (NER)

Almost all higher organisms including humans follow this sophisticated mechanism to repair certain DNA lesions, including photoproducts.^[93-96] Plants and lower organisms also utilize this pathway for lesion repair to a large extent. In this process the repair enzyme recognizes the DNA lesion and excises a short oligonucleotide segment, approximately twenty nucleotides in length from either sides of the lesion, in the single strand. Local DNA synthesis by polymerases, using the complementary strand as a template (gap filling) is followed by ligation by DNA-ligase (see Figure 1.12a). The following steps are involved.

recognition of a DNA lesion

separation of the double helix at the DNA lesion site

single strand incision at both sides of the lesion
 excision of the lesion-containing single stranded DNA fragment
 DNA repair synthesis to fill the gap and
 ligation of the remaining single stranded nick

In *E. coli* the damage removal proteins are *UvrA*, *UvrB* and *UvrC* and that in yeast are *RAD3*, *RAD10* etc.

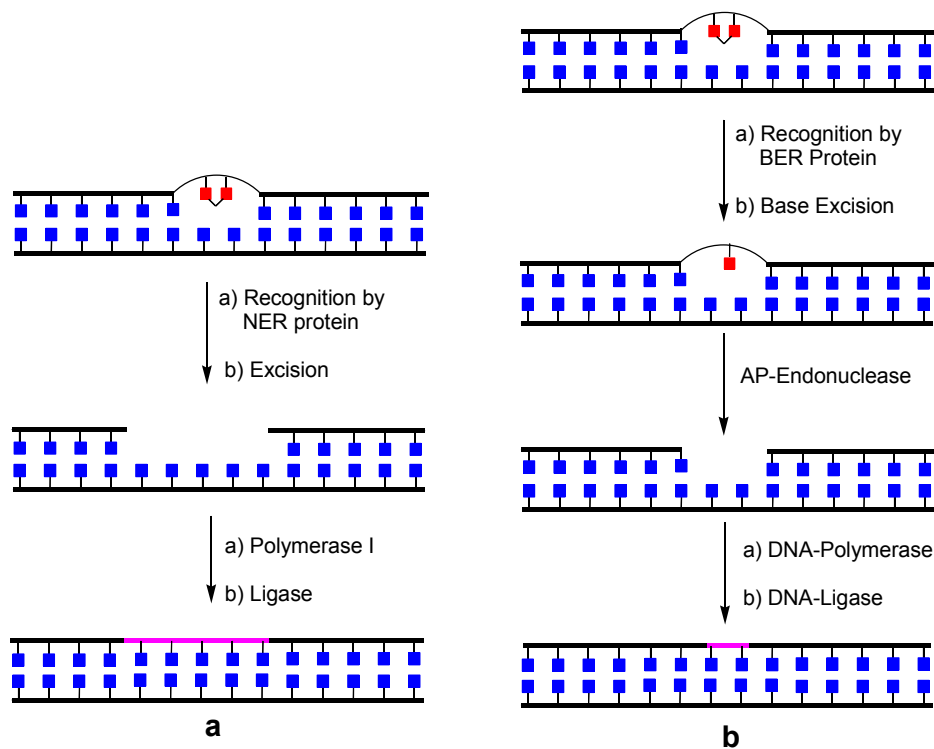


Figure 1.12: Representation of two important mechanisms to repair DNA-lesions, including photolesions, in the genome: **a)** Nucleotide excision repair and **b)** Base excision repair.

Base excision repair (BER)

The damaged DNA bases that are produced by deamination, oxidation and alkylation are repaired by this mechanism, as shown in Figure **1.12b**. BER enzymes are glycosylases which recognize the damaged bases and remove them from the DNA by cleaving the N-glycosidic bond between the heterocyclic base and the sugar moiety.^[72, 97] The abasic site is then removed by other enzymes involved in BER and replaced with the correct single nucleotide base by a repair polymerase.

Repair by photolyase

The majority of photoproducts in plants and lower organisms are repaired by photolyases.^[98, 99] Section **1.5** will describe the structures and functions of these enzymes in details.

Homologous-recombinant repair

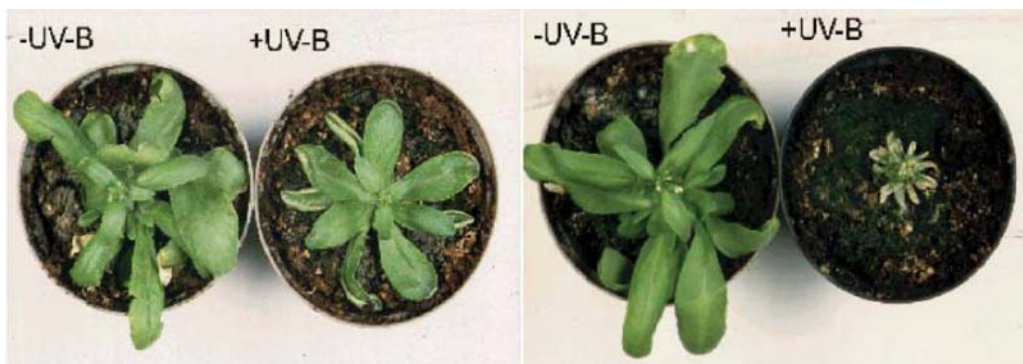
Recombinant repair is found in bacterial mutants which lack photolyases and excision repair proteins. This is a highly complex pathway coordinated by many homologous recombinant proteins.^[72]

Mismatch repair

Mismatched bases arise from replication errors during polymerase catalyzed DNA replication.^[72] This system recognizes and removes the base-base mismatches followed by insertion of the correct nucleotide bases by the polymerase.

1.5. DNA photolyases

DNA photolyases are monomeric proteins that directly repair the lethal and carcinogenic UV-induced DNA lesions in the genome of many organisms such as plants, lower organisms and some higher organisms like wood frogs, Australian kangaroos etc.^[98, 100] Photolyases are among the rare kinds of enzymes that are driven by light.^[41, 101, 102] Humans most probably do not possess this repair enzyme. Since plants are more exposed to sunlight and also absorb sunlight to a large extent for photosynthesis, they have a greater need of photolyases. Figure 1.13 demonstrates the development of a plant's growth which lacks photolyase gene. The growth of the photolyase-deficient, knock-out mutant plant, deteriorates very fast under UVB light compared to the wild-type plant which retains its photolyase activity.

a) *Ler* wild type**b) *Ler uvr2-1***

26 d old plant, UV-B: 14 d ($3.3 \text{ KJm}^{-2}\text{d}^{-1}$)

Figure 1.13: Essence of photolyase for plant's survival. Growth of 26 days old *A. thaliana* under UVB light is demonstrated for: **a)** *Ler* wild-type plant containing photolyase activity and **b)** *Ler uvr2-1* mutant which lack photolyase activity.

Depending upon the photolesions they repair, photolyases are divided into two categories: CPD-photolyase, that repairs cyclobutane pyrimidine dimers (CPD) and (6-4)-photolyase which reverts (6-4)PP lesions. The spore photoproduct is repaired by a non-photolyase enzyme known as spore photoproductlyase, which does not require light for its action.

1.5.1. The mechanism of action of CPD photolyase

CPD photolyase provides the major defense system for many organisms against UV radiation and thus prevents premature cell death, aging and prevalent diseases such as skin cancer. These photolyases effect the $[2\pi + 2\pi]$ cycloreversion of CPD lesions in a light-driven process.^[99, 103] All photolyases use the harmless

long wavelength radiation (450-550 nm) from sunlight to repair the photolesions.^[104, 105] All photolyases found to date are flavoproteins, containing an essential, non-covalently bound coenzyme FAD in the active site and a non-covalently bound second cofactor.^[99, 106-110] This second coenzyme is, however, probably not very essential for function of photolyase. The coenzyme FAD binds to the active pocket of the photolyase in a very unusual U-shape conformation (Figure 1.15). Depending on the nature of the second cofactor, CPD photolyases can be classified into two categories: Type-II photolyase e.g. *A. nidulans*,^[111] which uses 8-hydroxy-5-deazaflavin (8-HDF) and Type-I photolyase e.g. *E. coli*^[112, 113] that carries methenyltetrahydrofolate (MTHF) as the second cofactor. The chemical structures of the cofactors are depicted in Figure 1.14.

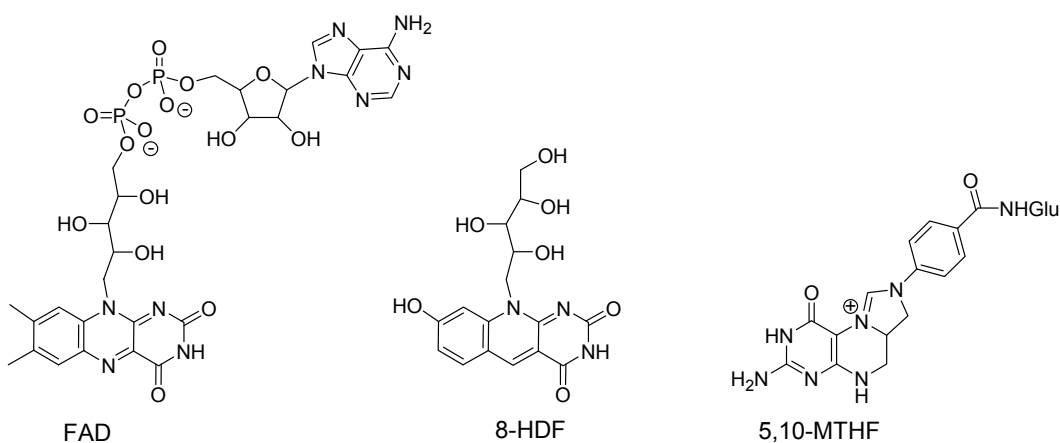


Figure 1.14: Chemical structures of the three coenzymes for photolyase (Glu = Glutamate)

Both the crystal structures from Type-I and Type-II photolyases (see Figure 1.15) published by *Sancar*^[112] and *Eker*,^[111] respectively, showed that the cofactor FAD is bound to the photolyase in an unusual U-shaped conformation.

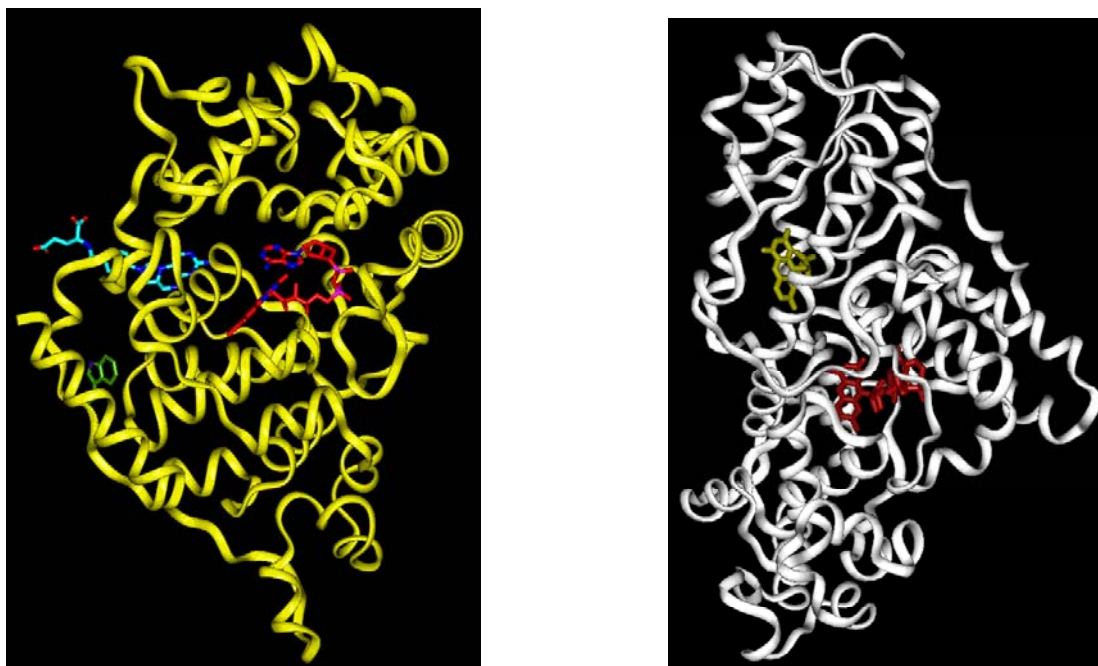


Figure 1.15: Obtained crystal structures of Type-I photolyase from *E. coli* (left) and Type-II photolyase isolated from *A. nidulans* (right)

It is believed that photolyases recognize the substrate lesion in a flipped-out conformation.^[114] In agreement with X-ray crystal structures obtained from other repair enzymes in complex with lesion-containing DNA,^[115-117] photolyase appears to effect a local conformational change to a large extent upon binding to a substrate lesion.^[114] A DNA bending of about 36° was observed from atomic force studies of the interaction between photolyase and substrate DNA.^[118, 119] Recently, a cocrystal structure of thymidine together with a photolyase from *T. thermophilus* has revealed that the thymidine, in the binding pocket of the protein, resides within *van der Waals* distance from the isoalloxazine ring of

FAD.^[120] This strong interaction, together with the stacking interaction of the thymine with the neighboring Trp₃₅₃ residue and *van der Waals* interaction with Trp₂₄₇, Met₃₁₄ and Gln₃₄₉ residues, is the driving force for the flip-out conformation of the thymidine.

Photolyases are one of the very rare types of enzymes that require light for action.^[121] Other light-dependent proteins are cryptochromes, rhodopsins etc. The second cofactor of photolyases (MTHF or 8-HDF), known as antenna cofactors, absorb long wavelength UV-visible light (450 nm to 550 nm) in order to activate the two-electron-reduced FADH⁻ to its first excited singlet state from where an electron transfer to the dimer occurs.^[98] The recognition of the dimer lesion by the photolyase is however, light independent. The intake of an electron by the dimer from fully reduced FADH^{*} governs the spontaneous cycloreversion of the dimer lesion into its monomers.^[99]

A schematic diagram of the CPD-repair phenomenon in *E. coli* is presented in Figure 1.16. In general, the partially reduced FADH^{*} in the active site of photolyase is activated through direct energy transfer from the second cofactor (MTHF, for *E. coli* photolyase). The excited FADH^{*} is then converted to the fully-reduced form FADH⁻, by the amino acid residues of the active site of the enzyme. Finally an electron is transferred to the CPD dimer which drives the cycloreversion into the monomers.

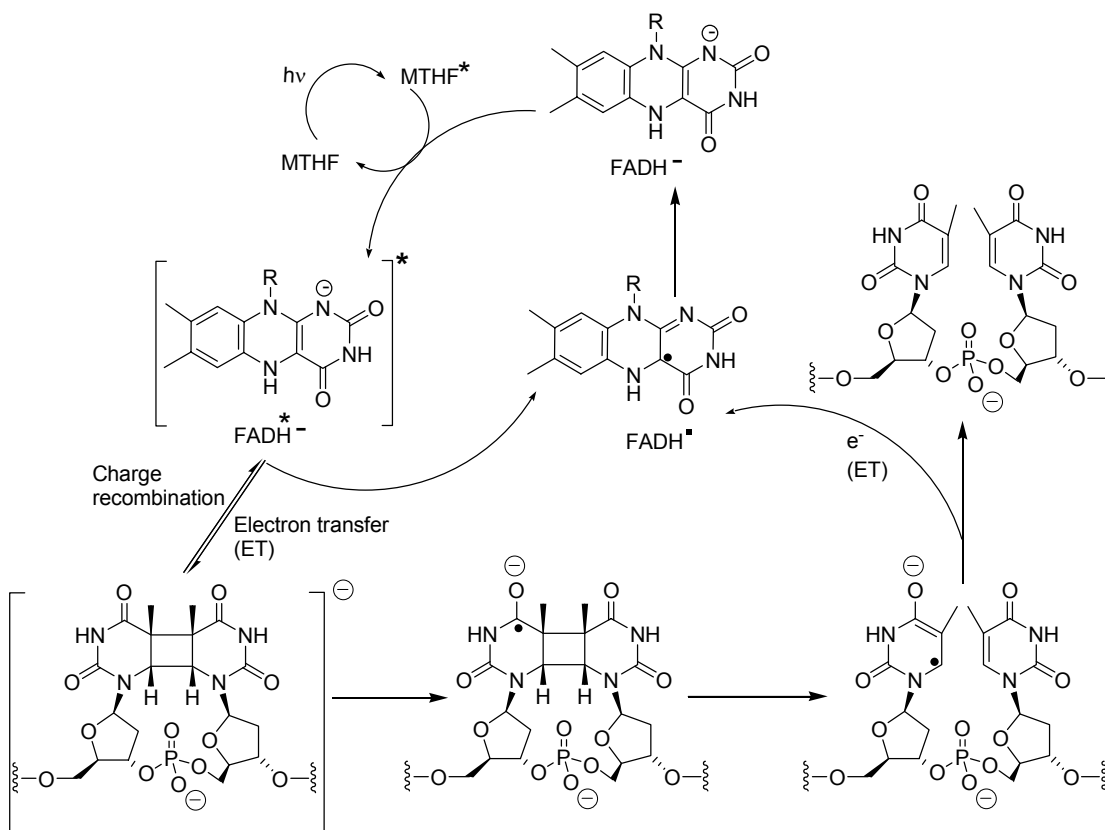


Figure 1.16: Electron transfer process and mechanism of photoinduced repair of *cis-syn* thymine-thymidine cyclobutane-pyrimidine dimer lesion (dTpdT-CPD) catalyzed by Photolyase. The cycloreversion is initiated by the fully reduced FADH cofactor which becomes activated through energy transfer from the second coenzyme such as MTHF.

1.5.2. Electron transfer mechanism between CPD and photolyase

Theoretical investigations on the DNA lesion-photolyase complex and the dimer-flavin electron transfer pathway have recently revealed that electron transfer to the CPD dimer occur from the fully reduced FADH *via* the adenine moiety, as adenine is presumably in close proximity to the lesion due to the rare U-shaped orientation of the flavin in photolyase.^[122, 123] Applying the DOCK 4.0 program to

a hypothetical DNA-photolyase complex, the study showed that the average distance between the dimer and the FADH⁻ can be as low as 3 Å,^[123] contradicting the other report suggesting a larger distance.^[124] This study also showed that electron transfer from the FADH⁻ to the dimer is not direct, rather an indirect process mediated by the adenine moiety of the FAD. Other studies of the dimer-photolyase complex using AMBER force field support a flipped-out conformation of the dimer lesion during recognition by photolyase and also suggest that the event is independent of DNA sequence.^[122]

Experimental studies have also been performed to investigate the electron transfer mechanism using synthetic model compounds by *Carell et al.*^[125] A systematic study with model compounds **1-4** (Figure 1.17) which contain a thymidine dimer-linked flavin moiety, has shown that deprotonation of flavin at N1 (pK_a = 6.5) is essential for dimer cleavage.^[126] No repair was observed at lower pH, with N1 of the flavin fully protonated. This investigation supports the necessity of fully reduced FADH⁻ during photolyase-derived dimer repair. Protonation at N1 would result in the FADH₂⁺-dimer⁻ charge-complex after electron transfer from neutral FADH₂ (see Figure 1.16), which would possibly undergo a fast charge recombination (backward reaction) that always competes with the dimer splitting process ($k_{\text{split}} = 2 \times 10^6 \text{ S}^{-1}$). Deprotonation at N1, on the other hand, would contribute a charge-shifted FADH-dimer⁻ complex which would reduce the charge recombination process, thus increasing the overall yield of dimer repair ($\Phi = 0.7-0.9$). Protonation of the dimer radical anion or hydrogen bonding had been suggested to accelerate the dimer cleavage.^[125, 127]

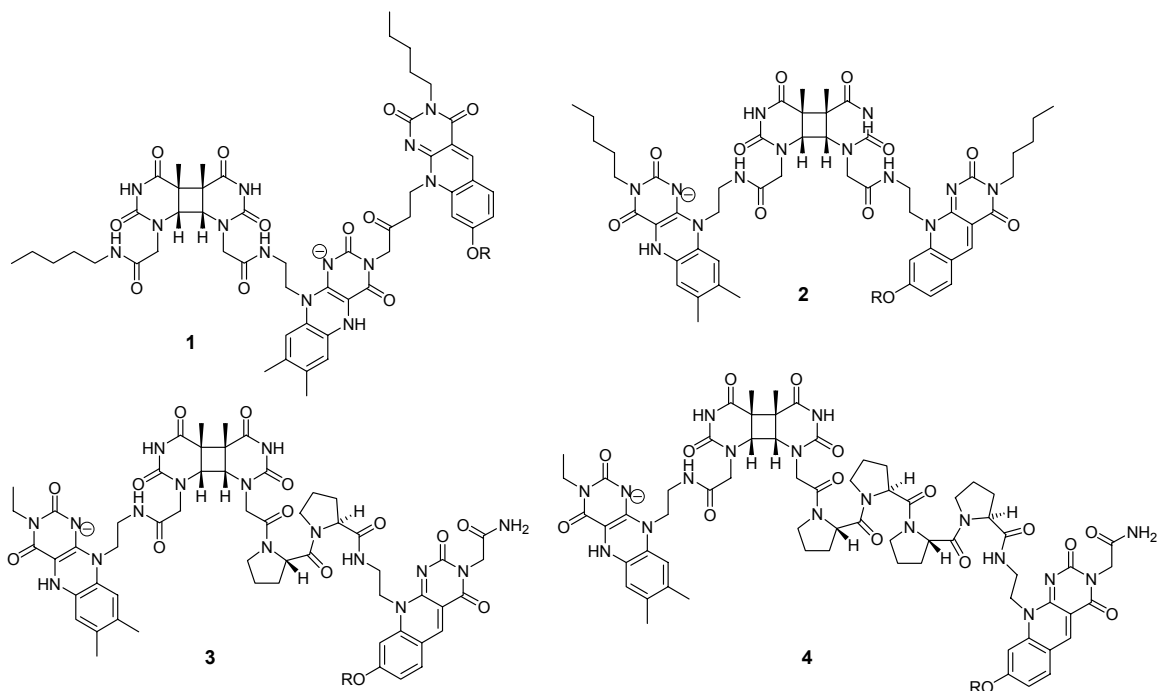


Figure 1.17: Model compounds **1-4** for the investigation of electron transfer and energy transfer phenomena in photolyase-catalyzed CPD repair. Model compounds **1-4** are covalently linked flavin-deazaflavin-thymine dimer systems. While the flavin-dimer separation is kept constant, the dimer-deazaflavin distance is increased systematically from **1** over **2** and **3** to **4**

1.5.3. Energy transfer between the cofactors

The non-covalently bound second cofactor (8-HDF or MTHF) serves as a photo-antenna for photolyase. The easily accessible long-wavelength radiation from sunlight is absorbed by these light-harvesting cofactors and is funnelled to the semi-reduced FADH[•].^[99] The incapability of FAD to absorb the most available long-wavelength light perhaps forced nature to select these auxiliary cofactors.

Since the energy transfer phenomenon is important for FAD activation, the relative separation between the cofactors should also play a role in this process, as, according to *Förster theory*, the rate of energy transfer (K_{EET}) is proportional to r^{-6} , where 'r' is the distance between the dipoles. The theory predicts that a short separation distance between the two cofactors will enhance energy transfer and hence dimer repair process. Model compounds **1-4** (Figure 1.17) with systematically varied FAD-deazaflavin distance, were carefully studied by *Epple et al.*^[128, 129], to address the energy transfer event. It was first being observed by *Deisenhofer et al.* that the large separation of the two cofactors in photolyase structure is difficult to rationalize considering *Förster theory*.^[112, 121] The model compounds **1-4** constituted of a flavin, a deazaflavin which is the second cofactor in Type-II photolyase and a photolyase substrate, the thymidine dimer (CPD). Keeping the flavin-dimer distance constant, the separation between flavin and deazaflavin was gradually increased from **1** to **4**. The investigation showed that a selective irradiation of deazaflavin by monochromatic light resulted in the most efficient dimer cleavage for the compound **4**, which has the largest cofactor-cofactor separation. The efficiency of dimer repair gradually decreases through **3** to **1**, although a systematic increase in fluorescence energy transfer rate was exhibited sequentially in that direction. This system is a reasonable mimic to photolyase structure and also supports the necessity for large cofactor separation in the protein, as observed by *Deisenhofer*^[112]. One explanation of this apparent anomaly is given by a possible 'short circuit' reaction which interferes with the dimer repair process. Figure 1.18 represents a schematic diagram of the possible electron transfer pathways from the activated and fully reduced FADH*.

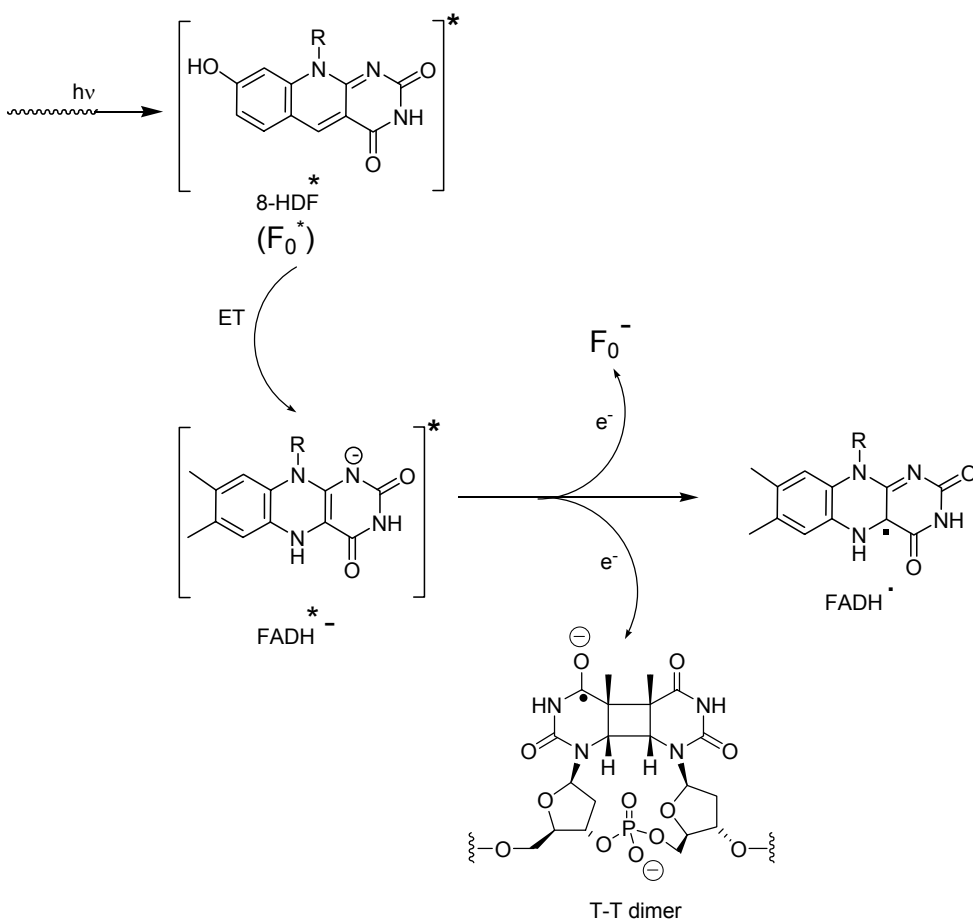


Figure 1.18: Mechanism of energy transfer from deazaflavin (F₀) to flavin coenzyme in *A. nidulans* photolyase. The photo-excited and fully reduced flavin effects an electron transfer either to the CPD-dimer lesion or back to the deazaflavin.

As demonstrated in Figure 1.18, the deazaflavin (F₀), due to its higher reduction potential than that of the CPD-dimer, is believed to serve as an alternative electron acceptor. The electron trap by the deazaflavin in this scenario competes with the electron transfer needed for dimer repair. The efficiency of this electron sink is clearly expected to increase with increasing proximity of the two cofactors.

1.5.4. *The photoactivation of FAD*

Flavin in the inactive form of photolyase exists in a semi reduced form as FADH[•]. Activation to the excited form FADH^{••} usually occurs due to excitation energy transfer (EET) from the second cofactor in presence of light (450-550 nm). The fully reduced, catalytic form FADH⁻ is obtained through one electron reduction with the participation of conserved amino acid residues in the active site of the protein. A study of the model compounds **1-4** showed that selective irradiation of deazaflavin strongly accelerates the reduction of the flavin chromophore in the presence of photoreductants such as EDTA. The photolytic reduction process involving flavin in both types of photolyases has been carefully investigated using time resolved absorption and electron paramagnetic resonance (EPR) spectroscopy.^[130-132] For *A. nidulans* photolyase a flash absorption spectroscopic study in the absence of deazaflavin has indicated that selective photoactivation of FADH[•] gives rise to the fully reduced form FADH⁻ in less than 500 ns, with a 7 ns laser flash.^[130] The reduction occurs by extraction of an electron from the neighboring tryptophan (TrpH) residue which is present in the active centre of photolyase (Figure **1.19a**). The resulting Trp[•] radical subsequently abstracts an electron from a tyrosine (TyrOH) residue with a half life of $t_{1/2} = 50 \mu\text{s}$, leaving behind a Tyr[•] radical which finally gets deactivated by an external electron donor, or reoxidizes the reduced flavin back to its inactive form, FADH[•]. The formation of the tyrosinyl radical was evident by time-resolved electron paramagnetic resonance spectroscopy.^[131]

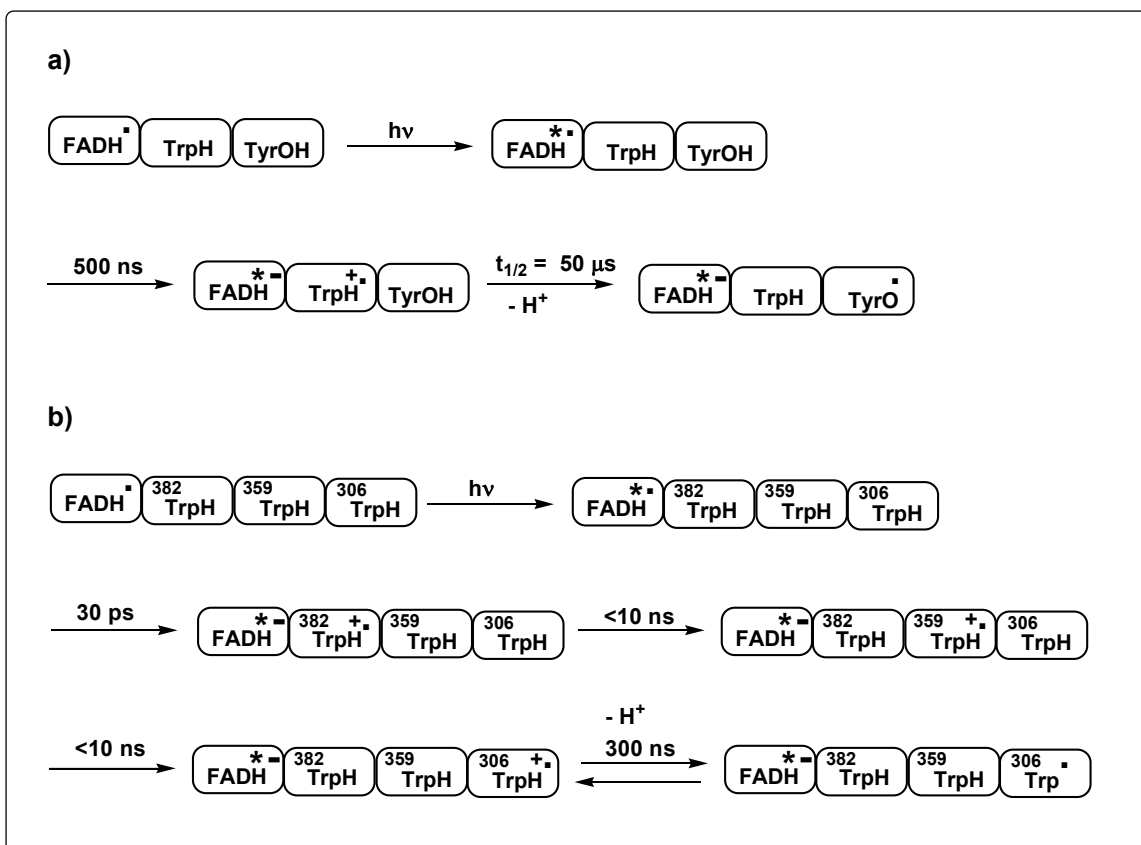


Figure 1.19: Radical transfer cascade for the photo-reduction of the FADH cofactor in Type-II photolyase (*A. nidulans*) and Type-I photolyase (*E. coli*). **a)** In Type-II photolyase, an electron transfer from a surface tyrosine (Tyr) residue *via* a tryptophan (Trp) residue causes reduction of the FADH radical to the two electron reduced form. **b)** In Type-I photolyase, the electron is donated by Trp₃₅₉ and Trp₃₈₂ residues to the semi-reduced FADH radical.

The photoactivation process of Type-I photolyase from *E. coli* was also investigated using short time spectroscopy.^[132-134] The data suggests involvement of a series of tryptophan residues in a multi-step radical transfer process (see Figure 1.19b). As with Type-II photolyase, the first electron abstraction by the excited FADH• occurs from a tryptophan (Trp₃₈₂) residue, resulting tryptophenyl

radical cation ($\text{TrpH}^{\bullet+}$). But this process is much faster (30 ps) than that of *A. nidulans* photolyase (500 ns). The radical transfer process propagates through two more steps involving Trp_{359} and Trp_{306} , each of which takes less than 10 ns to complete. The final deprotonation of the radical $\text{Trp}_{306}\text{H}^{\bullet+}$ to $\text{Trp}_{306}^{\bullet}$ which takes approximately 300 ns, seems to trap the radical at $\text{Trp}_{306}^{\bullet}$, positioned close to the surface of the protein. Deactivation of $\text{Trp}_{306}^{\bullet}$ takes place *via* electron abstraction from an exogenous electron source (e.g. reducing agent). The involvement and importance of Trp_{306} was proved by a site-specific mutagenic study, which showed that replacement of Trp_{306} by an alanine (Ala) residue prevents *E. coli* photolyase from being photoactivated. The tryptophan residues were understood to be properly aligned and the distances of each radical transfer step were calculated to be 4.2 Å, 5.2 Å and 3.9 Å respectively.^[135]

1.5.5. Photolyase-substrate co-crystal study

Although an extensive amount of theoretical work has been performed,^[122, 123] the lack of sufficient substrate prevented formation of a photolyase-substrate complex for structural studies. A photolyase-CPD complex structure has been elucidated recently by Mees *et al.*^[136] The co-crystal structure of *A. nidulans* photolyase in complex with a double-stranded DNA containing a synthetic thymidine dimer (CPD) with a formacetyl-bridge, in 1.8 Å resolution, has revealed plenty of information about the photolyase-substrate binding event (Figure 1.20). The CPD-lesion at the binding site has been found to be completely flipped out of the helical plane by about 50°, significantly higher than the theoretically predicted value (36°).^[137, 138]

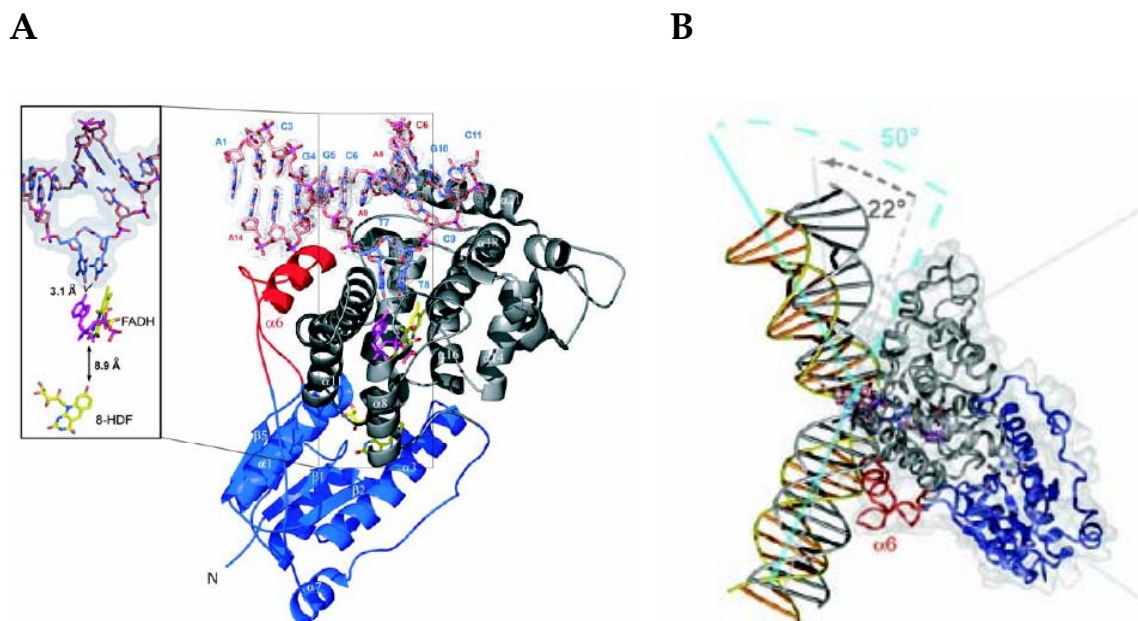


Figure 1.20: Co-crystal structure of a photolyase (*A. nidulans*) complexed with a DNA substrate in 1.8 Å resolution. The substrate DNA bears a synthetic, formacetyl-bridged *cis-syn* cyclobutane-thymine-thymidine dimer (CPD) which is recognized by the photolyase. **A)** The CPD lesion just after the cleavage in the active pocket of the photolyase. The thymidine dimer is highlighted in blue, the cofactors in yellow and the adenine moiety of the FAD in purple. **B)** The overall bend of the modeled DNA B-duplex with an internal CPD-lesion increased from about 22° (gray) to 50° on binding to the DNA polymerase (yellow)

1.5.6. (6-4) photolyases

The highly mutagenic (6-4)PP photoproducts and their Dewar isomeric lesions, in some organisms, are repaired by (6-4)-photolyases.^[139] Although a crystal structure of this protein has not yet been published, the strong sequence homology with CPD-photolyases suggests a similar catalytic pathway for both types of enzymes. The (6-4)-photolyase is known to possess a FAD cofactor as

with CPD-photolyase and possibly also a folate, as a second cofactor. Recently an EPR study of isolated (6-4)-photolyase from *X. laevis*, confirmed the involvement of a tyrosyl radical during the photoreactivation of the reduced FADH.^[140] A suggested repair mechanism of this enzyme is to proceed *via* conversion back to an oxetane intermediate, as depicted is Figure 1.21.^[141-143]

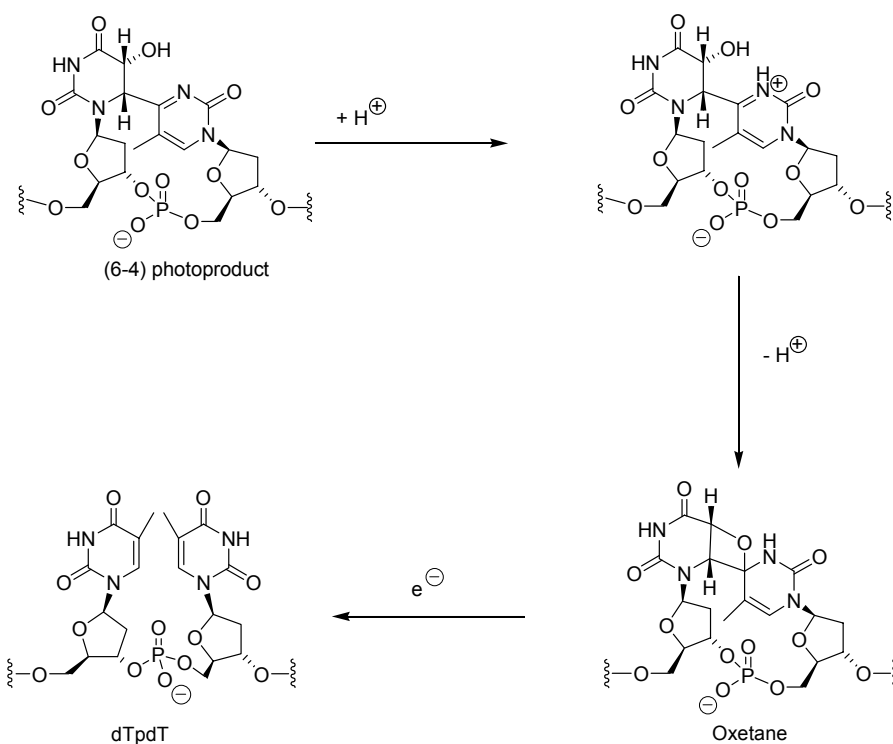


Figure 1.21: Proposed mechanism for the repair of (6-4)PP lesions by the (6-4) photolyase. The repair is believed to proceed *via* an oxetane intermediate.

1.6. **Molecular Beacons**

Detection of genetic and cellular disorders is a very important factor for successful disease diagnosis. Understanding the functions and malfunctions of genes and proteins at a molecular level occupies the majority of today's research and is a fast growing field. An extensive number of sophisticated techniques such as selective fluorescence labeling and DNA microchip arrays^[144-147] have already been developed for biomolecular recognition but there is still a strong demand for efficient techniques with high sensitivity and specificity.

Molecular beacons (MB) are excellent probes for target recognition and disease diagnosis, recently developed by *F. R. Kramer* and *S. Tyagi* in 1996.^[148-150] This technique has gained enormous popularity in the last 3-4 years and has a wide range of applications e.g. for the detection of single base mismatch,^[151-153] real time monitoring of PCR (RT-PCR),^[150] detection of DNA-RNA hybrid probes in real time,^[154] detection of pathogens^[155] and even as biosensors.^[156]

MB's are single stranded, hairpin shaped oligonucleotides with a stem-loop structure.^[149, 157] The loop of the hairpin is usually designed to serve as a probe region. The self-complementary stem contains a fluorophore at the 5'-end and a non-fluorescence quencher at the 3'-end as depicted in Figure 1.22. This fluorophore-quencher system serves as a molecular photo-switch.^[158, 159] In the absence of a target, the closed hairpin form turns the fluorescence 'off', whereas, recognition of the target will immediately switch the fluorescence 'on'. MB's are very sensitive and are extraordinarily target-specific. MB's are now used as probes for DNA and RNA detection in living cells and protein studies.^[160, 161]

1.6.1. Principles of MBs

MB's function as molecular switches, exploring the phenomenon of fluorescence resonance energy transfer (FRET).^[162] The extraordinary target-specificity of the MB's comes from their dual stability in both closed form (hairpin) and hybridized form (open) with the complementary target.^[163] The loop sequence of the MB is the functional part which is specific to the target, whereas the stem part remains un-engaged in molecular recognition. The self-complementary stem however, holds the closed structure of the MB and is responsible for signal transduction upon loop-target interaction. A schematic presentation of how a MB functions, is shown in Figure 1.22. In the hairpin conformation, the fluorophore is in close proximity to the quencher and efficient energy transfer occurs from the fluorophore to the quencher residue. This quencher molecule absorbs the fluorescence energy of the fluorophore, resulting in a loss of fluorescence signal, because the quencher moiety by itself is non-fluorescent.

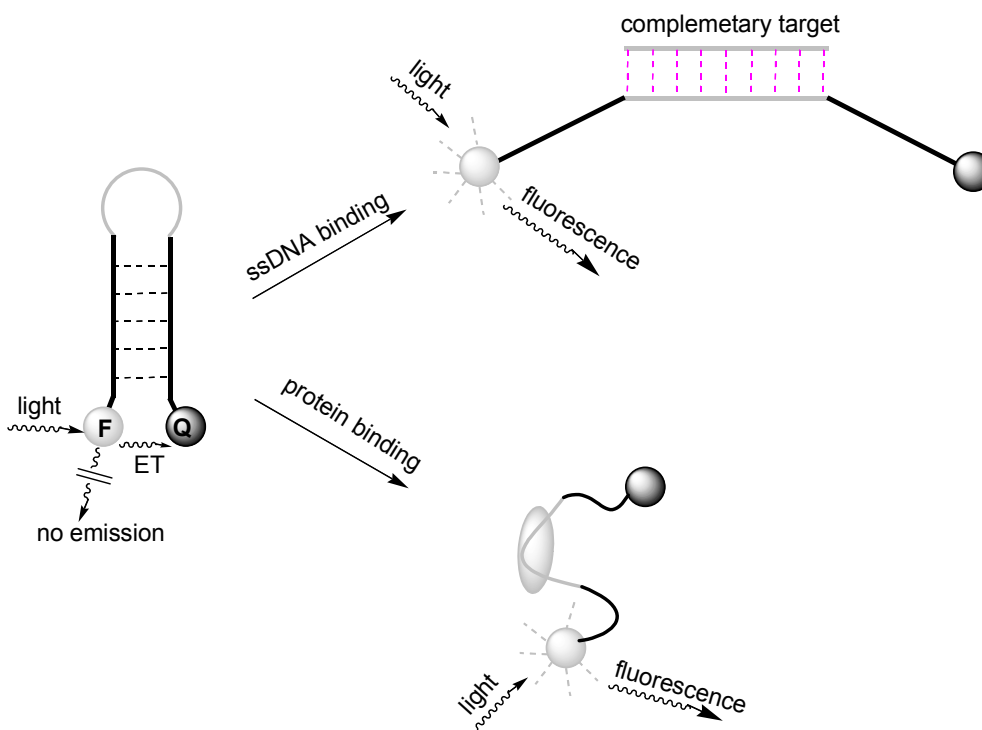


Figure 1.22: Basic principle of the molecular beacon (MB) as a sensitive probe. The figure describes opening of the MB structure upon hybridizing to a target DNA or on binding to a target protein. Opening of the hairpin results in loss of energy transfer from the fluorophore (FAM) to the quencher, thereby restoring the fluorescence of the FAM.

When the loop of the MB binds to a complementary sequence^[164-166] or a protein target,^[167, 168] the stem of the MB melts due to better loop-target interaction and consequently the fluorophore and the quencher falls apart (Figure 1.22), preventing energy transfer and thus restoring fluorescence. In the closed MB form, energy transfer can occur either *via* FRET,^[162] which requires spectral overlap between the fluorophore and the quencher, or *via* direct energy transfer.^[169, 170] Direct energy transfer occurs due to the formation of a transient charge-transfer complex between the fluorophore and the nearby quencher. It requires physical contacts of the two participating moieties. The quenching

results in a reduction of the emission of the fluorophore. A schematic presentation (*Jablonski* diagram) of FRET between a fluorophore and a dark-quencher is given in Figure 1.23.

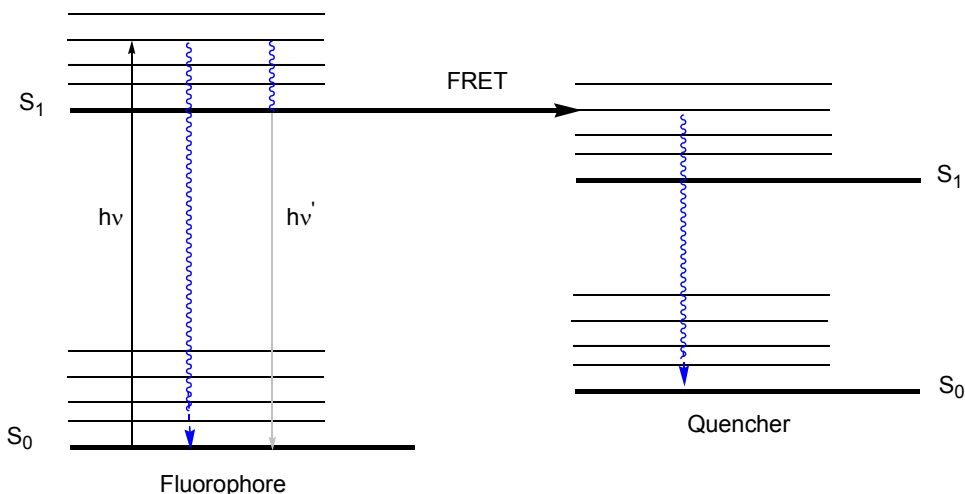


Figure 1.23: *Jablonski* diagram for FRET between a fluorophore and a non-fluorescent quencher. The black arrow represents excitation of the fluorophore to higher electronic state (S_1), squiggly line represents non-radiative relaxation to the ground state (S_0) and the gray arrow comprises for the radiative fluorescence emission.

FRET in a MB occurs within a spatial distance of 20-100 Å between the donor and the acceptor. The efficiency of FRET falls rapidly with increasing separation (r) of the two moieties.^[171] Energy transfer efficiency (%E) is given by the following equation:

$$\%E = \frac{R_0^6}{R_0^6 + r^6}$$

where R_0 is the average donor-acceptor distance when the energy transfer reaches 50% and is calculated from the equation:

$$R_0 = \frac{9.78 \cdot 10^3}{\left(n^{-4} \cdot f_d \cdot k^2 \cdot J \right)^6}$$

where n is the refractive index of the solution, f_d is the quantum yield of the donor (fluorophore), J is the overlap integral, which is the area of overlap between the emission spectrum of the fluorophore and the absorption spectrum of the quencher, k is called orientation factor of the two dipoles.

1.6.2. Designing molecular beacons

When designing a molecular beacon, an important factor to be considered is how to acquire the best sensitivity of the probe (high signal to background ratio). The length of the stem structure should be designed to be sufficiently strong to hold the duplex configuration. But at the same time, it has to be weak enough to be denatured upon binding to the target. A typical MB contains a loop sequence which is 15-40 nucleotides long, whereas the stem usually contains 5-7 nucleobases.^[149]

The design of a MB probe, specific to a target, is based on a number of parameters. The most important of which is the melting point study. Figure 1.24 shows a fluorescence-based melting point profile.^[172] The bottom-curve demonstrates the fluorescence change of a MB with rising temperature. At low temperature, the fluorophore and the quencher are in close contact, turning the fluorescence 'off', whereas at higher temperatures the stem of the MB denatures, resulting in a coiled structure and the turning 'on' of the fluorescence.

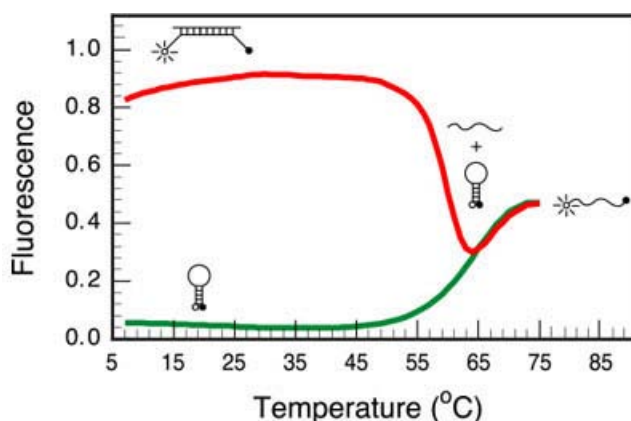


Figure 1.24: Designing molecular beacon on the basis of melting temperature study. The bottom-curve represents the melting curve of the MB on gradual heating, while the upper-curve shows the temperature dependent interaction of the MB with its complementary target DNA. While the MB-target hybrid predominates at low temperature, the relatively higher temperature favors the hairpin form to persist.^[172]

The upper-curve in Figure 1.24 shows a MB probe-target hybridization profile. The loop of the MB binds strongly with the target DNA below the melting point of the MB. However, as the temperature is increased the probe-target hybrid

gradually falls apart, causing the MB to fold back into the U-shape. In Figure 1.24 this temperature (55 °C) is the critical point. The MB assay in this case, should be performed below 55 °C to attain highest sensitivity.

Melting temperature study is very important for single mismatch detection using this MB technique. For this study the probe temperature is chosen as just slightly lower than the critical temperature. The target, with a single base mismatch, will not bind to the probe at this critical temperature because the probe-mismatch melting temperature will be slightly lower than the original probe-target hybrid.

1.6.3. *Kinetics and thermodynamics of MBs*

As described in section 1.6.1, a MB exists either in a folded hairpin (closed) or in a coiled (open) conformation.^[163] The equilibrium of this two state transition process is given by the following expression.^[173]

$$K_{\text{closed}} = \frac{k_{\text{closed}} \left[\text{open form} \right]}{k_{\text{open}} \left[\text{closed form} \right]}$$

$$\Delta G_{\text{closed}} = -RT \ln (K_{\text{closed}})$$

The stability of the closed state is determined by its lower enthalpy (high negative value), whereas the open conformation is sustained due to its higher

entropy (high positive value) which comes from the high degrees of freedom of the coiled form. It has been shown that the rate of opening of the hairpin form is governed by the supplied thermal energy or the amount of enthalpy gained upon probe-target hybrid formation. The rate of the opening strictly follows *Arrhenius* kinetics. The opening process of the hairpin is independent of the loop sequence and loop size. The rate of closing of the coiled form into the hairpin structure, however, deviates strongly from *Arrhenius* kinetics and is determined by both the entropy of the open form as well as the enthalpy of the closed state of the hairpin.^[174] Therefore the opening process of the MB is more regular than the closing phenomenon. The closing process also depends significantly on loop size and sequence.^[174] Hence it is always preferable to study MB-target kinetics on the basis of the opening of the MB rather than the closing process.

1.6.4. Surface immobilized MBs

This technique is used widely for molecular recognition and disease diagnosis. The MB, specific to a target, is first immobilized onto a solid support.^[164] The well-known biotin-avidin binding system is exploited for the immobilization process. The MB is synthesized with a biotin-linker which is able to recognize and bind to the avidin, immobilized on the surface of the solid support (Figure 1.25).

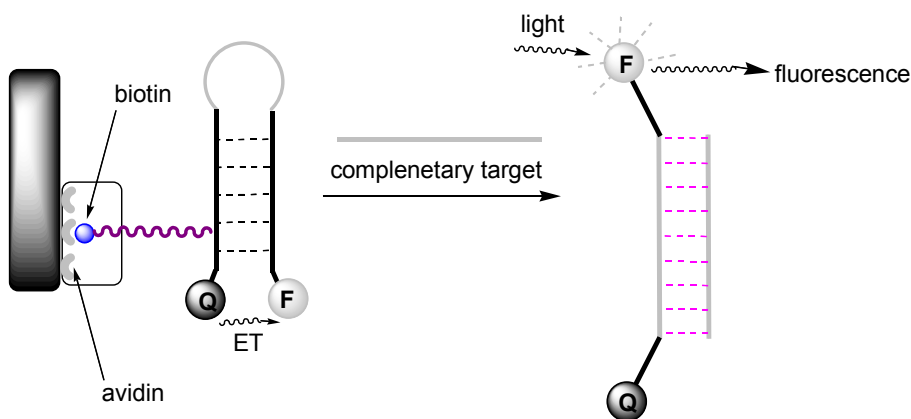


Figure 1.25: Surface immobilized molecular beacon technique. The non-fluorescent MB is immobilized on solid support (black box) *via* biotin-avidin interaction. Opening of the hairpin loop upon binding to the complementary target (gray bar), causes 5'-FAM which was non-fluorescent in MB to fluoresces.

It has been found that choosing the correct position of biotin in the MB stem is important. The biotin is usually positioned close to the quencher to avoid possible involvement in any energy transfer event with the fluorophore. The linker should be long enough to avoid any steric or chemical interactions between the biotin and the quencher molecule.^[149]

There are also other important MB-based surface techniques such as optical biosensors.^[144, 156, 175] The surface core of an optical fiber is exposed by a chemical etching process. An evanescent, generated out of the surface is used to excite the fluorophore of the MB which is immobilized onto the surface. This technique has been used to detect non-labeled DNA targets in real time with high sensitivity. The surface immobilized biotinylated MB's are also effective tools as multiple analyte biosensors.

1.6.5. **Applications of MBs**

Real time enzyme assay: molecular beacons are one of the most efficient probes to assay DNA-binding or DNA-cleaving enzyme activities.^[157, 167, 176, 177] Several enzymatic kinetics have been investigated using MB's as a probe. The protein functions can be studied efficiently in real time only by monitoring the fluorescence fluctuations.

The activities of DNA-cleaving enzymes^[178] and DNA-cleaving small molecules^[179] have also been investigated with high accuracy and sensitivity, using MB's as probes.

Single base mismatch detection: detection of a single base mismatch is of paramount importance in order to identify point mutations. MB's have proved to be excellent probes for detection of target DNA sequences which differ by a single nucleobases.^[153, 155, 166] Because of their high target sensitivity, MB's are currently used for single nucleotide polymorphism (SNP)^[180] and mutation detection assays.^[181] As described earlier, the designing of the probe MB is very important for this type of study.

Real-time monitoring of PCR: the most important and unique application of MB's is their potential to be used as real time probes for monitoring DNA/RNA amplification during PCR.^[151, 182-184] An excess of the MB probe is used for the experiment in a sealed PCR tube. The loop sequence of the MB-probe is complementary to a segment of the DNA/RNA sample of interest (amplicon). The fluorescence of the MB is measured at the annealing step of each cycle.^[149, 185]

The MB-amplicon hybrid is formed at the annealing temperature, resulting in an increase of MB-fluorescence. The MB-amplicon hybrid again denatures under PCR temperature, thus preventing the MB from interfering in the amplification process. The progress of the PCR reaction therefore, can be studied directly by monitoring the fluorescence increase of the MB. Recently, methods have been developed to monitor multiple PCR reactions simultaneously using an array of MB's. This multiplex assay is being widely used for detection of pathogens.^[186]

RNA detection in living cell: MB's are used to track the pathways of mRNAs in living cells.^[160, 187, 188] Cells transport mRNA from the transcription sites in the nucleus to the cytoplasm where they are translated into proteins. Nuclease resistant MB's which contain a loop sequence complementary to the mRNA of interest, have been explored to track the migration of the mRNA. The movement of the mRNA *in vivo* could be visualized by following the fluorescence of the MB, which is turned 'on' upon binding to the target mRNA.^[160] The change of transport pathway of the mRNA by employing genetic manipulation or chemical agents, has been found to alter the fluorescence distribution. This shows the sensitivity of the MB-probe to track mRNA transport process.

1.7. *Mass spectrometry for biomolecular analysis*

Mass spectrometry is a sensitive technique to detect the precise mass (and therefore its identity) of chemical compounds and biomolecules such as DNA, RNA and proteins. Recently, advanced mass spectrometric methods allowed studying proteomics and identification of genetic mutations, at very low concentrations.

In the present investigation to detect and characterize UV-induced DNA damages, an extensive amount of mass spectrometric analysis has been performed. Two kinds of mass ionizations were mainly used for the analysis: matrix assisted laser desorption ionization (MALDI-TOF) and electrospray ionization in combination with ion fragmentation (ESI-MS/MS).

Figure 1.26a shows a general skeleton of a modern mass spectrometer which primarily contains three components: an ion source, an ion analyzer and a detector. Mass spectrometers vary widely depending upon the principles of the analyzer and the detector.

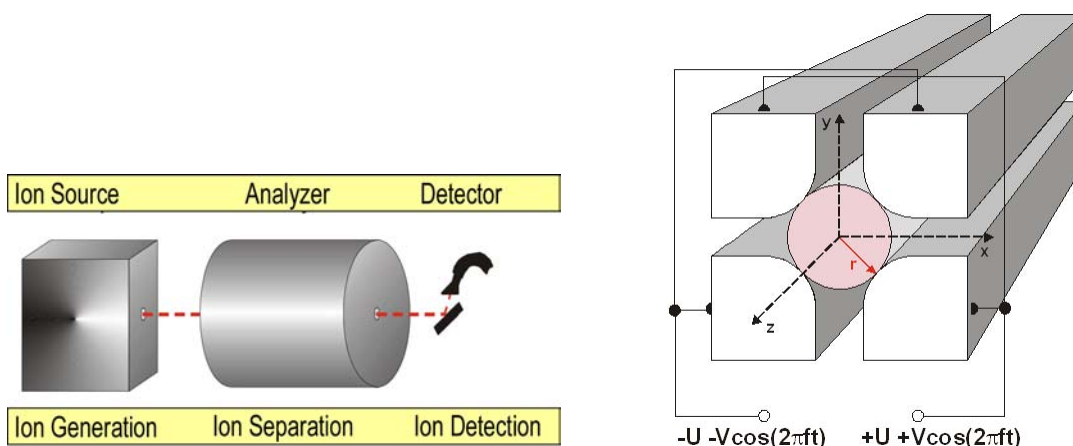


Figure 1.26: a) General principle of a mass spectrometer, b) depiction of a quadrupole in a Qstar i pulser MS/MS analyzer.

MALDI-TOF separates the ions based on their time of flight from the target containing the sample. The higher masses reach the detector later than the lower masses. In electro-spray ionization (ESI), the analyte, dissolved in a solvent, is allowed to pass through a channel where a high potential difference is applied and molecules become positively charged. A continuous flow of dry nitrogen evaporates the solvent to form small droplets of ions which subsequently undergo *Coulomb* explosion due to high charge density. The ions are then separated based on their relative velocities.

A mass fragmentation (MS/MS) technique is often employed to characterize the separated ions. For the work described here, a highly sensitive Qstar i pulser, quadrupole Time-of-Flight (TOF) mass spectrometer (Figure 1.27) was used which is capable of specific ion selection followed by its fragmentation and analysis using quadrupoles (see Figure 1.28).



Figure 1.27: Depiction of components of a mass spectrometer: **a)** Qstar pulser quadrupole mass analyzer, **b)** ion-spray source

The opposite rods of each quadrupole (Figure 1.26b) have same d.c. voltage. An a.c. voltage is overlaid in the second quadrupole (Q1) during the analysis. Depending on the frequency of the a.c. voltage, the second quadrupole can select only ions with a specific mass value (m/z) which migrates on a stable flight path. The mass selection, fragmentation and the detection of the ions by the quadrupoles is depicted in Figure 1.28.

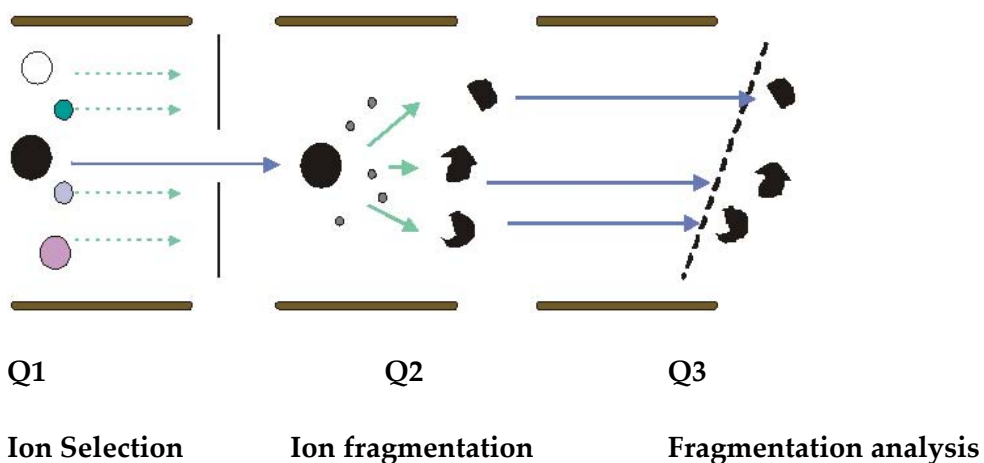


Figure 1.28: A schematic presentation of stepwise MS/MS analysis by the quadrupoles.

In the first quadrupole (Q0, not shown in Figure 1.28) collision occurs between the supplied gas and the analyte, due to a high applied potential. The ion selected by Q1 undergoes fragmentation in Q2, due to collision with the supplied nitrogen gas molecules. The fragmented ions are finally analyzed by the Q3 which is essentially a mass detector.

2. Aims of Research

The goal of this work was to investigate the formation and repair of UV-induced DNA-lesions. Understanding the effect of different chemical environments and conformations on DNA/RNA-damage formation event was a major focus of this research. Emphasis was made to establish efficient analytical methodologies for the separation, direct quantification and characterization of the photoproducts in DNA/RNA. In order to achieve this, short, hairpin-shaped oligonucleotides were chosen as probes. In order to attain highest sensitivity and accuracy of lesion quantification, these hairpins were labeled with a fluorescent molecule. DNA and RNA hairpins were chosen for comparative conformation-dependent studies.

Another major concern of this research was to investigate the mechanism of action of CPD-photolyase enzyme in repairing cyclobutane-thymidine dimers, and to develop methods that would yield information about the repair process in living cells. For this, efficient DNA-probes containing a synthetic CPD-lesion were designed, with the light-cycler molecular beacons (MB) strategy believed to be of use in these investigations. (Figure 2.1) This recently developed FRET-based technique is an efficient probe to study cellular processes. The CPD-lesion containing MB-probe has been strategically designed to induce DNA strand break after photolyase-catalyzed repair of the CPD-lesion.

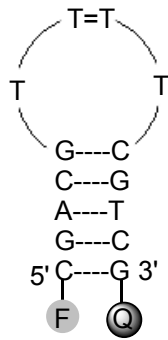


Figure 2.1: Molecular beacon (MB) substrate for photolyase-catalyzed CPD-lesion repair.

3. UV Induced Damage Formation Event

The UV-stimulated photoproduct formation and genomic damage is an important area of research to understand genomic mutation, aging and skin cancer. In the present context, the formation of various photoproducts has been studied under UVC radiation. Investigations of the UV-induced photodamage event have previously been performed but with cellular and/or chromosomal DNA irradiation,^[189-191] where the selective study of a particular dinucleotide in a particular region (and hence its environmental effect) was difficult to commence. In this investigation, a series of small DNA, RNA and/or DNA-RNA mixed hairpins were prepared. All the hairpins were labeled with 6-FAM fluorescence moiety at the 5'-end of the hairpins. These strategically employed fluorescence-labeled hairpin oligos have following advantages:

Hairpins possess a loop and a stem structure, the latter being self-complementary. The loop region of a hairpin acts as a single-stranded DNA whereas the stem part resembles a double-stranded oligonucleotide.^[48] Hence a comparative study of UVC induction on single and double stranded DNA or RNA could be performed. Hairpins are also rather small molecules which enabled us to determine the amount of photoproducts directly using HPLC.

The hairpin, although a short oligonucleotide, shows a high melting temperature and the melting is concentration independent.^[192-194] Hence a slight concentration difference among the probe solutions would not have much impact on damage formation event, provided the irradiation source is sufficiently powerful.

The hairpin, being self-complementary and having a high melting point, exists as a single entity in probe solution, without any concentration fluctuation. In contrast, a normal double-stranded oligonucleotide always imposes a concentration fluctuation of the two single-stranded entities, due to manual pipeting error or unsuccessful hybridization or both. Hence for a double-stranded DNA probe, at least three entities will co-exist in probe solution and an accurate damage analysis after UV irradiation could not be performed. The rate of photochemical reactions and the characteristics of the formed photoproducts from the free, unhybridized single stranded oligos might be very different compared to the hybridized double stranded probes, which is an important factor to be considered for such lesion analyses.

Advantages of 5'-FAM labeling are:

Labeling with a fluorescent molecule allows detection at a very low concentration level using fluorescence detector. Due to the concentration independent melting behavior of the hairpin, irradiation experiments performed at very low DNA concentration still generated a sufficient amount of UV-damaged lesions for direct analysis.

A dinucleotide after lesion formation loses its aromaticity and hence does not absorb as efficiently as individual bases at 260 or 280 nm.^[40] Hence accurate quantification of the photoproducts can not be performed on the basis of 260 or 280 nm UV-absorption. However, a precise measurement of photolesions can be achieved with a fluorescence detector which does not account for UV absorption. Moreover this fluorescent molecule does not interfere with the photoproduct formation.

Irradiation of small, fluorescence-labeled hairpins therefore, allowed direct measurements of the damage formation process. This is important because previously the lesions were quantified in an indirect way, back transferring the photoproducts into the monomers using enzymes like T4-endo V^[195] or DNA-photolyases.^[98, 112] However, the activities of these enzymes by themselves might be modulated by the sequence and structural context of the lesion.

All the DNA hairpins were constructed with 14 to 16 nucleotides as shown in Figure 3.1 (section 3.2) The hairpins contain a stem region of 5 to 6 nucleobase pairs, which is needed to form the necessary duplex structure. The loop is constructed either from four 2'-deoxycytidines, four 2'-deoxythymidines, four 2'-deoxyadenosines or from a C12 spacer. The 5'-end of the hairpins were labeled with 6-FAM. In order to avoid any possibility that this fluorescent moiety interferes with the lesion formation process, hairpin 5 and another hairpin, having a sequence as 5 but without the 5'-end-labeled FAM, were employed. Both solutions of equal concentrations were irradiated for 6 min under a 254 nm hand lamp (energy fluence rate 7 mW/cm²). The HPLC measurements of the probes showed exactly the same amount of damage (50%). This observation therefore showed that the FAM at the 5'-end, remains unreacted during UVC irradiation. However, it allowed detection of oligonucleotides even in very small quantities.

All the hairpins depicted in Figure 3.1 (section 3.2) were HPLC purified. The measured concentration of the stock solutions, observed mass (m/z) values, and their melting point are listed in Table 3.1.

Table 3.1: Tabulation of the observed molecular weights of hairpins 1-7, concentration of the stock solutions and their measured melting points (T_m)

Hairpin (5' to 3')	Observed m/z	Melting point (T_m)
1. FAM- <u>GCGCG</u> (CH ₂) ₁₂ <u>CGCGC</u>	3897	83 °C
2. FAM- <u>GCGCG</u> AAAA <u>CGCGC</u>	4821	78 °C
3. FAM- <u>GCGCG</u> CCCC <u>CGCGC</u>	4722	81 °C
4. FAM- <u>CATATG</u> CCCC <u>CATATG</u>	5339	52 °C
5. FAM- <u>GCGCG</u> TTTT <u>CGCGC</u>	4785	82 °C
6. FAM- <u>GTTTTG</u> AAAA <u>CAAAAC</u>	5435	50 °C
7. FAM- <u>CCCCC</u> AAAAA <u>GGGGG</u>	4821	77 °C

3.1. HPLC methodology

A new method of using HPLC (fluorescence detector, unless otherwise mentioned) for UVC induced photolesion detection was established in this study (for details see the experimental section). Photolesions that were produced after UVC irradiation of the oligonucleotides were directly analyzed by this method. This is for the first time an analytical separation method is established to separate the dimeric-lesions in an intact oligonucleotide from the undamaged oligonucleotide. A highly efficient ion-exchange SAX (1000-8) column was utilized for the separation of the damage-containing oligonucleotides from the undamaged ones. Since most of the photoproducts are dimers, which do not alter the number of negatively charged phosphate groups or establish a significant

polarity difference, they could not be detected directly with reversed-phase or other commonly employed HPLC columns. The SAX-column was found to be capable of and efficient in, quantifying the overall damage within an irradiated oligonucleotide. The separations were performed at pH~13 at room temperature ($T= 25\text{ }^{\circ}\text{C}$). These relatively harsh conditions were needed in order to denature the hairpins completely, especially those having a high G:C content. For the experiments the hairpins were dissolved in buffer of (150 mM sodium chloride, 10 mM Tris-HCl buffer, pH = 7.4). The concentration of the hairpins was kept as low as $0.2\text{ }\mu\text{M}$. The solutions, taken in a 2 mm fluorescence cuvette, were irradiated for 10 to 30 min at 254 nm ($\pm 10\text{ nm}$) inside a fluorimeter equipped with a single monochromator. During irradiation the temperature of the sample holder was kept constant at $10\text{ }^{\circ}\text{C}$. An aliquot of sample was taken out before and after irradiation and injected into the HPLC through an autosampler, with detection via a fluorescence detector (see experimental section).

Since FAM has an absorption maximum at 495 nm, the detector was set at an excitation wavelength of 495 nm and the emission was measured at 520 nm.

3.2. Lesion formation on the different of nucleobases

In order to test, using this direct method, which of the nucleobases are prone to UVC-induced lesion formation, single-stranded poly-dT, poly-dC, poly-dA and poly-dG oligonucleotides were irradiated for around 30 min at 254 nm. The observed damage formations, after HPLC analyses are listed in Table 3.2. Except for the oligo (FAM-TTTT-3'), all HPLC's were analyzed by SAX-column. The damage content of this short oligo was analyzed with a reversed-phase column

using a very flat gradient (see experimental section). The reverse phase HPLC analyses of all the other oligonucleotides listed in Table 3.1, were also performed, but no photolesions were identified.

Table 3.2: Depiction of the damage formation of the fluorescent (FAM) labeled single-stranded oligonucleotides under UVC light at 254 nm. Probe concentration = 0.2 μ M in buffer (150 mM NaCl, 10 mM Tris-HCl, pH = 7.4).

Oligonucleotides (5' to 3')	Time of irradiation (min)	Damage (%) at 254 nm
FAM-TTTTTTTTT	30	55
FAM-TTTT	30	36
FAM-CCCCC	30	0
FAM-AAAAAAAAA	60	0
FAM-GGGGGG	60	0

From Table 3.2 it can be understood that guanine and adenine are immune to UVC radiation, clearly supporting the established data that the pyrimidines and not the purine nucleobases are active targets under UVC light.^[196-198] Surprisingly, cytosine nucleobases were also found to be inert under UVC radiation in a single-stranded configuration under the chosen experimental conditions. This relatively new observation has been affirmed in the preceding experiments with hairpins. Only thymine, in a single stranded DNA-conformation, was found to be severely damaged under UVC, supporting the published data that thymine is most vulnerable site for photodamage.^[190]

In this work a systematic comparison was made between single-stranded and double-stranded oligonucleotide led damage formation, by comparing damage occurred in the loop and the stem structure of a hairpin, respectively. To this end hairpins 1-7 (Figure 3.1) were irradiated. Irradiation of hairpins 1-4 gave no detectable damage even after 1 hour of irradiation under UVC light (Table 3.3). The HPLC's of all four hairpins before and after irradiation were found to be unaltered (not shown).

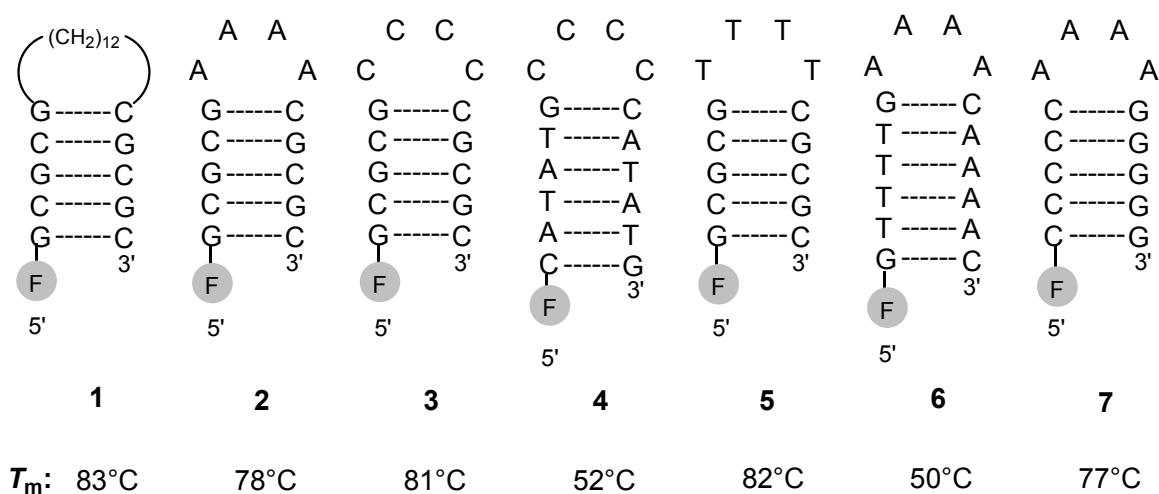


Figure 3.1: Depiction of the hairpins 1 - 7 prepared to study the reactivity of the various bases in the presence of UVC-light. F (6-FAM) = 5'-Fluorescein. Melting point (T_m) condition: $C_{\text{hairpin}} = 3 \mu\text{M}$ in buffer (150 mM NaCl, 10 mM Tris-HCl, pH = 7.4).

Hairpins 1 and 2, which both contain an alternate G:C duplex stem, were not expected to undergo a photo-reaction under UVC radiation, and were used in a control study. The loop of hairpin 1 contains a UV-unreactive C12 spacer, and that of hairpin 2 features four UVC-inert 2'-deoxyadenosines. The surprising

observation that hairpins **3** and **4**, both of which contain four 2'-deoxycytidines in the loop of the hairpins, remained undamaged under UVC irradiation affirms the result from poly-dC irradiation listed in Table **3.2**. This finding, that a poly-dC sequence in the single-stranded configuration remains undamaged to UVC light, was not previously known.

Any possibility of co-elution of the damaged hairpin with its undamaged counterpart was dismissed by further enzymatic digestion of the irradiated hairpins followed by mass spectrometric analysis described later in this section.

The efficiency of damage formation of the hairpins **1-7** is depicted in Table **3.3**.

Table 3.3: A comparative study of damage formation of the FAM labeled hairpins 1-7 after irradiation at 254 nm at 10 °C. Assay solution: hairpin concentration = 0.2 μ M in buffer (150 mM NaCl, 10 mM Tris-HCl, pH = 7.4). The amount of formed photoproducts was analyzed and quantified by analytical HPLC using SAX-column.

Hairpins (5' to 3')	Irradiation time (min)	Irradiation temperature (°C)	Damage (%)
1. FAM- <u>GCGCG</u> (CH ₂) ₁₂ <u>CGCGC</u>	30	10	0
2. FAM- <u>GCGCG</u> AAAA <u>CGCGC</u>	30	10	0
3. FAM- <u>GCGCG</u> CCCC <u>CGCGC</u>	30	10	0
4. FAM- <u>CATATG</u> CCCC <u>CATATG</u>	30	10	0
5. FAM- <u>GCGCG</u> TTTT <u>CGCGC</u>	20	10	32
6. FAM- <u>GTTTTG</u> AAAA <u>CAAAAC</u>	20	10	25
7. FAM- <u>CCCCC</u> AAAAA <u>GGGGG</u>	20	10	12

Unlike oligonucleotides 1-4, the hairpins 5-7 were found to be strongly degraded by UVC irradiation. Figure 3.2 shows chromatograms of all three hairpins before (bottom) and after (top) 20 min of irradiation at 254 nm. As can be evident from Figure 3.2, hairpins 5 and 6, both of which contain a short homo 2'-deoxythymidine sequence in the single-stranded loop and the duplex stem respectively, were found to be damaged significantly (32% and 25% respectively, after 20 min irradiation) confirming that thymine is the most sensitive target under UVC irradiation. The damage content of these two hairpins is comparable,

indicating that photoreaction of 2'-deoxythymidine is independent of oligonucleotide configuration or flexibility. Hairpin 7 which features a homo 2'-deoxycytidine duplex sequence, was also found to be degraded (12% after 20 min of irradiation), but to a much lesser extent compared to hairpins 5 and 6.

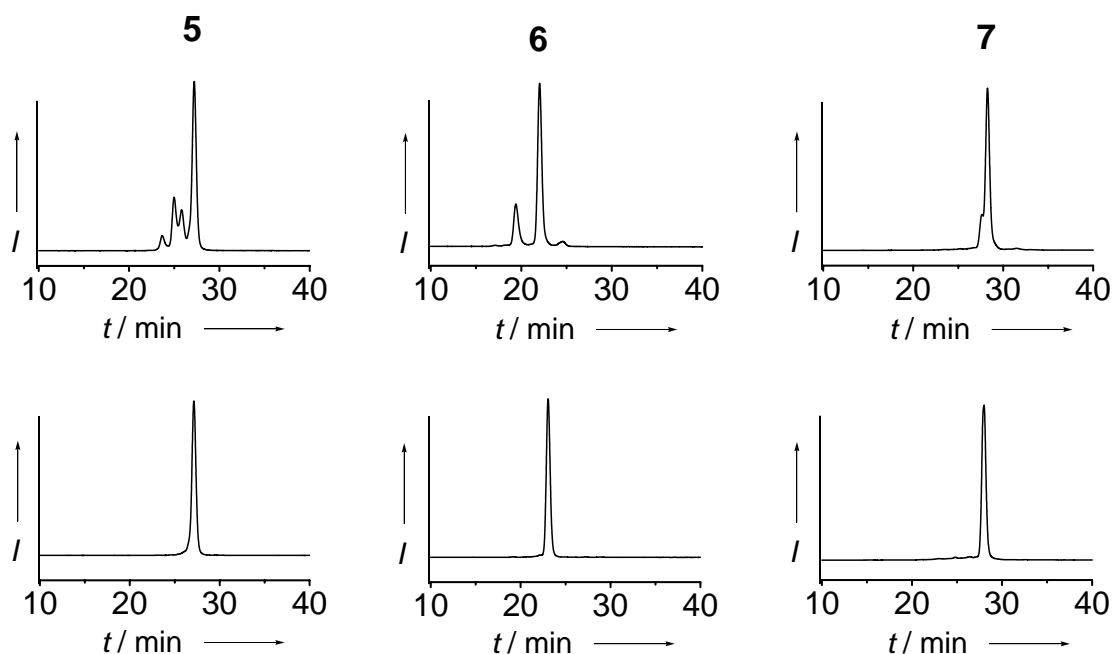


Figure 3.2: Depiction of the HPL-chromatograms before (bottom) and after (top) irradiation of hairpins 5, 6 and 7 with UVC light for 20 min. Assay solution: hairpin concentration = 0.2 μ M in buffer (150 mM NaCl, 10 mM Tris-HCl, pH = 7.4). λ_{irr} = 254 nm (\pm 10 nm), T = 20 $^{\circ}$ C. HPLC conditions: Nucleogel-SAX-column (1000-8); eluting buffers (buffer A: 0.2 M NaCl/0.01 M NaOH in H₂O, pH = 13; buffer B: 1 M NaCl/0.01 M NaOH in H₂O; pH = 13); Gradient: 0-75% B in 25 min and then up to 85% B in 35 min at a flow of 0.7 mL/min. t = retention time; I = relative fluorescence intensity.

Comparison of hairpin 7 with hairpins 3 and 4, which both gave no HPLC detectable photodamage, reveals that for a homo 2'-deoxycytidine sequence, a proper alignment of the two dC's is essential. The dCpdC dinucleotide in a well-organized duplex stem is just energetically fit for lesion formation, whereas a dCpdC dinucleotide in the loop/single stranded DNA sequence is poorly organized due to better flexibility. This pre-organization is probably not necessary for dTdT dinucleotides, resulting in a large amount of photolesions in both flexibly arranged single-stranded (5) and organized double-stranded (6) DNA under UVC light. Hairpin 4 was found to be undamaged by UVC light except for a very insignificant amount of dTpdA photolesions found only in mass spectrometric measurement. This result is interesting because it excludes any dTpdT lesion formation between the non-adjacent 2'-deoxythymidines, intervened by a 2'-deoxyadenosin, which is different from the early report with single strands.^[199] Under our irradiation conditions, inter-strand dTpdT lesions were not detected, contradicting what was previously observed by *Douki et al.*, that 2'-deoxythymidines present in opposite strands form cross-linked dTpdT photolesions under UV light.^[44] If at all, the formation of dTpdT photoproducts of non-adjacent 2'-deoxythymidines is of minor chemical significance and may require a much higher radiation dose.

3.3. Stability of the photoproducts under various pH conditions

Photoproducts are known to undergo degradation under highly basic conditions. *Cis-syn* and *trans-syn* dTpdT-CPD-lesions were reported to be converted into

their dicarboxylic acid salts when treated with 5-10 M sodium hydroxide at elevated temperatures.^[200-203] The (6-4)PP photoproduct and its Dewar valence isomer were also found to be unstable under these high alkaline conditions. In order to investigate whether the relatively alkaline condition (0.01 M NaOH, pH = 13) used in our chromatographic detection of the damage oligonucleotides interferes with precise lesion analysis, the stability of the damaged DNA hairpins was tested. For this, a very short, single-stranded oligonucleotide sequence [5'-TTTT-3'] was irradiated. A fraction of the probe was analyzed by ion-exchange chromatography at pH = 13 and another fraction by reversed-phase chromatography. Detection of damaged oligonucleotides using this reversed-phase column was possible only with a very short oligonucleotide such as that used, with a very flat gradient (C-18 column, *Nucleosil* 250*4 mm, 3 μ m; buffer A: 0.1 M AcOH/NEt₃ in water, pH = 7.0; buffer B: 0.1 M AcOH/NEt₃ in 80% acetonitrile, pH = 7.0; gradient: 0 to 30% B in 90 min). Both analytical methods produced the same result (30% damage after 20 min irradiation). This result was further strengthened with two other experiments. In one, the hairpin 6, which produced a significant amount of damage, was irradiated. One fraction of this sample was measured immediately after the irradiation using ion-exchange SAX-column and another fraction was injected into the HPLC after incubation for 1 hour in a buffer of pH = 13 (buffer A of SAX analysis was used). The obtained HPLC profiles were identical with an error margin of 1%, confirming that the chromatographic condition used for damage analysis was not harsh enough to degrade the formed lesions. In another experiment, an oligonucleotide hairpin containing a synthetic *cis-syn* thymidine dimer (dTdT-CPD-lesion, see Figure 4.2 for structure) which was site specifically incorporated (FAM-CGACGTXTCGTCG-3', where X= dTdT CPD-lesion), was incubated in SAX-A buffer for over an hour. The HPLC analysis showed no degradation of the CPD-

lesion. This observation together with the literature data, affirm the conclusion that the formed photolesions are stable under the HPLC conditions used for analysis.

3.4. Enzymatic digestion and lesion analysis

The HPLC profiles of the hairpins allowed precise quantification of the photoproducts. This technique, however, could not determine the identity of the lesions. In order to identify the produced damages, irradiated oligonucleotides were enzymatically digested following a method developed by Cadet *et al.*^[190, 204] This digestive system generates individual monomers and dinucleotide lesion dimers with a phosphate group (dNpdN lesion). The functions of the enzymes are briefly described below.

Nuclease P1 was used to hydrolyse double-stranded DNA (hairpins) into shorter fragments. It also removes the 3'-phosphate group from the nucleotides produced after action of calf spleen phosphodiesterase (phosphodiesterase II).

Phosphodiesterase II recognizes the 5'-hydroxy terminal of a nucleotide and releases the 3'-phosphomononucleotides.

Alkaline phosphatase cleaves the 5'-phosphate from DNA or RNA.

Phosphodiesterase I (snake venom) hydrolyses 5'-mononucleotides from 3'-hydroxy terminated DNA. The detail of this enzymatic digestion is described in the experimental section.

The dinucleotide lesions were separated from the individual monomers after the enzymatic digestion, by reversed-phase HPLC using a HDO column and the lesions were analyzed by HPLC coupled mass spectrometry (ESI-MS).

3.5. HPLC-ESI-MS for damage detection

In order to analyze which lesions were predominantly formed due to UVC irradiation, a short single-stranded oligonucleotide [5'-TTTT-3'] was irradiated and the solution was analyzed (without enzymatic digestion) by reversed-phase HPLC coupled to electrospray mass spectrometry (ESI-MS). All the new peaks obtained after irradiation (Figure 3.3) had the same molecular weight as the unirradiated oligonucleotide ($m/z = 1154$). This result is in full agreement with the formation of mainly CPD, (6-4)PP and its Dewar valence isomeric dTpdT lesions, all of which have the same molecular weight, indistinguishable from a dTpdT dinucleotide. In order to identify these photoproducts, further experiments were performed by total enzymatic digestion of the irradiated hairpins. First of all, a methodology was established for the separation of the individual nucleosides and the photoproducts. For this, unirradiated DNA hairpin **9** and a mixed DNA-RNA hairpin **16** were enzymatically digested.^[190, 204] Individual monomers were separated by a HDO column using a very slow gradient as described in the experimental section 5.2.1.10. The UV-detector of the

HPLC was set at 210 nm which is the absorption maximum of most of the dTpdT photoproducts. Samples were analyzed by coupling HPLC with a mass spectrometer (HPLC-ESI). Figure 3.4 depicts crude LCMS spectra of the unirradiated hairpins **9** and **16**. Both the LCMS spectra showed all the individual nucleosides from the DNA (**9**) and the RNA hairpin (**16**), characterized by their m/z values.

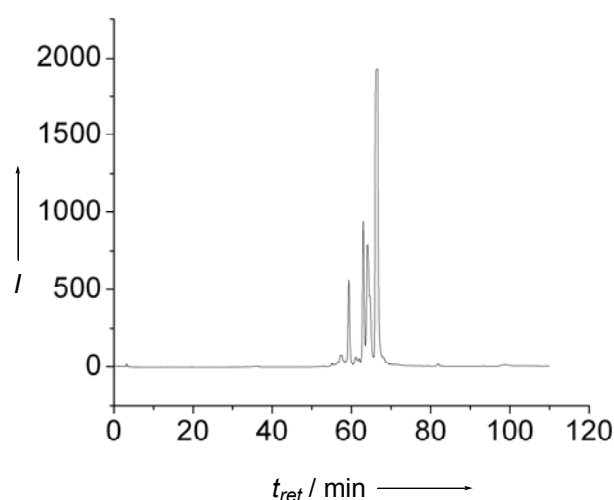


Figure 3.3: Reversed-phase HPLC separation and characterization of the photoproducts upon irradiation of a short single-stranded oligonucleotide [5'-TTTT-3']. Probe concentration = 0.2 μM in buffer (150 mM NaCl, 10 mM Tris-HCl, pH = 7.4). $\lambda_{\text{irr}} = 254 \text{ nm}$ ($\pm 10 \text{ nm}$), $T = 10 \text{ }^\circ\text{C}$. HPLC conditions: Nucleosill 120-3 C18 column; eluting buffers: A = 0.1 M AcOH/ NEt_3 in water, pH = 7.0, B = 0.1 M AcOH/ NEt_3 in 80% acetonitrile, pH = 7.0; Gradient: 0 to 30% B in 90 min. t_{ret} = retention time; t_{irr} = irradiation time; I = relative fluorescence intensity

For the identification of the photolesions, the UV-vulnerable hairpin **5** was irradiated at 254 nm and enzymatically digested. Figure 3.5 shows a LCMS

spectrum of the irradiated hairpin **5** followed by enzymatic digestion. It should be noted from Figure **3.5**, that the presence of photoproducts could not be identified from the LCMS spectrum, due to their very low yield compared to the individual nucleosides. However a thorough scan over the LCMS spectrum (ion-extraction) revealed new peaks compared to the non-irradiated reference spectrum. All the new peaks had masses (m/z) of 545, the mass of dTpdT photoproducts. Hence it can be concluded from the LCMS spectrum, that irradiation of hairpin **5** yielded only the dimeric dTpdT photolesions. A selective extraction of ions with $m/z = 545$ is shown in the subset of Figure **3.5**.

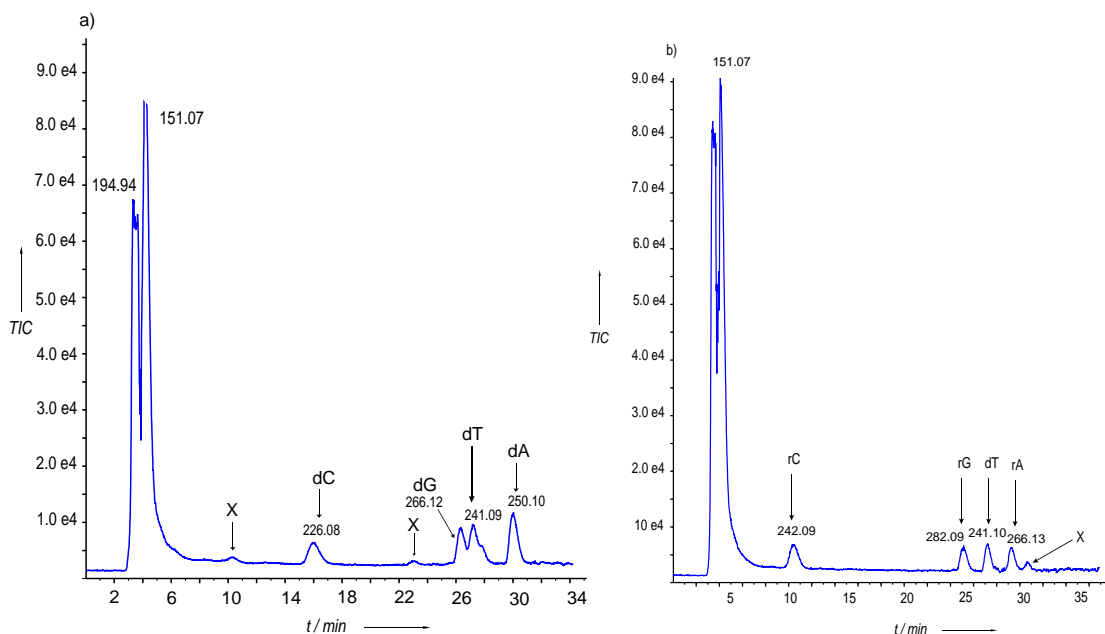


Figure 3.4: LCMS analysis of the digested DNA hairpin **9** (a) and the DNA-RNA mixed hairpin **16** (b). The chromatograms show all the individual DNA and RNA monomers. X = unknown peaks. HPLC condition: *Uptisphere 3 HDO* column (150*2.1 mm), eluting buffers: A = 2 mM AcOH/NEt₃ in water, pH 7.0, B = 2 mM AcOH/NEt₃ in 80% acetonitrile, pH 7.0; Gradient: 0-3% B in 12 min and then up to 20% B in 30 min.

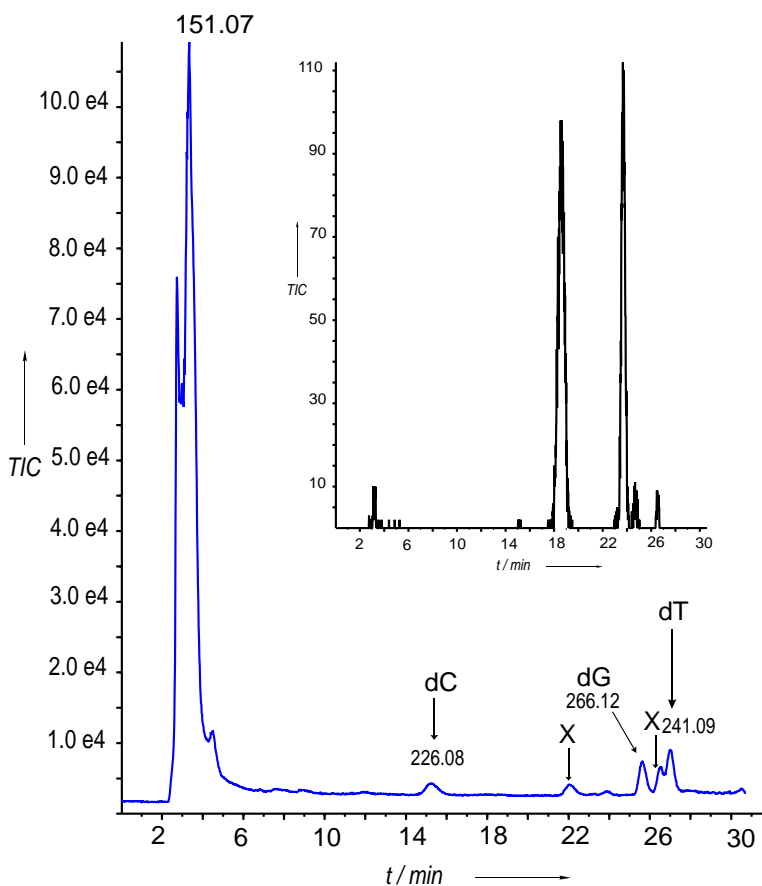


Figure 3.5: LCMS analysis of the irradiated and digested DNA hairpin 5. X = unrecognized peaks, might also contain dimer lesions. The subset shows all the new peaks obtained after ion-extraction at $m/z = 545.0$ to 545.2 .

3.6. Characterization of photoproducts by HPLC-ESI-MS/MS

The characterization of the photoproducts was performed by mass spectrometry using ion selection followed by further fragmentation of the ions (MS/MS). With this method ions of a particular m/z value were selected by the first quadrupole followed by fragmentation of each ion by the second quadrupole. For hairpin 6, the first quadrupole was set $m/z = 545$, the mass of dimeric dTpdT lesions. Part of

the chromatogram obtained after HPLC-ESI-MS/MS is presented in Figure 3.6. The assigned peaks correspond to the dTpdT photoproducts. The non-assigned peaks are unspecific with no characteristic fragmentations and were also present in the control experiment with non-irradiated hairpin 6. These peaks might be due to a dTpdT dinucleotide, which might have arisen from incomplete digestion.

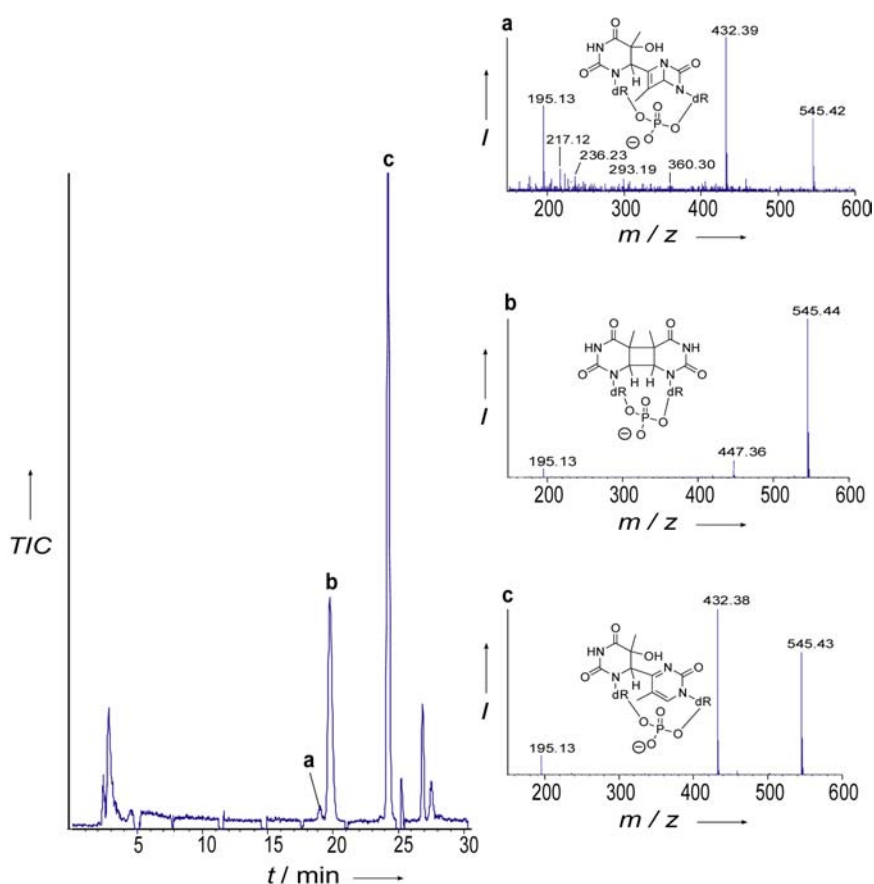


Figure 3.6: Depiction of the HPLC-MS/MS data obtained for hairpin 6 after irradiation and complete digestion. The insets show the fragmentation pattern of the detected lesions. The first quadrupole (Q1) was set to $m/z = 545$, and the fragmentation was measured in a mass range of 150 - 600 amu. The polarity was set to the negative ion

mode. **a**: dTpdT Dewar photoproduct, **b**: dTpdT *cis-syn*-CPD, **c**: dTpdT-(6-4)PP lesion; dR: 2-deoxyribose, *t* = retention time, *TIC* = total ion current, *I* = relative signal intensity.

The insets of Figure 3.6 represent the fragmentation pattern of the assigned peaks. The photoproducts were identified by this characteristic fragmentation pattern. At 19 min, a compound (signal **a**) was detected with a fragmentation pattern reported as that of Dewar valence dTpdT photoproduct. The fragmentation of the peak at 20 min (signal **b**) was found to be identical with the reported fragmentation of CPD-dTpdT lesion. At approximately 24.5 min a new peak was obtained which had a fragmentation matching that of the (6-4)PP dTpdT lesion (signal **c**). All these structural assignments were performed on the basis of elution time and fragmentation pattern of the lesions following the published data of *Cadet et al.*^[49, 190, 205] The characteristic fragmentations are briefly discussed bellow.

Abbreviation: dR = deoxyribose; dRp = deoxyribose phosphate.

Dewar dTpdT: 195 [dRp]⁻, 217 [bases-H₂O-OH-H]⁻, 236 [bases-OH]⁻, 293 [dRpdR]⁻, **432** (uncharacterized)

CPD dTpdT: 195 [dRp]⁻, **447** [CPD dTpdT-dR]⁻

(6-4) dTpdT: 195 [dRp]⁻, 217 [bases-H₂O-OH-H]⁻, 236 [bases-OH]⁻, 293 [dRpdR]⁻, **432** (uncharacterized)

It might be noteworthy to observe that (6-4)PP and its Dewar valence dTpdT lesion showed similar fragmentation patterns. These two lesions were

differentiated by their relative elution time from the column. The Dewar isomer, reported to be more polar than the (6-4)PP lesion, was assigned to the faster eluting peak.

Similar results were obtained from the irradiation and digestion of the hairpin 5, containing four 2'-deoxythymidine residues in the hairpin loop. The HPLC-ESI-MS/MS showed only CPD, (6-4)PP and Dewar valence dTpdT lesions with their characteristics fragmentations.

In order to analyze the damage sustained by the C-rich hairpin 7, similar HPLC-ESI-MS/MS experiments were performed. Hairpin 7 was irradiated under UVC light and was enzymatically digested as above. The sample was analyzed by LCMS and MS/MS. For MS/MS, the first quadrupole was set at $m/z = 515$ in low resolution. The resolution was kept low deliberately, to detect ions in the range of 515 (dCpdC dimeric lesions) to 516 (dUpdC lesions). The dCpdC lesions were found to undergo fast deamination into their corresponding 2'-deoxyuridine photoproducts.^[49] A parallel reference experiment was always performed with unirradiated hairpin 7. The obtained chromatogram together with the fragmentations of the assigned peaks is shown in Figure 3.7.

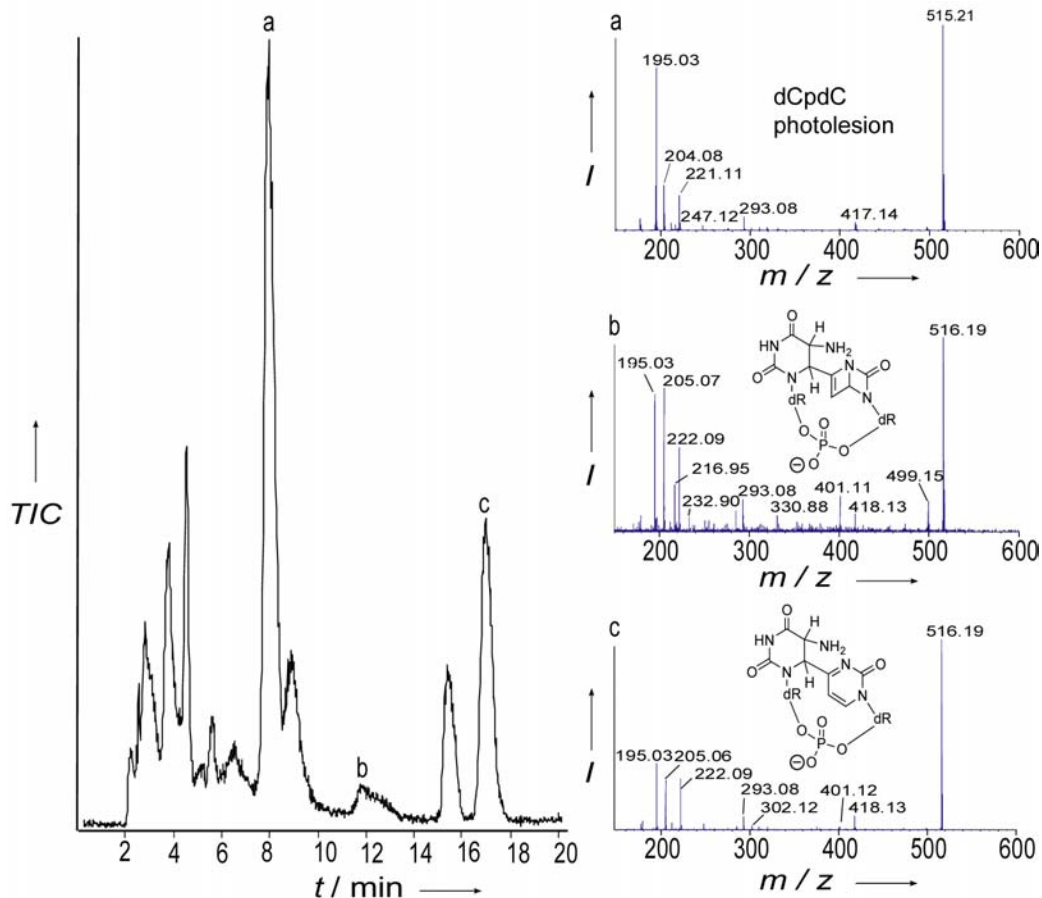


Figure 3.7: Depiction of the HPLC-MS/MS data of hairpin 7 after irradiation and complete digestion. The insets show the fragmentation pattern of the detected lesions. The first quadrupole (Q1) was set to $m/z = 515$, and the TOF range was chosen from 150 - 600 amu. The polarity was set to the negative ion mode. a: dCpdC photolesion, b: dUpdC-Dewar valence isomer, c: dUpdC-(6-4) lesion, dR: 2-deoxyribose, t = retention time, TIC = total ion current, I = relative signal intensity. (The structures of the photoproducts were drawn in accordance with literature data)

As can be seen, the peak obtained between 8 and 9 min (signal **a**), showed a mass (m/z) of 515, which is the mass of a dCpdC dinucleotide and that of other dimeric

photolesions. The fragmentation pattern proved these lesions to be CPD dCpdC lesion: **417** [CPD dCpdC-dR]⁻, 195 [dRp]⁻

At retention times of 12 and 17 min, peaks were observed with masses of (*m/z*) 516. These lesions should correspond to the dUpdC lesions. The fragmentation of signal **b** was found to match with the characteristic fragmentation of Dewar valence dUpdC lesion. The fragmentation of signal **c** was found to be similar compared to peak **b**. The higher elution time of this lesion was the basis to assign it as the (6-4)PP dUpdC photoproduct.

Abbreviation: dR = deoxyribose; dRp = deoxyribose phosphate.

Dewar dUpdC: 195 [dRP]⁻, 205 [bases-NH₃-H]⁻, **418** [dUpdC-dR]⁻, **401** [dUpdC-dR-NH₂-H]⁻

(6-4) dUpdC: 195 [dRP]⁻, 205 [bases-NH₃-H]⁻, **418** [dUpdC-dR]⁻, **401** [dUpdC-dR-NH₂-H]⁻

The MS/MS measurement was also performed with the irradiated hairpin **7**, setting the detector at a precise mass (*m/z*) of 517, the mass of dUpdU lesions, which might have formed due to fast deamination of both cytosines from dCpdC lesions. All the three kinds of lesions *i.e.* dUpdU CPD, (6-4)PP dUpdU and its Dewar valence isomer, were clearly detected and characterized from their fragmentation pattern.

From the MS/MS experiments it can be concluded that irradiation of hairpins **5** and **6** under UVC light leads to the formation of CPD, (6-4) and Dewar valence

dTpdT photolesions, whereas hairpin 7 produces the commonly formed dCpdC, dUpdC and dUpdU photoproducts.

In order to prove that the damaged peaks obtained during direct ion-exchange HPLC analysis of the irradiated hairpins were indeed due to the above photoproducts, two experiments were performed. Firstly, the damaged hairpins, after irradiation of 5, 6, and 7, were isolated using analytical ion-exchange chromatography (SAX-column). The fractions were desalted and enzymatically digested. HPLC-MS (followed by ion-extraction) and HPLC-MS/MS experiments showed all the usual dTpdT and dCpdC lesions, confirming that the hairpin degradation was indeed due to photoproduct formation. The undamaged oligonucleotides were also isolated from the ion-exchange HPLC and treated similarly. Here, however, no lesions were found, which excludes any possibility of co-elution of the damaged products with the undamaged ones.

Similar experiments were performed with hairpins 1-4, which did not give any damage under UVC light. The hairpins were enzymatically digested after irradiation and HPLC-MS was performed followed by ion-extraction. No lesions were found for hairpins 1-3, confirming that no co-elution occurred. In the case of hairpin 4, which contains an alternating A:T sequence, however, a very small amount of new peaks were observed in the HPLC-MS (followed by ion extraction). More careful analysis of these peaks by HPLC-MS/MS confirmed these compounds to be dTpdA photoproducts, which support previous observations by Zhao *et al.*^[206] These damages were not visible during ion-exchange HPLC analysis due to their very low quantum yield.

In order to search for the presence of any other photoproducts apart from the commonly observed ones, thorough scans of HPLC-MS chromatograms were performed, using a sensitive ion-extraction method. This method allows the user

to search for new peaks with specific a mass value (m/z) and several masses can be checked from a single HPLC-MS run. Many kinds of hypothetical photolesions were searched including hydration and oxidation products of thymine and cytosines. However, neither these reported lesions nor any new photoproduct was found, indicating that they were either not formed under our irradiation conditions or under UVC light in general.

The mass spectroscopic analysis confirmed that detection and quantification of the damaged photoproducts using this newly established ion-exchange chromatographic method is indeed a good measure of the total amount of the UVC induced photoproducts.

3.7. Dose-dependence study

UVC-mediated photochemical reactions of the nucleobases are reversible processes. Photoproducts were found to undergo cyclo-reversions at 254 nm into the respective monomers.^[207] The relative dose of the irradiation source, therefore, should have a strong impact on the overall yield of the photoproducts. Hence under the experimental irradiation conditions, the lesion formations should be consistent and linearly dose-dependent, to acquire precise comparison of the damage formation obtained from the hairpins irradiation. This was confirmed by irradiation of the UVC-vulnerable hairpin 6 for increasing periods of time. A plot of the amount of degradation, quantified by HPLC, against the irradiation time is shown in Figure 3.8. Up to as long as 30 min irradiation, the damage formation process was found to depend linearly on the dose of UVC

light under our conditions (see experimental section). From 40 min onwards, the damage formation starts to deviate from linearity (not shown in Figure 3.8) due to the reversibility of the UV damage formation process. Hence only the amount of DNA damage formed up to 30 min of irradiation were considered.

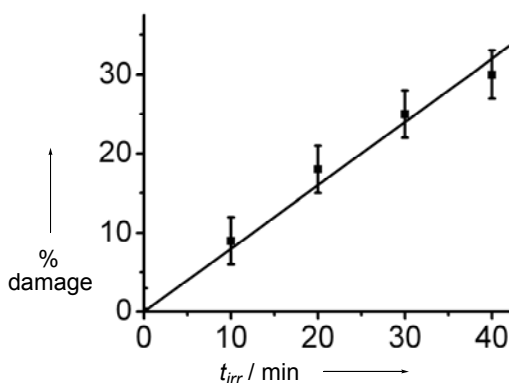


Figure 3.8: Dose-dependence of the lesion formation process measured by irradiation of hairpin 6 at 254 nm. Assay solution: $C_{\text{hairpin}} = 0.2 \mu\text{M}$ in buffer (150 mM NaCl, 10 mM Tris-HCl, pH = 7.4). $\lambda_{irr} = 254 \text{ nm}$ ($\pm 10 \text{ nm}$), $T = 20 \text{ }^\circ\text{C}$. HPLC conditions: Nucleogel-SAX-column (1000-8); eluting buffers (buffer A: 0.2 M NaCl/0.01 M NaOH in H_2O , pH = 13; buffer B: 1 M NaCl/0.01 M NaOH in H_2O ; pH = 13); Gradient: 0-75% B in 25 min and then up to 85% B in 35 min at a flow of 0.7 mL/min. t_{irr} = irradiation time.

3.8. Sequence context

Under UVC conditions, only 2'-deoxythymidines and well-paired 2'-deoxycytidines were found to be degraded into photoproducts. Since genomic DNA's were found to be non-homogeneously damaged under UV light,^[208] the

neighboring nucleotides might have some effect on photoproduct formation. Although a few studies have been performed to understand this environmental effect,^[209-211] a lack of efficient methodology has left plenty of space for further investigations. In order to rationalize how the nearest neighbors participate in damage formation, oligonucleotide hairpins **8-15** were implemented. All these hairpins, shown in Figure **3.9**, contain a UVC-reactive dTpdT dinucleotide in various sequential environments in the stem structure of the DNA hairpins.

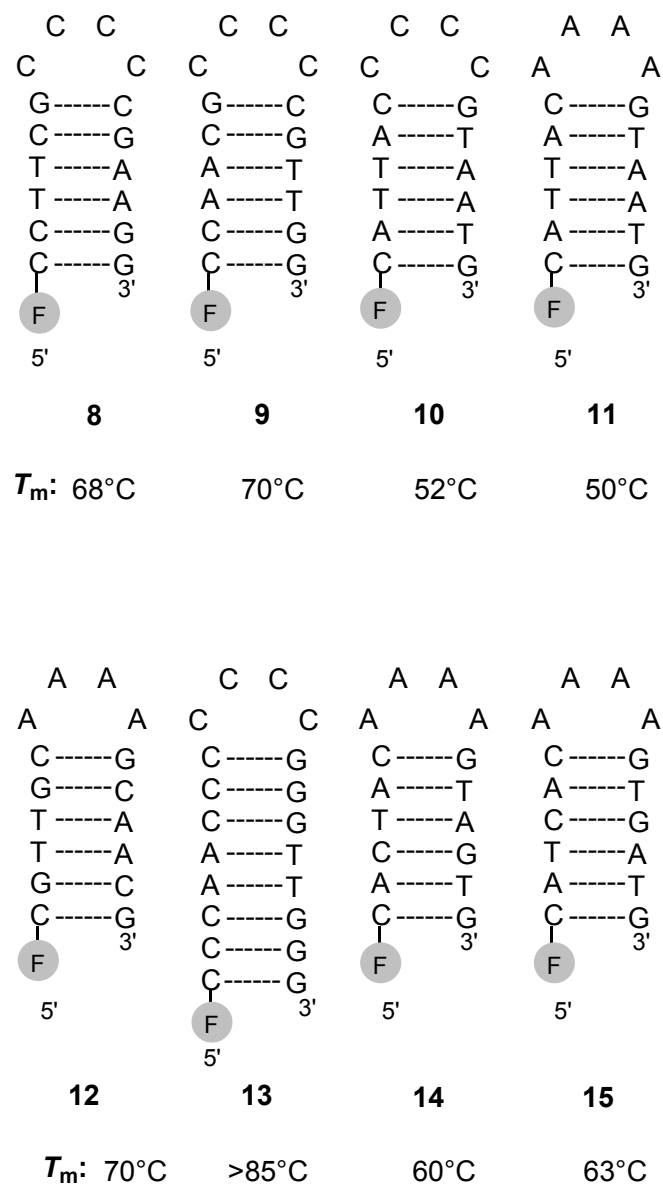


Figure 3.9: Depiction of the eight hairpin molecules **8 - 15** analyzed in order to assess how the nearest neighbors influence the UV lesion formation process in a dTpdT-dinucleotide sequence. F: (6-FAM) = 5'-Fluorescein. Melting point (T_m) condition: $C_{\text{hairpin}} = 3 \mu\text{M}$ in buffer (150 mM NaCl, 10 mM Tris-HCl, pH = 7.4)

All these hairpins were characterized by their molecular weights which were measured by MALDI-TOF. Concentrations and melting points were measured (depicted in Table 3.4) using a UV-spectrometer. The high melting temperature of the hairpins confirmed the duplex structure at room temperature.

Table 3.4: Tabulation of the observed molecular weights of hairpins 8-15, concentration of the stock solutions and their measured melting points (T_m)

Hairpins (5' to 3')	Observed molecular mass (m/z)	Melting point (T_m)
8. FAM- <u>CCTTCG</u> CCCC <u>CGAAGG</u>	5341	68 °C
9. FAM- <u>CCAACG</u> CCCC <u>CGTTGG</u>	5340	70 °C
10. FAM- <u>CATTAC</u> CCCC <u>GTAATG</u>	5359 [M+Na] ⁺	52 °C
11. FAM- <u>CATTAC</u> AAAA <u>GTAATG</u>	5433	50 °C
12. FAM- <u>CGTTGC</u> AAAA <u>GCAACG</u>	5434	70 °C
13. FAM- <u>CCCAACCC</u> CCCC <u>GGGTTGGG</u>	6577	>85 °C
14. FAM- <u>CACTAC</u> AAAA <u>GTAGTG</u>	5436	60 °C
15. FAM- <u>CATCAC</u> AAAA <u>GTGATG</u>	5436	63 °C

All of these hairpins 8-15 were irradiated with UVC light at 254 nm in a cuvette inside a fluorimeter, at a constant temperature of 10 °C. The efficiency of damage formation of these hairpins is summarized in Table 3.5. The damaged hairpins were separated by ion-exchange (SAX-column) HPLC and detected with a

fluorescence detector. The chromatographic profiles of the hairpins **8-10** before (bottom) and after (top) irradiation for 30 min are shown in Figure **3.10**.

Table 3.5: A comparative study of damage formation of the FAM labeled hairpins **8-15** after irradiation at 254 nm at 10 °C. Assay solution: hairpin concentration = 0.2 μ M in buffer (150 mM NaCl, 10 mM Tris-HCl, pH = 7.4). The photoproduct containing DNA was separated and quantified by analytical HPLC using SAX-column.

Hairpins (5'-3')	Irradiation time (min)	Temperature (°C)	Damage (%)
8. FAM- <u>CCTTCG</u> CCCC <u>CGAAGG</u>	30	10	40
9. FAM- <u>CCAACG</u> CCCC <u>CGTTGG</u>	30	10	< 3
10. FAM- <u>CATTAC</u> CCCC <u>GTAATG</u>	30	10	20-25
11. FAM- <u>CATTAC</u> AAAA <u>GTAATG</u>	30	10	20-25
12. FAM- <u>CGTTGC</u> AAAA <u>GCAACG</u>	30	10	< 2-3
13. FAM- <u>CCCAACCC</u> CCCC <u>GGGTTGGG</u>	30	10	3-4
14. FAM- <u>CACTAC</u> AAAA <u>GTAGTG</u>	35	10	25
15. FAM- <u>CATCAC</u> AAAA <u>GTGATG</u>	35	10	35

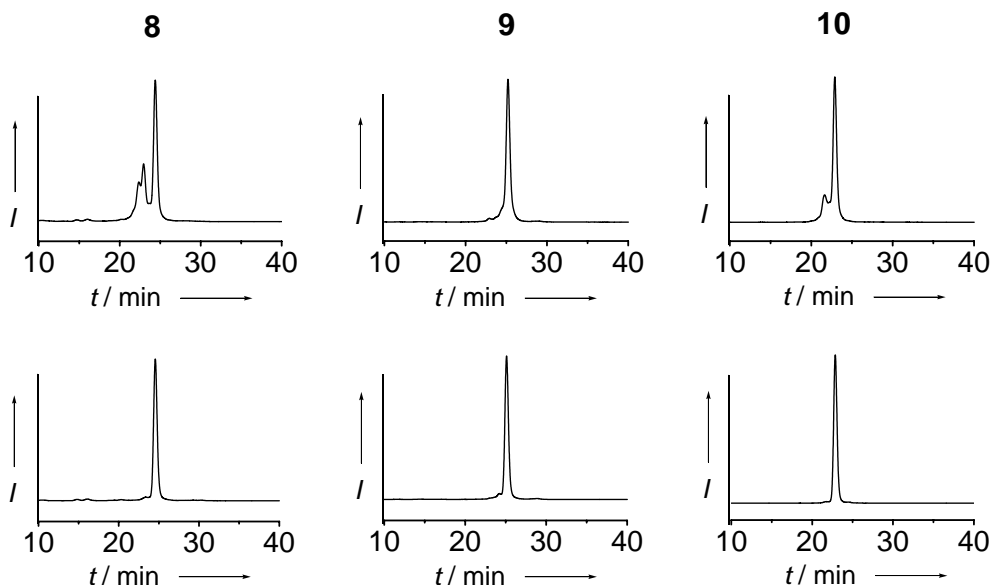


Figure 3.10: HPL chromatograms of the hairpin molecules **8**, **9** and **10** before (bottom) and after (top) irradiation with UVC light (254 nm) for about 30 min. Assay solution: $c_{\text{hairpin}} = 0.2 \mu\text{M}$ in buffer (150 mM NaCl, 10 mM Tris-HCl, pH = 7.4). $\lambda_{\text{irr}} = 254 \text{ nm}$ ($\pm 10 \text{ nm}$), $T = 20 \text{ }^\circ\text{C}$. HPLC conditions: Nucleogel-SAX-column (1000-8); eluting buffers (buffer A: 0.2 M NaCl/0.01 M NaOH in H_2O , pH = 13; buffer B: 1 M NaCl/0.01 M NaOH in H_2O ; pH = 13); Gradient: 0-75% B in 25 min and then up to 85% B in 35 min at a flow of 0.7 mL/min. t = retention time; I = fluorescence intensity.

From the chromatograms it can be interpreted that the neighboring nucleotides play an important role in dTpdT photodamage. The damage formation was severe for hairpin **8**, where a dTpdT dinucleotide is flanked by two 2'-deoxycytidine residues. Approximately 40% of the hairpin damage was observed with this hairpin, after 30 min irradiation. The high occurrence of lesions in this hairpin could be due to formation of dTpdT and dTpdC (or dCpdT) photoproducts. In this hairpin the 2'-deoxythymidines can react not only with one another but also with the neighboring 2'-deoxycytidines, making this (5'-

CTTC-3') stem-sequence highly vulnerable to UVC light. In hairpin **10**, on the other hand, the dTpdT dinucleotide is flanked by two 2'-deoxyadenosines. Since it has been shown in the previous section that 2'-deoxyadenosines were not found to undergo UVC degradation, except for a very small amount of dTpdA photolesion formation, hairpin **10** was not found to be as reactive as hairpin **8**. Here, about 20-25% damage was estimated from the chromatogram, mainly due to sole formation of dTpdT photoproducts. Similar amounts of degradation were observed from hairpin **11**, where the loop sequence of the hairpin was changed from (dC)₄ (as in hairpin **10**) into (dA)₄. Comparing the photoreactivities of hairpin **10** and **11**, it can be stated that degradation of hairpin **10** does not depend on the loop structure of the hairpin: the observed damage was formed in the stem structure. Hairpin **9** features a dTpdT dinucleotide sandwiched between two 2'-deoxyguanosines. Irradiation of this hairpin for more than 30 min, surprisingly, yielded almost no damage. This data was confirmed by irradiation and subsequent HPLC analysis of the hairpin **12** which also contains a dTpdT dinucleotide between two neighboring 2'-deoxyguanosines. Hardly any photodamage of **12** could be identified even after prolonged irradiation. When the number of G:C base pairs in both 3' and 5' directions were increased in the neighborhood of dTpdT dinucleotide as in hairpin **13**, the large protective effect of the guanines continued.

Hence it can be concluded that neighboring nucleobases play an important role during photoreaction of UVC-sensitive dTpdT dinucleotides. 2'-deoxythymidines locked between 2'-deoxyguanosine residues appear to be shielded most. This observation shows that our genome will be inhomogeneously damaged under such UVC light. So photo-induced damage formation and hence

mutation frequency will vary from genome to genome due to their different sequential environments.

The reason for this neighboring group participation can be explained by considering the flexibility of the duplex hairpin and the energetics of the photoproduct formation process. 2'-deoxyguanosin residues, in the neighborhood of a dTpdT dinucleotide, has better stability than dA residues. Hence, neighboring dG:dC base pairs offer more local rigidity than dA:dT base pairs. It's well known that a dTpdT dimer, after its formation, induces a local DNA distortion. The dTpdT dinucleotide, locked between two nearby 2'-deoxyguanosines, may require higher activation energy to react in order to undergo photoproducts formation.

The photoreactivity of dTpdC dinucleotides was also investigated using the direct HPLC-analysis method. For this, hairpins **14**, with a 5'-dCpdT-3' sequence and **15**, with a 5'-dTpdC-3' sequence were used (see Figure 3.9). The hairpins were irradiated for about 35 min under identical conditions as above. The HPLC analyses of these two hairpins yielded about 25% damage formation for hairpin **14** (5'-dCpdT-3'), whereas almost 35% degradation (Table 3.5) was detected from hairpin **15** (5'-dTpdC-3'). The result that 5'-dT in a dTpdC dinucleotide is more UVC-reactive than 3'-dT, supports earlier observation by *Douki et al.*^[49] The explanation of this higher reactivity of 5'-dT is given by the better compatibility of the methyl group of the 5'-dT in a dTpdC dimer into the duplex DNA.

In order to again characterize the types of photolesions formed in this sequence context, all the hairpins **8-15** were again irradiated at 254 nm using the hand lamp (see experimental section) and enzymatically digested as described earlier

in section 3.4. The digested solutions were separated with HPLC and the lesions were identified by ESI-MS and ESI-MS/MS coupled to HPLC. A systematic scan over the ESI-MS spectrum followed by ion extraction revealed the dimeric lesions of dTpdT and dTpdC/dCpdT for hairpins 8, 10, 11, 14 and 15. No oxidation or hydration products were detected. However, very small amount dTpdA photoproducts were obtained along with dTpdT lesions in the HPLC-MS followed by ion extraction for hairpins 10 and 11. These dTpdA photolesions were not detectable in HPLC analysis. The mass spectrometric analysis showed no lesion formation for hairpins 9, 12 and 13, supporting the results obtained from HPLC profiles (see Figure 3.10 and Table 3.5) and rules out any co-elution of the damage photoproducts with the undamaged ones during HPLC profiling. The ESI-MS/MS spectra obtained from the hairpin 8 is shown in Figure 3.11 and 3.12. Here the detector was, in one experiment, set at a mass (m/z) of 530 to detect dTpdC photoproducts (Figure 3.11) and in another, the mass (m/z) value of 545 was chosen to identify the dTpdT induced photoproducts (Figure 3.12). The fragmentations of the new peaks compare to the control experiments are shown in insets.^[51] The fragmentation analysis of Figure 3.11 resulted Dewar valence and (6-4)PP photolesions of a dTpdC dinucleotide. Detection at $m/z = 531$ also yielded characteristic lesions of dUpdT dinucleotides. The dU resulted from fast deamination of dCpdT photoproducts. Figure 3.12 again shows all the major dTpdT photoproducts with identical fragmentation pattern as in Figure 3.6 from hairpin 6.

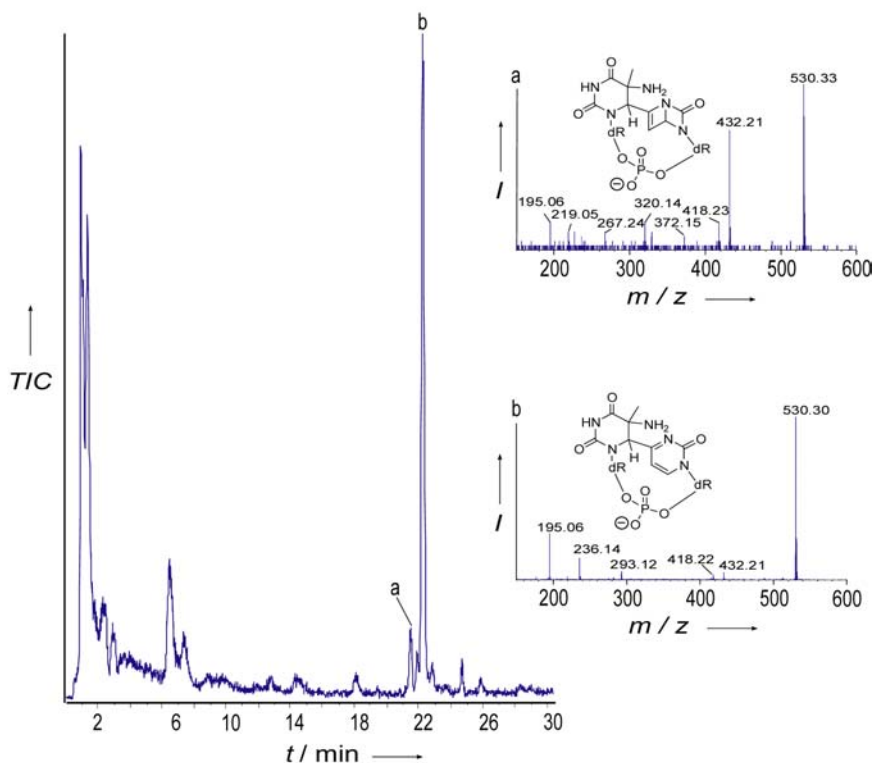


Figure 3.11: HPLC-MS/MS experiment at $m/z = 530$ after digestion of irradiated hairpin **10**. The insets show the fragmentation pattern. The first quadrupole (Q1) was set to $m/z = 530$, and the TOF range was chosen from 150 - 600 amu. The polarity was set to the negative ion mode. Peaks **a** and **b**: dTpdC derived photo lesions, t = retention time, TIC = total ion current, I = relative signal intensity.

For irradiated hairpin **10**, the detector was set at $m/z = 545$ and all three dTpdT photolesions, the CPD, (6-4)PP and its Dewar valence isomer were characterized.

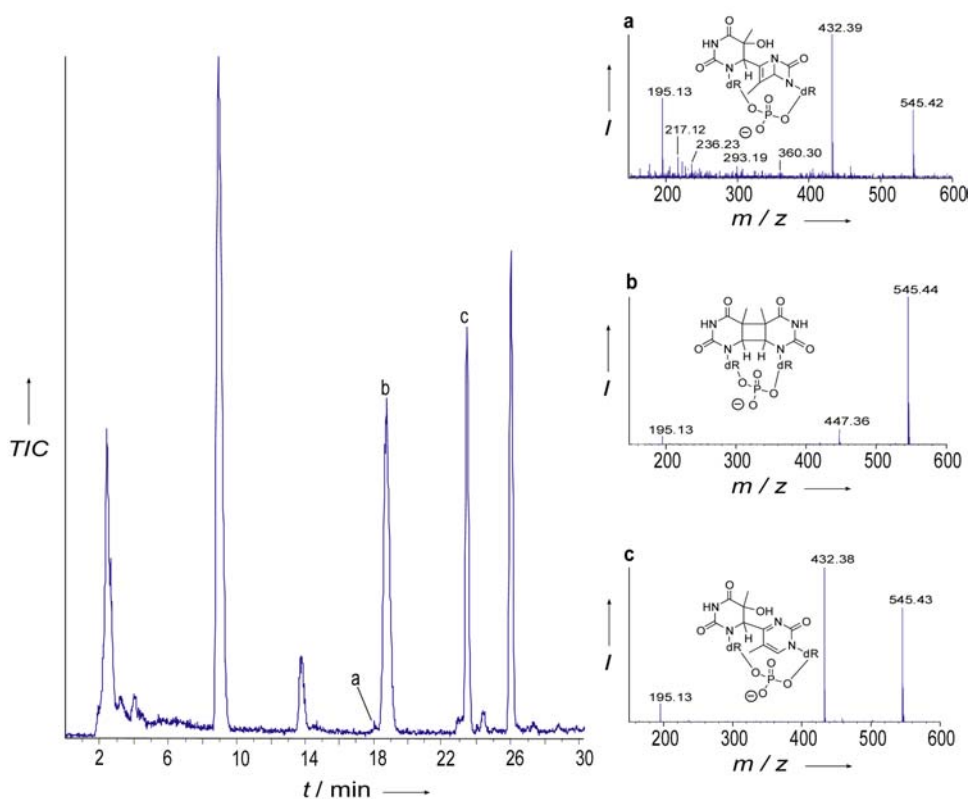


Figure 3.12: HPLC-MS/MS experiment at $m/z = 545$ after the digestion of irradiated hairpin **16**. The first quadrupole (Q1) was set to $m/z = 545$, and the TOF range was chosen from 150 - 600 amu. The polarity was set to the negative ion mode. **a:** dTpdT Dewar photoproduct, **b:** dTpdT-CPD, **c:** dTpdT-(6-4)PP lesion. dR: 2-deoxyribose, t = retention time TIC = total ion current, I = relative signal intensity. For the fragmentation pattern see Figure 5.

Irradiated hairpin **10** also yielded some dTpdA photoproducts when the mass detector was set at $m/z = 553$. However, the analysis of the fragmentation pattern is still open to interpretation due to lack of model compounds.

3.9. Conformation-dependence on photoproduct formation

The poly-dC's arranged in a single-stranded DNA were seen to behave differently under UVC light than a well-organized double-stranded hairpin DNA. The neighboring nucleotides are also understood to have a significant influence on the photoproduct formation. These observations indicate that the overall conformation of an oligonucleotide might also have a considerable impact on photoreactivation process. The conformation effect on photoproduct formation has not been well studied and therefore only limited data is available.^[47, 208, 212, 213] By changing the DNA conformation due to complex formation with small acid soluble proteins from *Bacillus* species only spore photoproduct and no CPD lesions was formed upon UV irradiation.^[214]

In the present research, a systematic investigation was performed to understand the influence of overall secondary structure on the damage formation event. To this end a set of well-organized RNA and DNA-RNA mixed hairpins **16-19**, depicted in Figure **3.13**, were employed.

All the bases written in bold red, represent 2'-deoxyribonucleosides (DNA bases) and those in italics are ribonucleosides (RNA bases). The RNA environment was chosen because it induces a more A-like conformation in contrast to DNA which preferentially forms a B-type duplex.^[62, 215] The DNA-RNA heteroduplexes have been found to adopt more A-like helix conformation as well.^[216]

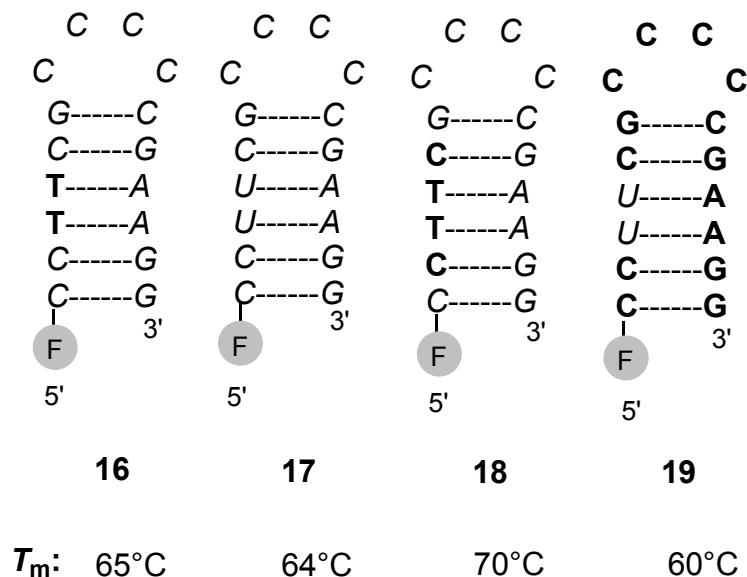


Figure 3.13: DNA/RNA hairpins **16 - 19** prepared for the investigation of how strongly the duplex conformation influences the UVC damage formation process. RNA bases are shown in italics, DNA bases are printed in bold. F: (6-FAM) = 5'-Fluorescein. Melting point (T_m) condition: $C_{\text{hairpin}} = 3 \mu\text{M}$ in buffer (150 mM NaCl, 10 mM Tris-HCl, pH = 7.4)

Hairpins **16**, **18** and **19** are mixed DNA-RNA strands whereas **17** is a pure RNA hairpin. The hairpin **16** contains a dTpdT dinucleotide in a RNA environment. Hairpin **17** is a pure RNA structure where thymine was replaced with uracil. In hairpin **18**, the DNA stretch was increased to four bases. Hairpin **19** contains two uracil moieties embedded in a DNA duplex. The concentrations, observed mass (m/z) values and melting points of these hairpins are listed in Table 3.6. The DNA-RNA mixed duplexes are known to show a little higher melting temperature than respective DNA-DNA duplexes. The similar trend is visible here as hairpin **18** was found to possess slightly higher melting point (70 °C) than hairpin **16** or **19**.

Table 3.6: Tabulation of the observed molecular weights of hairpins **16-19**, concentration of the stock solutions and their measured melting points (T_m)

Hairpins (5' to 3')	Observed molecular mass (m/z)	Melting point (T_m)
16. FAM- <u>CCTTCG</u> CCCC <u>CGAAGG</u>	5657 [M+Na] ⁺	65 °C
17. FAM- <u>CCUUCG</u> CCCC <u>CGAAGG</u>	5891 [M+Na] ⁺	64 °C
18. FAM- <u>CCTTCG</u> CCCC <u>CGAAGG</u>	6965 [M+Na] ⁺	70 °C
19. FAM- <u>CCUUCG</u> CCCC <u>CGAAGG</u>	5635 [M+Na] ⁺	60 °C

3.9.1. CD spectral analysis

The conformations of the hairpins **16-19** were analyzed by CD-spectroscopy. After melting point studies, the solutions were used as probes for CD measurements. Figure 3.14 shows the CD spectra obtained for hairpins **12**, **17** and **18**. Hairpin **12** is a pure DNA strand, **17** being a pure RNA hairpin whereas hairpin **18** has a mixed DNA-RNA sequence. From the CD data, the DNA hairpin **12** (solid black) was found to have a B-like conformation showing two maxima at 284 nm and 218 nm and a minimum at 250 nm. These observed values tally properly with reported data on DNA hairpins which state that DNA hairpins deviate slightly from normal double stranded DNA.

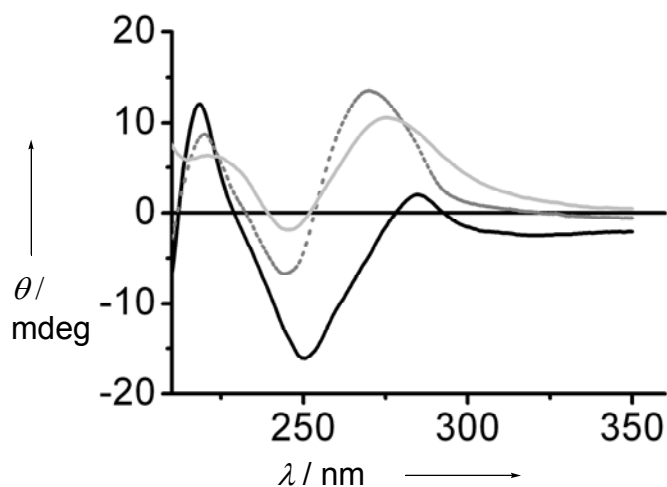


Figure 3.14: CD-spectra of the DNA hairpins **12** (solid black), **17** (dotted black) and **18** (solid gray). $C_{\text{hairpin}} = 3 \mu\text{M}$ in 150 mM NaCl, 10 mM Tris-HCl buffer, pH = 7.4. $T = 20 \text{ }^\circ\text{C}$.

The pure RNA hairpin **17** (solid gray) was found to adopt a more A-type conformation. Here the maxima were detected at 271 nm and 221 nm while the minimum appeared at 242 nm. The maxima of the mixed DNA-RNA hairpin **18** were shifted compare to hairpin **12**, to 276 nm and 223 nm whereas the minimum was found at 250 nm, confirming that it possesses more of A-like conformation in comparison to pure DNA hairpin **12**. The CD data of the other hairpins **16** and **19**, not shown in Figure 3.14 due to clarity reason, were observed to adopt an almost identical conformation to **18** (see Table 3.7). From analysis of the CD data it can be concluded that RNA hairpins adopt a more A-like conformation, fully supporting the literature data.^[62, 217, 218]

Table 3.7: Determination of conformations of the DNA hairpin **12**, DNA/RNA mixed hairpins **16**, **18** and **19** and the pure RNA hairpin **17** by CD-spectroscopy. Assay solution:). $C_{\text{hairpin}} = 3 \mu\text{M}$ in 150 mM NaCl, 10 mM Tris-HCl buffer, pH = 7.4. $T = 20 \text{ }^\circ\text{C}$.

Hairpin (5' to 3')	Maxima at (nm)	Minimum (nm)	Conformation
12. FAM- <u>CGTTGC</u> AAAA <u>GCAACG</u>	284 and 218	250	B
16. FAM- <u>CCTTCG</u> CCCC <u>CGAAGG</u>			A-like
17. FAM- <u>CCUUCG</u> CCCC <u>CGAAGG</u>	271 and 221	242	A
18. FAM- <u>CCTTCG</u> CCCC <u>CGAAGG</u>	276 and 223	250	Between B and A
19. FAM- <u>CCUUCG</u> CCCC <u>CGAAGG</u>	275 and 223	248	Between B and A

All these hairpins were irradiated at 254 nm inside the fluorimeter as described earlier, at the same concentration of 2 μM taken in a fluorescence cuvette. The RNA hairpins were handled carefully on a pre-sterilized bench, as RNA oligonucleotides are known to be degraded very fast with RNase present in skin. All the materials used for RNA, e.g. eppendorf cups, cuvettes, eppendorf tips, HPLC vials and buffers were autoclaved prior to use. The amount of damaged oligonucleotides, after UVC irradiation was quantified by HPLC using our direct method. Table 3.8 depicts radiation impact on the hairpins **16-19**. The chromatography profiles of these hairpins before (bottom) and after (top) irradiation are shown in Figure 3.15.

Table 3.8: A comparative study of damage formation of the FAM labeled hairpins 1-7 after irradiation at 254 nm at 10 °C. Assay solution: hairpin concentration = 0.2 μM in buffer (150 mM NaCl, 10 mM Tris-HCl, pH = 7.4). The amount of formed photoproducts was analyzed and quantified by analytical HPLC using SAX-column.

Hairpin (5' to 3')	Irradiation time (min)	Temperature (°C)	Damage (%)
16. FAM- <u>CCTTCG</u> CCCC <u>CGAAGG</u>	60	10	0
17. FAM- <u>CCUUCG</u> CCCC <u>CGAAGG</u>	60	10	0
18. FAM- <u>CCTTCG</u> CCCC <u>CGAAGG</u>	30	10	5
19. FAM- <u>CCUUCG</u> CCCC <u>CGAAGG</u>	20	10	10

For hairpin **16**, no lesion formation was observed even after 60 min of irradiation. This observation was unexpected as, hairpin **8** which has same sequence as that of hairpin **16** but in a pure DNA environment, produced 40% damage after 20 min of irradiation. The same unusual UVC resistance was observed for hairpin **17**, which contains a UpU dinucleotide instead of dTpdT as in hairpin **16**. Even after 60 min of irradiation no photoproduct formation could be detected in HPLC. This data suggests that pyrimidine bases, in a compact A-like structural environment are very much protected from UVC light.

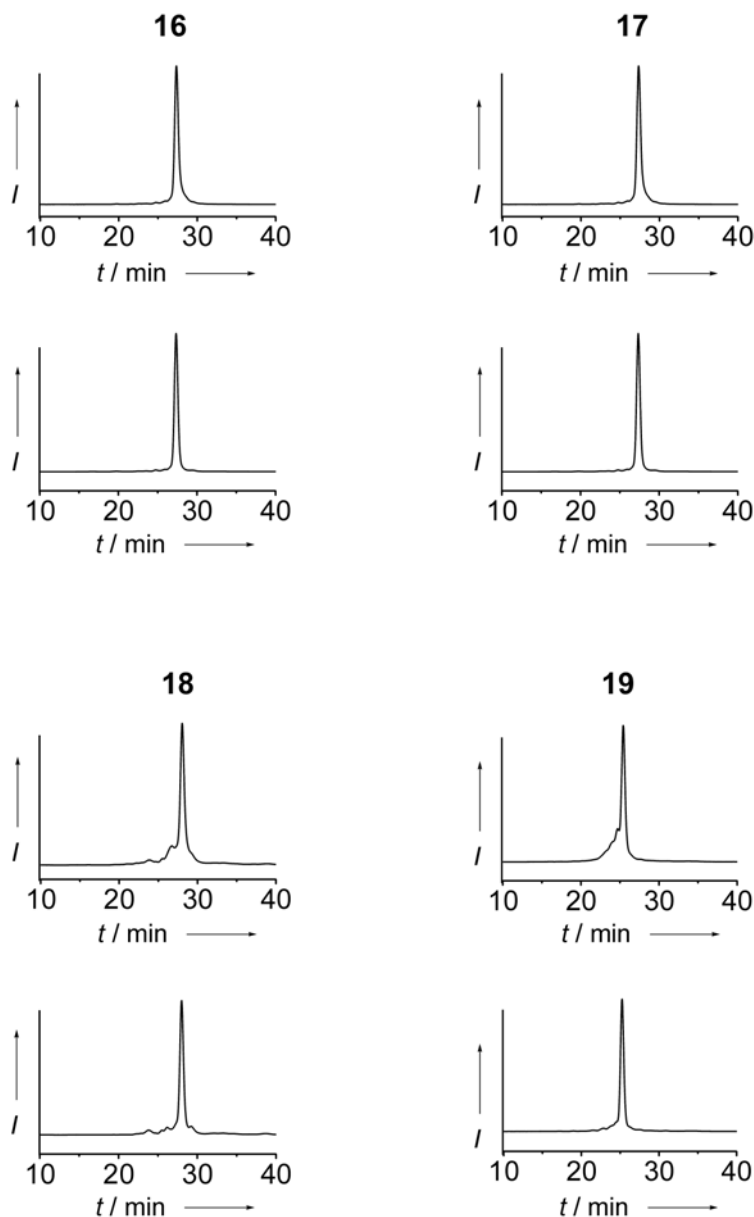


Figure 3.15: HPL chromatograms of the four hairpin **16 - 19** before (bottom) and after (top) 20 min of irradiation under UVC light. Assay solution: $C_{\text{hairpin}} = 0.2 \mu\text{M}$ in buffer (150 mM NaCl, 10 mM Tris-HCl, pH = 7.4). $\lambda_{\text{irr}} = 254 \text{ nm} (\pm 10 \text{ nm})$, $T = 20 \text{ }^\circ\text{C}$. HPLC conditions: Nucleogel-SAX-column (1000-8); eluting buffers (buffer A: 0.2 M NaCl/0.01 M NaOH in H_2O , pH = 13; buffer B: 1 M NaCl/0.01 M NaOH in H_2O ; pH = 13); Gradient: 0-75% B in 25 min and then up to 85% B in 35 min at a flow of 0.7 mL/min. t = retention time; I = relative fluorescence intensity.

This observation was supported by HPLC-MS/MS analysis of the irradiated and subsequently digested hairpins **16** and **17**, which also gave no detectable lesions confirming the results obtained from the HPLC experiments. The fact that a UpU sequence is in principle able to form UV lesions upon irradiation was proven with hairpin **19**, containing the UpU sequence within a DNA hairpin. Here, about 10% degradation was measured within 20 min of irradiation.

If the dTpdT containing DNA stretch was enlarged within the RNA hairpin as in **18**, we still observe a strong reduction of the amount of UV lesions, proving that it is indeed the A-conformation of the hairpin stem and not the contact of the dTpdT sequence with RNA-nucleotides that is responsible for the protective effect.

In order to analyze which lesions are formed in these A-like structures, hairpin **18** was irradiated for an extended time period (60 min) to produce enough lesions for HPLC-MS/MS analysis. The irradiated sample was then digested enzymatically as described earlier and was analyzed by HPLC-MS/MS.^[49, 219] The enzyme mixture was found to digest RNA hairpins as well. For the lesion characterization, two HPLC-MS runs were performed. In the first run, the quadrupole was set at $m/z = 530$, to detect the dTpdC derived photoproducts. Here two kinds of photolesions were observed. The mass and the fragmentation showed clearly that the lesions are either dTpdC (6-4)PP or dTpdC-Dewar lesion. The obtained HPLC-MS spectrum and the fragmentations of these peaks were very similar to those observed for DNA hairpin **10** (Figure 3.11 and 3.12). Since the Dewar lesions are generally more polar, we speculate that the peak (**a**) may be due to the Dewar lesion and the peak (**b**) is the (6-4)PP lesion. However, this data is not sufficient for a clear assignment of these structures. At a detection

mass of $m/z = 545$ which is the mass (m/z) of a dTpdT-dinucleotide and hence their photoproducts, again all the usual photoproducts, the dTpdT-CPD, the dTpdT-(6-4)PP and its Dewar valence isomer were detected (Figure 3.12). This clarifies that a dTpdT-dinucleotide sequence embedded in a RNA environment produces the same photoproducts as in a DNA environment, but to a lesser extent due to the conformation adopted by RNA.

It can be concluded that an A-like double helix structure dramatically reduces the reactivity of dTpdT and UpU dinucleotides in the presence of UVC light. In summary, RNA is much more UV stable than DNA if exposed to UVC light.

3.10. Summary and conclusion

UV irradiation leads to severe genomic damage. The DNA lesions formed upon UV irradiation are mainly cyclobutane pyrimidine dimers, (6-4)PP photolesions and Dewar valence isomers of the (6-4)PP photoproducts. These lesions are predominantly responsible for the development of non-melanoma skin cancers.

In the present work small fluorescein-labeled DNA, RNA and mixed DNA-RNA hairpins, which form stable folded oligonucleotide duplex structures at room temperature, were employed to investigate the UVC-induced DNA or RNA damage formation event. The concentration-independent melting behavior of the hairpins allowed irradiation at very low concentrations, which produces a significant amount of lesions even under very mild UVC conditions. Due to the small size of the hairpins it was possible to quantify the amount of UVC degradation directly, using a newly developed ion-exchange chromatographic method at pH = 13 (fluorescence detection) at room temperature. The quantification of the damaged oligonucleotides by fluorescence detection, instead of detection by UV-absorption, enabled an accurate measurement of DNA degradation. Irradiation of hairpins possessing various sequences once again established that 2'-deoxythymidine is the most vulnerable DNA base in UVC light. Direct HPLC studies of the total damage yield, together with MS/MS structure determination of the formed lesions, prove that homo 2'-deoxythymidine stretches form rapidly UVC induced lesions in large quantities. The Dewar valence isomer lesion is formed in much smaller amounts. 2'-Deoxythymidines give rise to these lesions in flexible DNA regions as well as in

the well structured, double helical stem area. 2'-Deoxycytidines, in contrast, react in the presence of UVC light only in the well organized B-duplex. Flexible homo dC-sequence regions are UVC resistant.

Investigation of the reactivity of a dTpdT-dinucleotide in various sequence contexts revealed the surprising result that the reactivity is strongly reduced when a dTpdT dinucleotide is locked between two neighboring 2'-deoxyguanosines. The reason for the protective effect is probably due to a reduced flexibility of the 2'-deoxythymidines embedded between 2'-deoxyguanosines. First of all, the dT's are stacking on top of large purine bases and secondly, the flanking sequences are G:C base pairs which have significantly higher pairing strength than an A:T base pair, making the duplex more rigid which may hinder the re-orientation of the duplex upon photolesion formation. The sequence dependence on lesion formation suggests that genomic DNA will be inhomogeneously damaged under such UV exposure.

The most surprising observation is that the oligonucleotide hairpins, possessing more A-like conformations are very much resistant to UVC degradation. RNA hairpins containing UpU dinucleotides sequence were found to be fully protected from being damaged. The dTpdT stretches, embedded in an A-like RNA environment, showed surprising stability under UVC light. This could be explained by more compact structure of A-duplex compared to B-duplex. The activation energy required for structural arrangement of the dTpdT lesions inside a compact A-conformation might be too high to pay off.

This observation is particularly interesting in a biological context, since DNA in eukaryotes is densely packed in chromatin. DNA which is present in the nucleus

of the cell does not possess an ideal B-conformation because genomic DNA's are wrapped around nucleosomes. This study shows that this distortion from B-duplex structure will tremendously affect the UV stability of the duplex.^[220, 221]

The observation of high UVC stability of RNA oligonucleotides can be co-related to prebiotic research which study the origin of life. A widely-acknowledged theory of prebiotic world is the RNA world theory. ^[222, 223] The theory hypothesizes that RNA was the first biomolecule on earth that was synthesized from the constituents present in the primordial soup, and hence it was the precursor of life. Due to the lack of ozone at the very beginning of life on the earth, it is believed that UV radiation dose on earth's surface was quite higher than it is today. The present observation that RNA is immune to UV light compared to DNA provides one more clue that might have encouraged RNA to evolve on the primordial earth and hence supports the RNA world theory.

4. Photolyase Catalyzed CPD-Lesion Repair Study

4.1. Activities of CPD-photolyase

Cis-syn Cyclobutane-thymidine-dimer (CPD) is the major photoproduct in genomic DNA and is responsible for aging and skin cancer.^[36] CPD-photolyase is the major defense system in plants and many other organisms, repairing the CPD-lesion inside the cell nucleus.^[99] This light-driven enzyme uses long wavelength radiation (350 to 450 nm) for its function. Photolyase therefore, can act only in tissues and cells that are exposed to daylight.

Although CPD-photolyases were isolated from different organisms and their structural features were studied, the activities of the photolyases have not yet been understood properly. Type-I photolyases are well studied microbial enzymes. Type-II enzymes are present in higher organisms such as plants. These photolyases are not well understood. The *Carell group* has a long-standing research interest in photolyase-catalyzed CPD-repair phenomenon. Towards this end, various model compounds have been synthesized and their repair mechanisms have been investigated using photolyases.^[128, 157, 224]

In the present investigation, a molecular beacon (MB) probe technique was explored to assay the photolyase-mediated CPD-repair process. The probe, which contains a synthetic CPD-lesion, serves as a substrate for photolyase. The activities of both Type-II (*A. nidulans*) and Class-II (*A. thaliana*) CPD-photolyases were profiled with this new probe methodology. Investigation was performed to

fish-out the photolyase activity from a protein-pool, in a wild-type cell extract. Attempt was also made to monitor the CPD-repair process within living cell, using this reporter probe.

4.2. Molecular beacon based photolyase-substrate DNA

Molecular beacons (MB) are U-shaped oligonucleotides that are efficient and highly target-specific probes. MBs in the past, have been used as probes for DNA-binding and DNA-cleaving proteins,^[167, 168] DNA-cleaving small molecules and self-replicating systems.^[179, 225] In the present work, a molecular beacon was designed to assay photolyase repair process. The molecular beacon **21** contains a CPD-lesion in its loop structure. This was for the first time that a synthetic target was incorporated in a molecular beacon structure. This *cis-syn* thymidine-dimer-lesion (see Figure 4.2 for structure), which has a open backbone structure, was synthesized by *L.T. Burgdorf*,^[157] and is analogous to a natural photolyase substrate first synthesized by *J. -S. Taylor*.^[226] The CPD-containing MB-probe **21** therefore, serves as a DNA-substrate for the CPD-photolyases. Figure 4.1 describes the MB-photolyase interaction process.

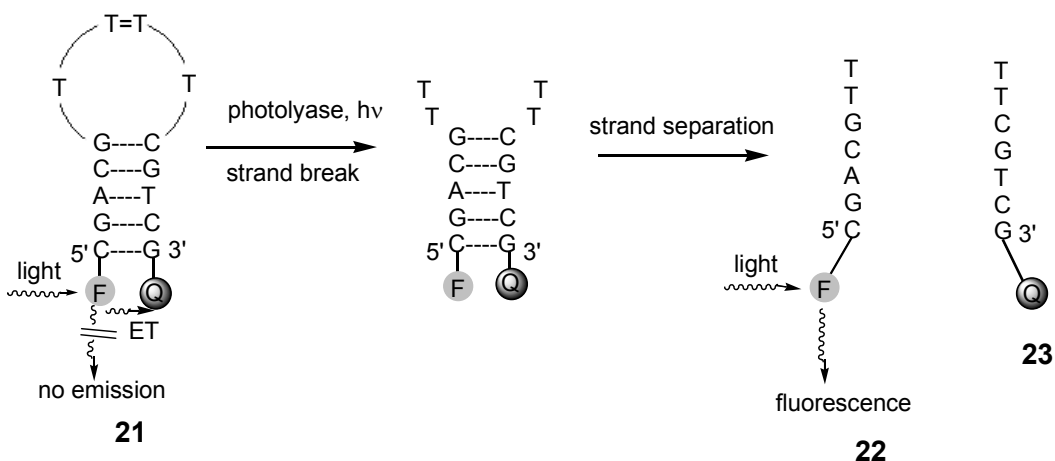


Figure 4.1: Depiction of the molecular beacon strategy employed to quantify DNA-repair activity. The beacon contains a 5'-Fluorescein (6-FAM), a 3'-Diazabenzylsulfonyl- (Dabsyl) quencher and the substrate analog **21** in the loop of the hairpin.

The synthesized CPD-lesion, which forms an open-backbone structure (see Figure 4.2) after the DNA synthesis followed by deprotection,^[227, 228] is a potential substrate for CPD-photolyase and was thus designed in order to translate photolyase activity into a strand break, as depicted in Figure 4.2. This CPD-lesion was found to be efficiently recognized by the repair enzymes. Photolyases accept this open-backbone substrate analog, most probably because they do not contact the central phosphodiester group in the photolyase-DNA complex. This fact was established by *A. Sancar* by using data from detailed footprinting studies.^[98]

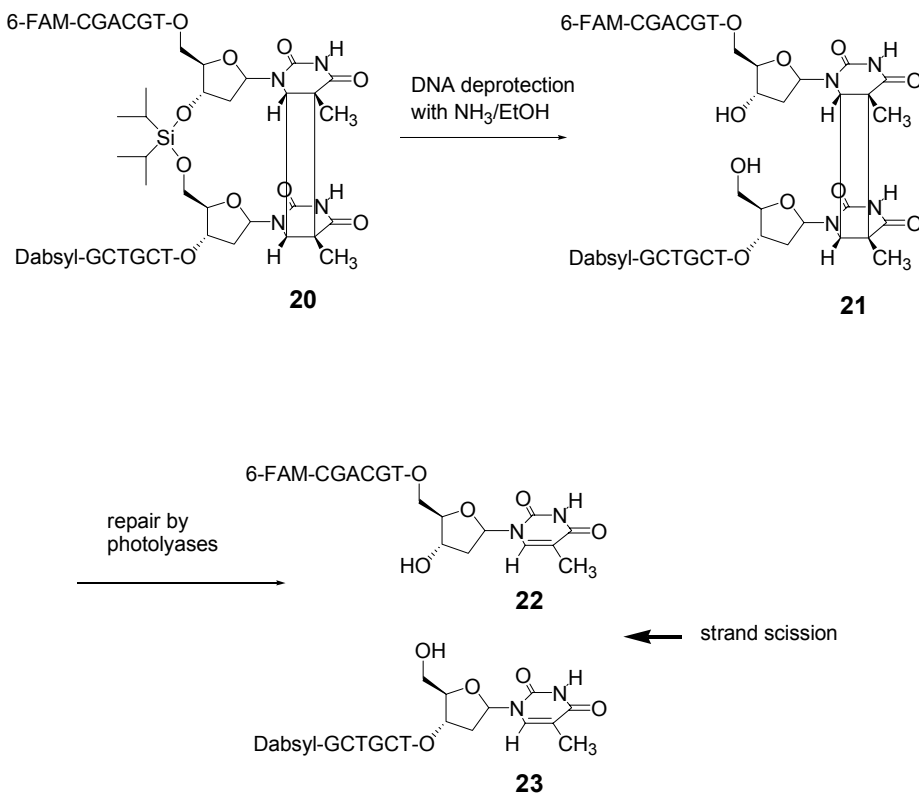


Figure 4.2: A schematic presentation of the CPD-lesion containing molecular beacon which induces strand break after photolyase-catalyzed repair the dimer.

As depicted in Figure 4.1, the MB **21** contains a fluorescence moiety (6-FAM, excitation: 495 nm, emission: 520 nm) at the 5'-end and a fluorescence quencher Dabsyl, at the 3'-end. The structures of these two molecules are shown in Figure 4.3. Dabsyl was used as the first base attached to the solid support in the cartridge, while FAM was a 5'-end terminator during the synthesis of the MB **21**.

The molecular beacon, in its closed form, is non-fluorescent due to efficient energy transfer from FAM to Dabsyl. When treated with photolyase and irradiated with light of suitable wavelength, the CPD-lesion undergoes cleavage due to cycloreversion of the thymidine-dimer (see Figure 4.2). The temporary

double-stranded DNA thus obtained, separates readily at room temperature, due to its very low melting point (less than 20 °C). As a consequence, the fluorescence of 6-FAM will be restored after the strand break (see Figure 4.1).

The 6-FAM phosphoramidite, which is a white solid, was non-fluorescent before the DNA synthesis. However, after the DNA synthesis, followed by deprotection from the solid support, it exhibited brilliant green fluorescence in aqueous solution of pH above 7.0 (see Figure 4.3). The red colored, controlled pore glass (CPG) supported 3'-Dabsyl was used as a universal fluorescence quencher.

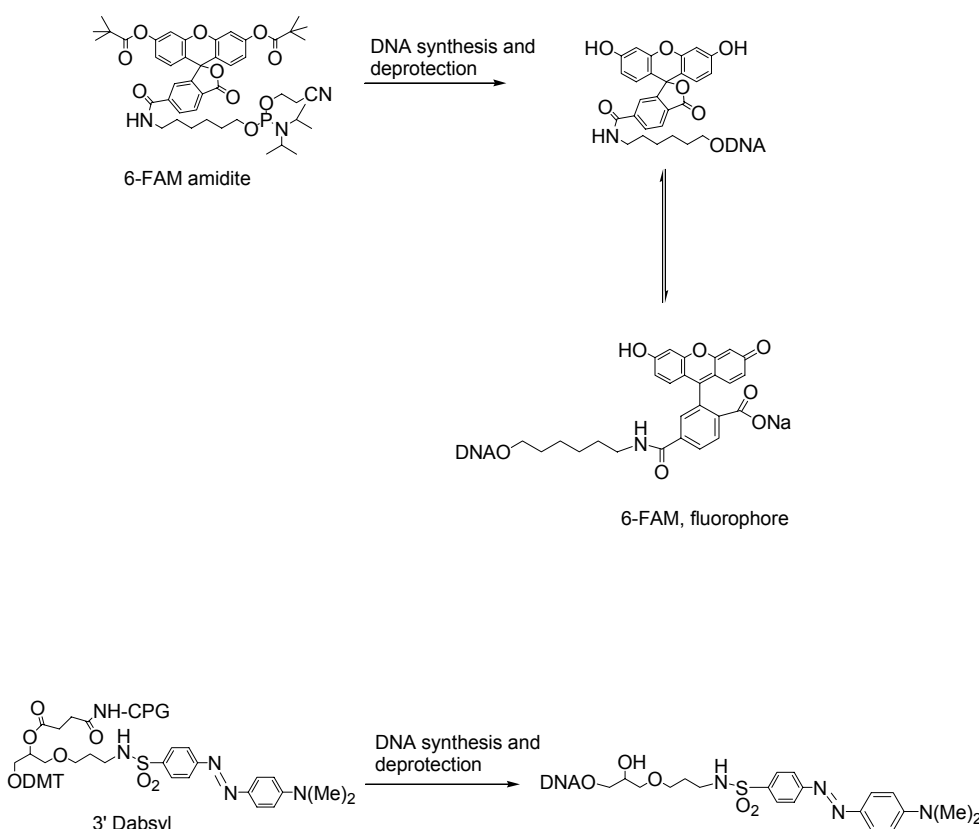


Figure 4.3: Structural presentation of the 5'-end (6-FAM) and 3'-end quencher Dabsyl before and after deprotection. CPG = Controlled pore glass.

With an intention to obtain a very short molecular beacon probe for photolyase, at first a molecular beacon with CPD-dimer was synthesized, having a sequence: 5'-FAM-GACGTXTCGTC-Dabsyl-3' (where X= CPD lesion, shown in Figure 4.2). This sequence which is one base pair shorter in the stem region than the hairpin probe **21**, did not show any melting behavior. This indicates that the short stem-sequence was incapable of forming a self-complementary stem structure which is an essential requirement for a molecular beacon. So MB-hairpin **21** was the shortest molecular beacon probe with a desired loop and stem structure, employed in this study to assay photolyase activities.

4.2.1. *Synthesis of the molecular beacon*

The synthesis of the molecular beacon was performed in an automated DNA-synthesizer using standard phosphoramidite synthesis protocol, developed by *Caruthers et al.*^[229-231] The solid phase synthesis was performed on a CPG-supported cartridge from 3' to 5' direction. A schematic diagram of the important steps of automated synthesis is presented in Figure 4.4.

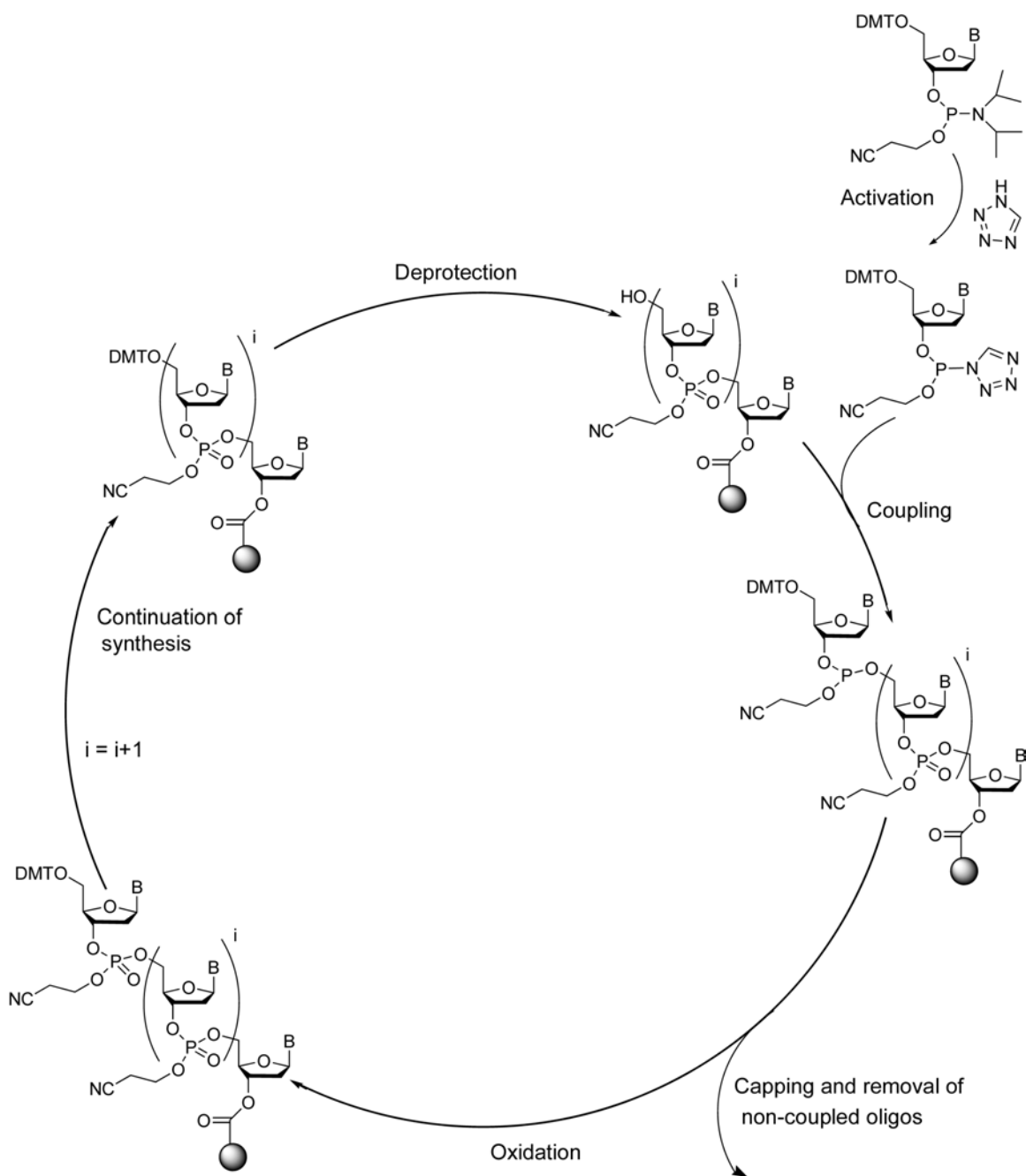


Figure 4.4: Demonstration of the important steps involved during solid phase DNA-synthesis in automated DNA-synthesizer.

4.2.2. Characterization of the molecular beacon

To obtain the required sensitivity of the assay method, particular attention was paid to the purity of the molecular beacon **21**. The purity of the synthesized photolyase-cleavable molecular beacon was examined by reversed-phase HPLC which showed a single, sharp peak at a retention time of about 20 min (Figure 4.5). However, presumably due to the strong self-pairing property of the designed molecular beacon, which forces the oligonucleotide into the U-conformation, the HPLC analysis had to be performed at an elevated temperature (55 °C) with a RPC18- HPLC column having a particle size of 3 μm . Colder conditions or the use of the standard 5 μm column gave broad and unresolved peaks.

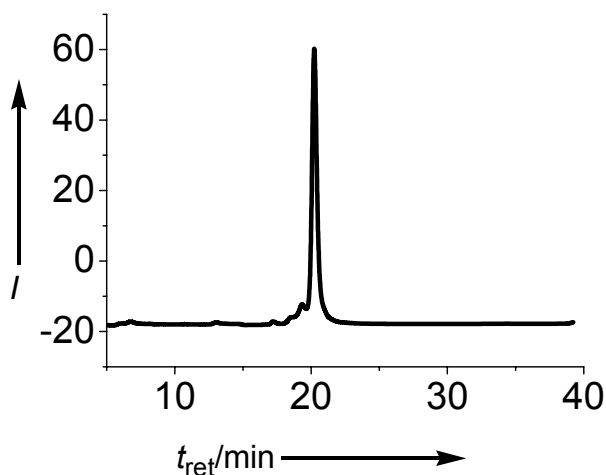


Figure 4.5: HPL-Chromatogram of the molecular beacon **21**. Buffer: A = 0.1 M AcOH/NEt₃ in water, pH 7.0, B = 0.1 M AcOH/ NEt₃ in 80% acetonitrile, pH 7.0; Gradient: 0 to 45% B in 35 min. 55 °C, Column: Nucleosil 250 mm x 4 mm, 120Å, 3 μm . t_{ret} = retention time; I = relative fluorescence intensity.

The MALDI-TOF spectrum depicted in Figure 4.6 displays the expected molecular weight (21^+ : MW = 5218) and the potassium adduct ($[21+K]^+$: MW = 5257) of the threefold modified molecular beacon **21**.

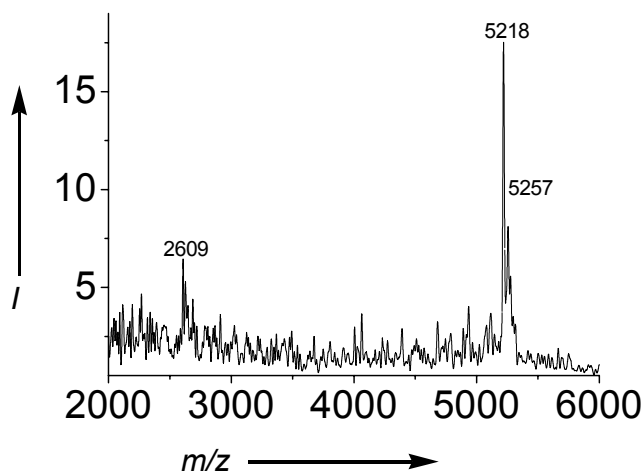


Figure 4.6: MALDI-TOF mass spectrum of the molecular beacon **21**. Matrix: THA/Citrate (2:1) in ethanol.

The self-complementary behavior of the molecular beacon **21** was tested by melting point (T_m) analysis. The melting temperature analysis based on UV absorption at 260 nm, showed high T_m of about 72 °C. In order to investigate the fluorescence quenching efficiency of the MB **21** and also to study the fluorescence signal to noise ratio, resulted from unwinding of the hairpin stem, fluorescence melting point measurement was performed. Figure 4.7 shows a temperature dependent fluorescence change of this molecular beacon. The probe was excited at 495 nm while the emission was recorded at 520 nm.

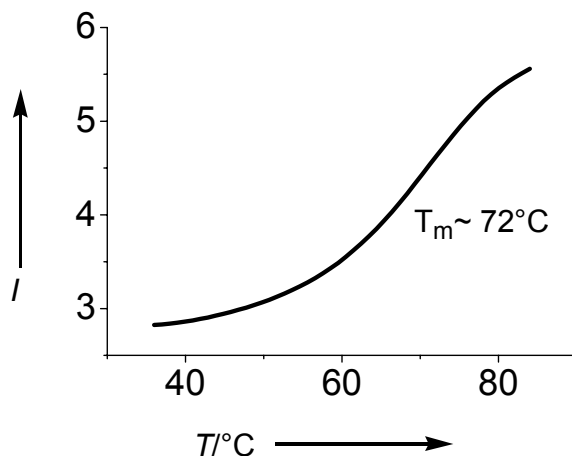


Figure 4.7: Fluorescence melting curve of the hairpin **21** ($C_{DNA} = 3 \mu M$, 150 mM NaCl, 10 mM Tris, pH 7.4). $T_m \approx 72^\circ C$. I = relative fluorescence intensity.

It is clear from Figure 4.7 that the molecular beacon **21** at room temperature (not shown in Figure 4.7), possesses a well paired, duplex stem structure. The fluorescence of FAM was virtually quenched at room temperature, due to FRET or direct energy transfer between the FAM and the 3'-quencher Dabsyl.^[149, 169] With increase in temperature, the stem of the molecular beacon starts melting, thus gradually increasing the spatial distance between the fluorophore and the quencher. The fluorescence signal of FAM, therefore, started increasing as a result of depression of FRET efficiency (fluorescence quenching efficiency falls down sharply in increasing the distance between the interacting moieties). At very high temperature, the molecular beacon acts as a coiled, single-stranded DNA, resulting in a stable fluorescence signal intensity (plateau of the Figure 4.7). As can be seen in Figure 4.7, the melting of the hairpin resulted in the

fluorescence intensity to increase only by a factor of two. This confirms that the length of the MB-oligonucleotide is short enough to enable efficient energy transfer even in the stretched-out single-stranded DNA-conformation. The fluorescence signal change due to melting of the MB is in fact an estimation of the background signal for photolyase-catalyzed repair of the MB **21**, as the stem of the MB might unwind during recognition of the CPD-lesion by the photolyase. In contrast to stem opening, the cleavage of the MB **21** should result in a high fluorescence signal (theoretically, the signal to noise ratio should be at least, more than 10), due to complete loss of fluorescence energy transfer between FAM and Dabsyl which become separated as a result of the hairpin cleavage (see Figure 4.1).

The fluorescence melting study of this short, cleavable molecular beacon **21** thus showed that it might act as a sensitive probe with high signal to background ratio for activity profiling of the photolyases.

The thermal stability of the duplex strand (5'-CGACGTT-3': 3'-GCTGCTT-5') which presumably would be formed after the cleavage of molecular beacon **21** at the dimer position, was also investigated. These two strands, partially complementary to each other, gave no detectable melting temperature, confirming that cleavage of the thymidine dimer substrate will lead to complete stem dissociation at room temperature.

4.3. Activity profiling of Type-II photolyase with molecular beacon substrate

Using the molecular beacon **21** as a substrate, the light-induced repair of the thymidine-dimer was studied using Type-II photolyase. The progress of the repair process was monitored by recording fluorescence signal of the molecular beacon as a function of time. Well characterized, pure, Type-II photolyase from *A. nidulans* was generously provided by Prof. A. P. M. Eker. This pure photolyase has a molecular weight of about 54 kDa and possesses 8-HDF as the light-harvesting cofactor along with the essential FAD cofactor.^[232, 233] A 100 μ L solution was prepared containing *A. nidulans* photolyase (0.10 μ M, 10 pmol) and molecular beacon **21** (0.25 μ M) in a buffer (NaCl: 150 mM, Tris: 10 mM, DTT: 10 mM, pH = 7.4). The semi-reduced FADH^{*}, in the protein environment, was expected to undergo reduction into its fully reduced form FADH, under this pH condition. The solution was irradiated under a white-light source at 27 °C. As *A. nidulans* photolyase is known to absorb light around 435 nm, a 380 nm cut off filter was used during the irradiation, to avoid high-energy radiation (above 380 nm). The irradiation was paused from time to time and fluorescence of the solution was measured inside a fluorimeter. The temperature inside the fluorimeter was kept constant at 27 °C. The obtained fluorescence growth is shown in Figure 4.8 with respect to irradiation time (curve **a**). Two control experiments were also performed in order to quantify the background activities. Curve **b** in Figure 4.8, represents the fluorescence fluctuation of an identical solution kept in dark. Another control experiment was carried out with a solution containing only the molecular beacon **21** of same concentration but without any photolyase, and was irradiated in parallel, under the identical

condition. This was performed to test the stability of the molecular beacon substrate under the irradiation condition (depicted in curve **c**). It is clearly evident from curve **a** that the expected thymidine-dimer repair, followed by a strand cleavage, gives rise to a strong fluorescence elevation. The fluorescence signal intensity was found to be increased by a factor of 10 compared to the background signal. A comparison of curve **a** with the background signal (curve **b** or **c**) clearly demonstrates a high signal to noise ratio as result of photolyase-substrate reaction. The continuum of curve **a**, after 60 min of irradiation, indicates the completion of substrate cleavage, reaching the fluorescence signal intensity to a constant value. Comparing the high fluorescence-signal turn-out (curve **a**) with the thermal denaturation profile (Figure 4.7) where only two-fold fluorescence increment was observed, it can be clearly stated that this high fluorescence signal intensity is indeed caused of a strand break of the MB 21, separating the FAM and the Dabsyl to a infinite distance.

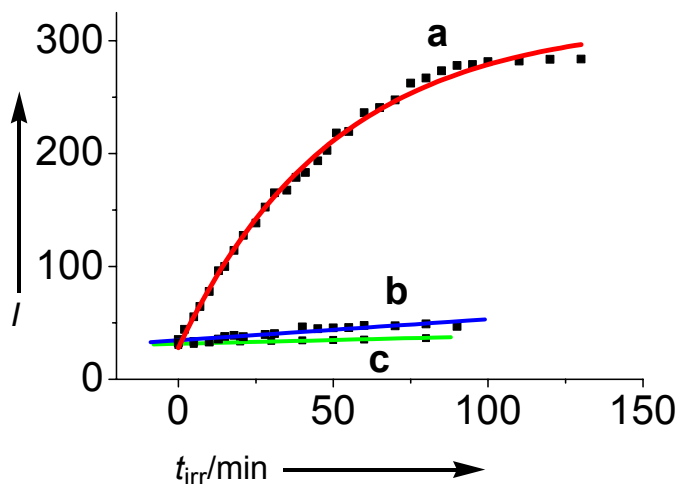


Figure 4.8: Fluorescence-based repair study with the *A. nidulans* photolyase. Assay solution: Molecular beacon **21** (0.2 μM), buffer (150 mM NaCl, 10 mM Tris, pH 7.5), DTT (10 mM) and *A. nidulans* photolyase (0.15 μM), Temperature: 27 $^{\circ}\text{C}$. **a)** assay solution irradiated with white light. **b)** Dark control. **c)** Assay solution containing no photolyase enzyme irradiated with white light. t_{irr} = irradiation time; I = relative fluorescence intensity.

4.3.1. HPLC profiling of photolyase activity

In order to prove further, that the fluorescence increment in Figure 4.8 (curve **a**) is in fact due to cleavage of the molecular beacon **21** at the thymidine-dimer position, time dependent HPLC studies were performed with the assay solution. For this, a 400 μL assay solution was prepared containing the molecular beacon substrate **21** (4 μM) and *A. nidulans* photolyase (0.2 μM , 20 pmol). The mixture was irradiated under identical condition as above. A small amount of aliquot samples were taken out at regular intervals and were injected into the HPLC. The obtained analytical HPLC profile using fluorescence detector is shown in Figure

4.9. The Z-axis represents the irradiation time coordinate. All the HPLCs were performed with a 3 μ m column at 55 °C. As can be seen from Figure 4.9, at a retention time of about 20 min, a small peak was observed (before irradiation), due to elution of hairpin **21**. With the progress of irradiation, a new peak started arising at a retention time of about 10 min. Co-injection studies with reference oligonucleotides confirmed that this peak was due to the FAM labeled single stranded oligonucleotide 5'-FAM-CGACGTT-3' (**22**), which is in fact, the short oligonucleotide fragment expected to be produced after the thymidine-dimer cleavage. MALDI-TOF analysis of the irradiated sample also showed a peak with a mass (m/z) of 2630, which is the mass of the FAM-containing fragmented strand **22**, along with the hairpin mass (m/z) of 5218. Analytical HPLC of this irradiated solution was carried out also with UV-detection at 260 nm. The HPLC clearly showed two new peaks at 10 min and 14 min of retention time, along with the intact molecular beacon **21** eluted at 20 min. By co-injection studies, both of these new peaks were identified as the expected fragmented-oligonucleotides **22** and **23** (see Figure 4.2) generated from cycloreversion of the thymidine-dimer.

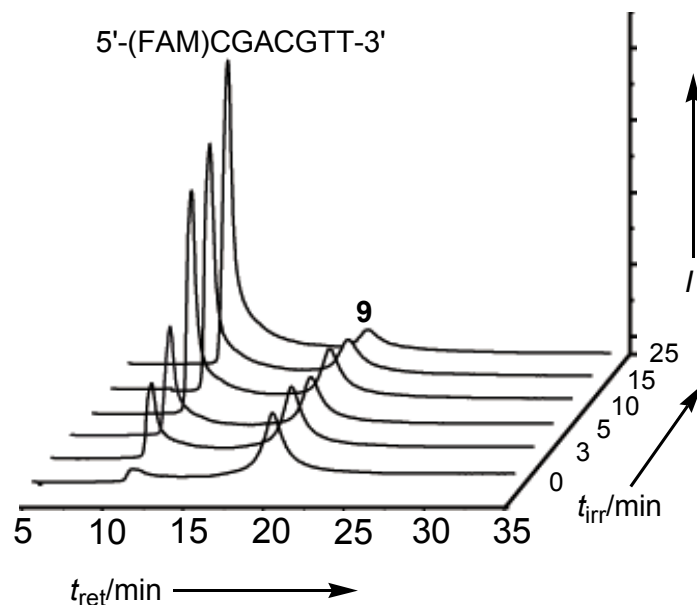


Figure 4.9: Series of HPLC-chromatograms of the assay solution irradiated with white light. Assay solution: Molecular beacon **21** (4 μM), buffer (150 mM NaCl, 10 mM Tris, pH 7.5), DTT (10 mM) and *A. nidulans* photolyase (0.15 μM). Temperature: 27 $^{\circ}\text{C}$. HPLC-conditions: Nucleosil column 250 nm \times 4 mm, 120 \AA , 3 μm ; buffer: A = 0.1 M AcOH/ NEt_3 in water, pH 7.0, B = 0.1 M AcOH/ NEt_3 in 80% acetonitrile, pH 7.0; Gradient: 0 to 45% B in 35 min. Temperature: 55 $^{\circ}\text{C}$. t_{ret} = retention time; t_{irr} = irradiation time; I = relative fluorescence intensity

The second fragmented strand 5'-TTCGTCG-Dabsyl-3' (**23**) could not be visualized in the HPLC diagram 4.9, as this strand is non-fluorescent. The much higher fluorescence signal intensity of the FAM-labeled fragment **22** (also see Figure 4.2) in comparison to the original hairpin **21**, proves again the huge loss of energy transfer (FRET) from FAM to the Dabsyl, as a consequence of hairpin cleavage. This energy transfer is strong enough in the hairpin **21**, even in its single stranded, denatured form, due to its short length (see Figure 4.7). Because of this non-linearity of the fluorescence energy transfer, which falls down rapidly

with increasing distance between the interaction moieties, the quantification of the photolyase-catalyzed dimer repair, could not be performed with this HPLC profile followed integration of the newly developed peak.

4.4. Repair study with Class-II photolyase from *A. thaliana*

The goal of this study was to investigate whether this molecular beacon technique allow quantification of the dimer repair even in crude cell extracts, particularly in plant cell extract. Towards this target, investigation was first performed to analyze if the CPD-lesion containing MB **21** is accepted as a substrate also by a Class-II photolyase from a higher organism. Here the enzyme (*At-PHR1*) from the plant *A. thaliana* was chosen. The enzyme, carrying a C-terminal 6xHis tag, was expressed in *E. coli* and affinity-purified on a Ni-column.^[234] It was isolated containing the FAD-cofactor but without any detectable second antenna pigment, which should strongly decrease the activity of the recombinant enzyme. Despite the low activity, the molecular beacon substrate enabled rapid analysis of the *A. thaliana* photolyase activity as depicted in Figure 4.10, even without an excess of the hairpin. Curve **a** shows the rapid fluorescence increase of an assay solution (100 μL) containing 0.2 μM of the beacon **21** and 1.2 μM of the *A. thaliana* enzyme, upon irradiation of the assay at 366 nm (energy fluence rate 44 Wm^{-2}). Curve **b** represents the fluorescence change obtained from a control experiment with an identical solution kept in the dark.

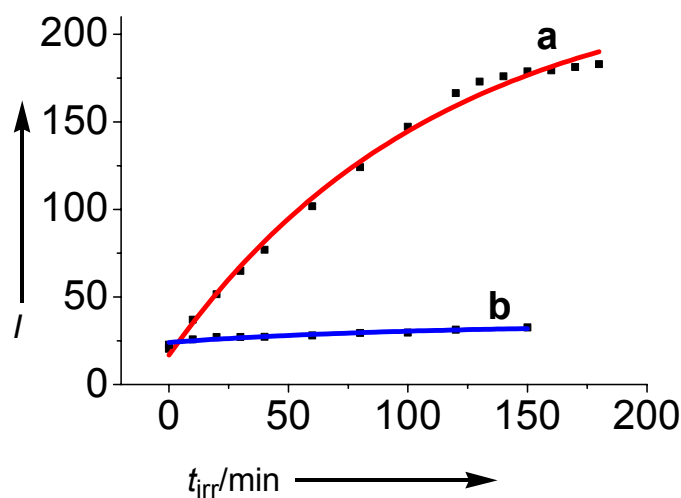


Figure 4.10: Fluorescence-based repair study with the *A. thaliana* enzyme. Assay composition: Molecular beacon **21** (0.2 μM), buffer (150 mM NaCl, 10 mM Tris, pH 7.5), DTT (10 mM) and *A. thaliana* enzyme (1.2 μM). Temperature: 27 °C. **a)** Assay solution irradiated at 366 nm (44 Wm^{-2}). **b)** Dark control. t_{irr} = irradiation time; I = relative fluorescence intensity

To prove that the large fluorescence signal (curve **a**, Figure 4.10) was indeed due to a result of the hairpin cleavage at the thymidine-dimer position, analytical HPLCs were also performed with the irradiated solution using both fluorescence and UV detection. Both HPLCs confirmed the extra peaks were the fragmented oligonucleotides after the expected dimer cleavage. These data therefore prove that the molecular beacon is indeed an efficient assay to allow rapid and reliable analysis of even the Class-II photolyase enzymes.

4.5. Activity profiling of Class-II photolyase in crude cell extracts

With a desire to study the damage repair within living cells (chemistry inside living cells), this molecular beacon **21** was employed to fish-out photolyase activity in crude, wild type cell extract. Identification and characterization of a target protein from a mixture is important in proteomics research.^[235, 236] Currently, two-dimensional gel electrophoresis or other powerful separation techniques in combination with mass spectrometry^[237] are most frequently employed for the direct investigation of the proteom of cells. Most recently, novel small molecule based techniques were described. In this context, *B. F. Cravatt* coupled protease suicide inhibitors to the molecule biotin thereby creating compounds which enabled selective extraction and quantification of proteases or other proteins with an accessible nucleophile from the complete proteom of cells (activity based protein profiling).^[238, 239] Along a similar line, *P. G. Schultz* reported synthesis of constructs made up of a small molecule inhibitors linked to a PNA-strand and a fluorophore. Addition of these compounds to a protein mixture specifically allowed to "hunt" for certain proteins, which were subsequently quantified on a DNA-array.^[240] Activity or affinity based protein characterization would be a descent way for their separations. In connection with the ongoing current effort to investigate DNA repair processes, it would be useful to develop methods that will allow quantification of DNA repair activities in the proteom of cells.

Using the molecular beacon as probe, the wild-type cell extract from *A. thaliana* plant was analyzed. Figure **4.11** shows the data obtained from the cell extracts

studies. All the cell extracts were prepared and supplied by *Prof. A. Batschauer*, our long standing collaborator. As a control, cell extract was also prepared from *A. thaliana* plants lacking the *PHR1* photolyase gene (*phr1* mutant).

In order to study the possibility of detection of photolyase activity in these cell extracts, a 100 μL assay solution was prepared containing 0.2 μM of the hairpin **21** and a cell extract solution with a concentration of 0.7 μg of total protein per μL (70 μg of total protein extract in the assay solution). This assay solution was irradiated for 1 h at room temperature at $\lambda = 366 \text{ nm}$ (44 Wm^{-2}). The background (Figure 4.11b, line 2) was determined by keeping an identical reference assay solution, containing the same amount of protein extract in the dark.

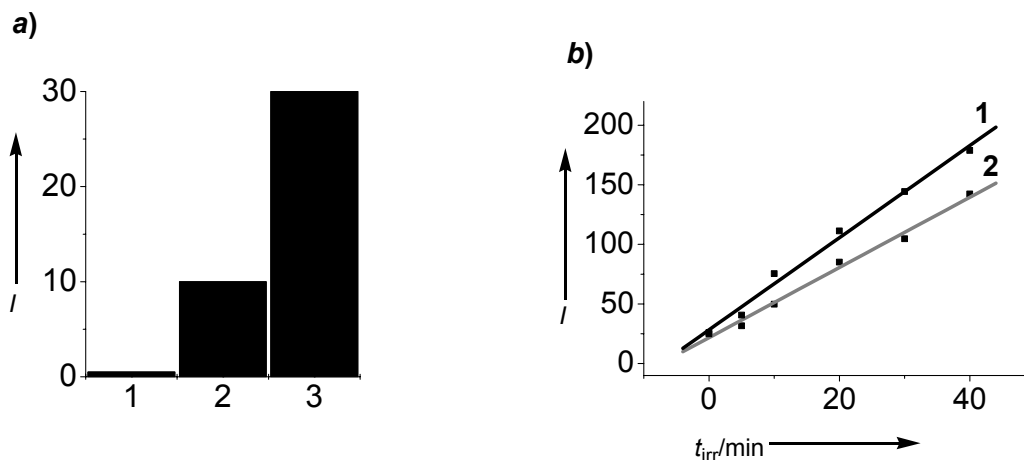


Figure 4.11: Fluorescence based repair study in cell extracts. Assay composition: Molecular beacon **21** (0.2 μM), buffer (150 mM NaCl, 10 mM Tris, pH 7.5), DTT (10 mM). Total protein concentration 0.7 μg per μL assay solution. Temperature: 27 $^{\circ}\text{C}$.

a) Bar graph representation of the assay data. Each bar shows the difference of the fluorescence response between a sample, which was kept in the dark and a sample

irradiated at 366 nm (44 Wm^{-2}) for 60 min: **1**) an assay containing just the molecular beacon. **2**) an assay containing protein extract from the photolyase mutant UVR2-1. **3**) an assay containing protein extract from wild type plants. I = relative fluorescence intensity.

b) Time dependent increase of the fluorescence response from a sample containing the wild type cell extract and the molecular beacon **21.1**: Irradiated assay solution with wild type extract. **2**: Assay solution kept in the dark

Relative to the mutant control, depicted in Figure **4.11a**, bar **2** in which the difference of the fluorescence response between the irradiation (366 nm , 44 Wm^{-2}) and the dark control was plotted, a reproducible threefold increase in fluorescence signal was observed in the assay solution containing the wild type cell extract (Figure. **4.11a**, bar **3**). This indicates reduced photolyase activity in the mutant plant. Bar **1** (Figure **4.11a**) shows an identical experiment as above but with an assay containing only the molecular beacon, and no cell extract, which shows almost no change in fluorescence response.

As evident from Figure **4.11a** that the molecular beacon **21**, containing a reporter unit (the thymidine dimer), is able to detect photolyase specifically from a protein-pool. The efficiency of this probe, though, is not up to the mark as expected. The mutant extract which should lack the photolyase enzyme also showed some light-induced DNA cleaving activities as can be seen from Figure **4.11a**, bar graph **2**. This can be due to presence of some other light-active proteins.

Figure **4.11b**, where the fluorescence change of the hairpin with wild-type extract irradiated at 366 nm is plotted compared to its dark control, reflects a significant

amount of background activity (curve 2). As it is a dark control, this unexpected background signal could not result from photolyase activity, although according to recent scientific believe, the presence of photolyases which are also active in dark can not be ruled out. This large background signal might have generated from DNA cleaving protein. In order to further investigate the detection limit, a small amount of purified *A. nidulans* photolyase was added during wild type cell extract assay and the increase of repair rate was recorded. A systematic study showed that an amount of 5-10 pmol of purified photolyase was clearly detectable with the hairpin dissolved in cell extract.

In order to address the prominent dark control activity obtained from Figure 4.11a, line 2, stability of the molecular beacon 21 in the cell extract was studied carefully, which is described later in this chapter.

4.6. Study with living cell: single cell detection

With an aim to study CPD-repair inside living cell, first, attempt was taken to incorporate the MB-probe 21, containing the CPD-lesion, into a plant cell. This was done by 'transformation from *A. thaliana* protoplast'. All experiments were performed in collaboration with Prof. A. Batschauer. In short, membrane free cells (called protoplast) were obtained from *A. thaliana* cell-culture solution by incubating it at 22 °C for 5 min, followed by re-suspension of the precipitate in an enzyme mixture containing membrane cleaving proteins. MB-probe 21 was incubated with a carrier DNA (plasmid) and transformation was performed by incubating this mixture with the protoplast solution.

Detection of the MB-probe inside cell was performed by a laser scanning fluorescence microscope. Figure 4.12 shows the abundance of fluorescence in the cell-nucleus compared to the control study. Further analysis of the fluorescence spectrum yielded an emission maximum of 515 nm (see Figure 4.13), which is in fact, matches with the emission of the FAM which is labeled at the 5'-end of the MB-probe **21**. This confirms that the fluorescence obtained in the cell-nucleus (Figure 4.12) is due to the incorporation of the MB-probe containing the CPD-lesion. Further experiments to study the actual repair of the CPD-lesion inside the cell, is currently underway.

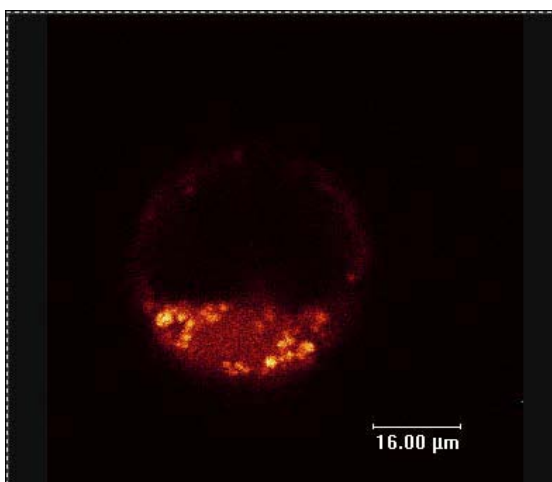


Figure 4.12: Image obtained from confocal fluorescence microscopic study. The bright fluorescence spot represents the incorporation of the MB **21** inside the cell-nucleus.

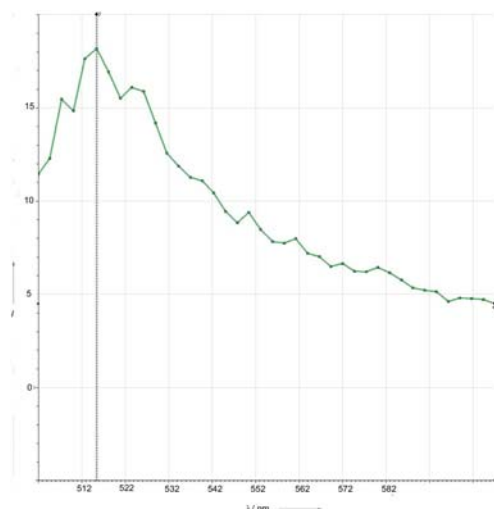


Figure 4.13: The fluorescence spectrum obtained from the Figure 4.12. The strong emission signal at 515 nm proves that its due to the fluorophore FAM.

4.7. Stability of the MB-probe in cell extract

In order to address the significant fluorescence signal in the dark control in Figure 4.11a, line 2, in section 4.5, the stability of the MB-probe 21 in the wild-type cell extract was performed. As cell extract contains many different proteins, it might react with the non-biological compounds such as the CPD-lesion, FAM and Dabsyl present in MB 21, and thereby degrade the MB.

A systematic study was performed, first with a hairpin strand 24 (5'-FAM-CGACGTXTCGTCG-3', where X= CPD-lesion), which has exactly the same sequence as MB 21 but without the 3'-Dabsyl labeling. Hairpin 24 was diluted in the cell extract. A fraction of this solution was incubated for about 30 min in dark at 20 °C. The other fraction was irradiated in white light (to see the CPD-repair). Both samples were then analyzed by HPLC (fluorescence detection) using ion-exchange SAX-column. Figure 4.14 shows the HPLC profiles of the unirradiated

(Figure 4.14a) and irradiated (Figure 4.14b) samples. The sharp, single peak of the hairpin **24** in Figure 4.14b, clearly explains that the FAM and the incorporated CPD-lesion are fairly stable in cell extract. On the other hand, the HPLC of the irradiated sample (Figure 4.14b) showed a new peak at about 21 min of elution time which is proved, by co-injection study, to be the FAM containing repaired strand **22**. This experiment proves that photolyase is active and is recognized by the hairpin **24** in the cell extract. Similar experiments were performed to test the stability of this hairpin in mutant cell extract. The dark control, after 30 min of incubation in a dark room, showed no change in HPLC (not shown in Figure). The irradiated sample also did not yield any new peak in HPLC analysis proving that neither hairpin degradation nor CPD-repair occurred in the mutant cell extract which devoid of any photolyase.

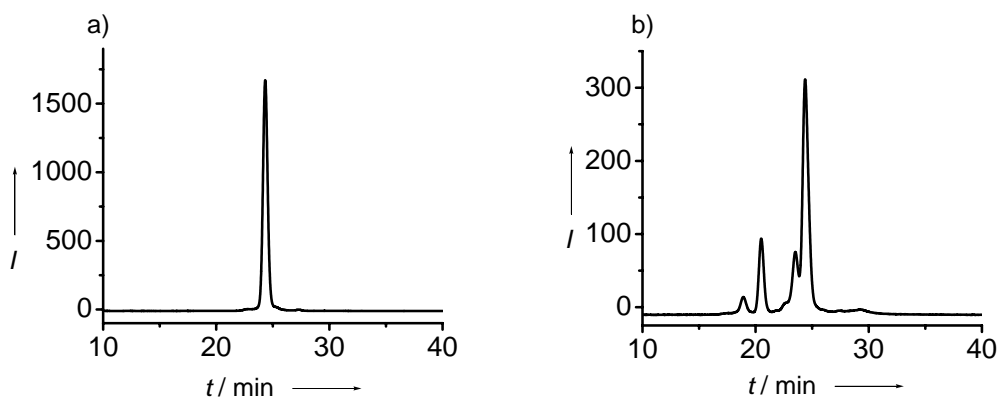


Figure 4.14: Depiction of HPLCs of the hairpin **24** in wild-type cell extract: **a)** probe taken in cell-extract was incubated in dark for 30 min and **b)** probe in cell extract was irradiated in white light for about 30 min.

Incubation of the MB **21** in wild-type cell extract in dark for 60 min, followed by HPLC analysis produced about 30% degradation of the MB **21** (not shown in

Figure). The main degraded peak is assumed to be due to lose of the 3'-Dabsyl. The reason might be due to presence of a sulphamide group in Dabsyl (see Figure 4.3, section 4.2 for structure of Dabsyl) instead of a biologically relevant amide group.

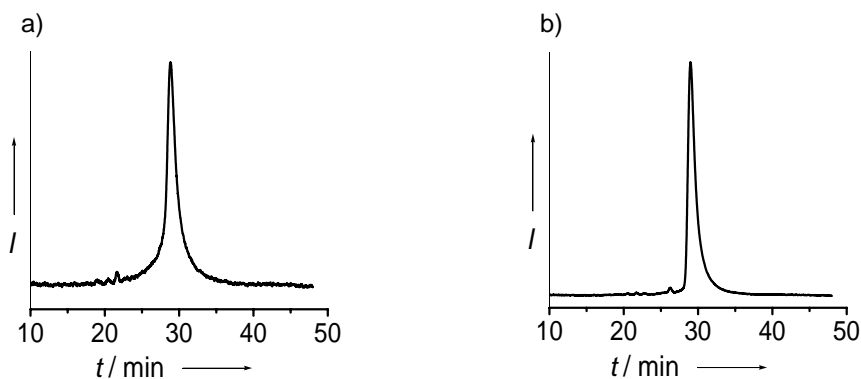


Figure 4.15: HPLC profiles for the stability of the MB 25 in wild-type cell-extract: a) HPLC of the probe before addition of the cell-extract and b) HPLC after incubating MB 25 in cell extract in dark for 60 min.

In order to improve the sensitivity of the MB-probe to study CPD-repair in cell extract and in future, in living cell, a new MB-probe was synthesized with same sequence as MB 21 but replacing 3'-Dabsyl by 3'-Dabcyl which contain an amide group instead of a sulphamide group (see Figure 4.3). The stability of this probe (MB 25: 5'-FAM-CGACGTXTCGTCG-3'-Dabcyl where X= CPD-lesion) was tested after incubating in cell extract. Incubation of this probe in cell extract in dark for about 60 min yielded no degradation of this strand, as depicted in Figure 4.15. Hence, this MB 25 can be an efficient DNA-probe with required sensitivity to study CPD-repair in wild-type cell extract and also in living cell.

4.8. Summary and conclusion

The detailed analysis of the DNA, RNA, and protein-content (genome, transcriptome and proteome) of cells is of paramount importance for our understanding of the complex functional networks that control life. Knowledge gained in the areas of genomics^[146] and proteomics^[235, 236] may lead to the discovery of new pharmaceutical targets and the development of novel therapeutic strategies.

Genomic DNA in cell is constantly undergoing damages due to various factors. The DNA-lesions are mutagenic and hence are harmful for the cell. DNA-photoproducts are the damages formed due to UV-exposure and need to be repaired to maintain healthy cell divisions. Photolyase was found to be the major defense system of the plants as well as many other organisms. CPD-photolyases are known to repair the CPD-photolesions in a light-driven process.

In the present work, the photoreversion of a thymidine CPD-lesion by photolyase enzyme, isolated from *A. nidulans* and *A. thaliana*, was studied using a recently developed molecular beacon probe technique. The photolyase-substrate MB **21** contained a synthetic thymidine CPD-lesion which mimics naturally occurring CPD-lesion. This lesion was designed to induce a strand break during photolyase-catalyzed dimer repair. The MB **21** served as an efficient and sensitive probe to profile photolyase-activities. The activities of both Type-II (*A. nidulans*) and Class-II (*A. thaliana*) CPD-photolyases were profiled with this new probe methodology.

The sensitivity of the probe DNA **21** was tested with wild-type and over-expressed cell extracts isolated from *A. thaliana*. The probe could successfully detect photolyase activity even within a wild-type extract, despite of the fact that a significant background activity was observed. Effort was made to investigate the repair process within a living cell, using fluorescence microscopy. Towards this goal the MB **21** was injected into the living cell. The insertion of this artificial, chemically modified DNA-substrate in the cell nucleus was achieved.

5. Experimental Section

5.1. Materials and methods

5.1.1. Equipments used in this study

Oligonucleotide Synthesis: The oligonucleotide strands were synthesized on a *Perseptive Biosystems' Expedite™ 8900* DNA synthesizer, *Model: 8909*, a versatile dual column instrument. The model 8909 of the 8900 series can use up to nine nucleotide monomer reservoirs and eight ancillary reagent reservoirs with a total capacity of 800 cycles at 0.2 μ mole scale. The protected phosphoramidites were purchased from *Glen Research*. The solid CPG-supported oligonucleoside cartridges were bought from *PE Biosystems*. The other ultra dry reagents (*p.a*) were purchased from *Fluka*, *Aldrich* and *Roth*. The solvent acetonitrile for activator and the phosphoramidite monomers were bought from *Roth* with a water content of less than 10 *ppm*. The synthesis was carried out by following standard DNA synthesis protocol provided by *Perseptive Biosystems'*.

UV/Vis Spectrometry for melting point measurement: Absorptions, concentrations and melting temperatures (T_m) of the oligonucleotide strands were measured with a *Varian Cary Bio 100* UV-spectrometer equipped with a *Cary Temperature Controller*, *Sample Transport Accessory* and *Multi Cell Block*. A constant flow of nitrogen kept the sample block^[241] free from air/moisture. The

temperature of the probe was measured from a reference cuvette containing only water. A constant gradient of 5 °C/min was used for melting point measurements. Cuvettes of 4 mm inner-diameter and 10 mm path length, purchased from *Helma*, were used. The extinction-coefficient (ϵ_{260}) of the oligos were calculated by algebraic addition of the ϵ_{260} of the individual monomeric nucleobases. The used values are given in Table 5.1. The extinction-coefficient of the thymidine dimer (CPD) was approximately taken as twice that of a 2'-deoxythymine monomer.

Table 5.1: Tabulation of the extinction coefficient (ϵ_{260}) of the nucleosides at 260 nm.

Nucleobases	dA	dC	dG	dT	6-Fam	T=T dimer
ϵ_{260} (mmol ⁻¹ . cm	15.01	7.11	12.01	8.41	21.00	16.81 (2*dT)

The concentration of a DNA oligonucleotide was determined by its relative absorptivity at 260 nm and was calculated using standard program. The melting point (T_m) was determined as follows: an array of melting curves of a given DNA-strand were plotted in *Origin^R* and fitted with 9th order polynomial function. The null point of the second derivative of the polynomial function gave the value of 'point of inflection' which is the melting point of the oligonucleotide strand.

Fluorescence Spectroscopy: Fluorescence spectra were measured using *JASCO-FP-750* fluorescence spectrometer (150 W Xe-lamp, single monochromator) equipped with a *Temperature Controller*. A DNA concentration of about 0.2 μM (200 μL) was used in a 2 mm fluorescence cuvette (*Helma*).

Circular Dichroism (CD) Spectroscopy: The conformations of the oligos were determined with a *J810 spectropolarimeter* from *JASCO*. A *CDF426 temperature controller* was used to monitor the temperature during measurements.

HPL-Chromatography: The synthesized oligos were purified and analyzed by HPL-Chromatograms. For analytical studies, a *Merck-Hitachi HPL-Chromatogram (Darmstadt, Germany)* with *D-7000* interface module, *L-7480* fluorescence detector, *L-7400* UV-detector, *L-7200* autosampler, *L-7100* pump and a *L-7612* degasser were used along with an external column thermostat from *JASCO*. The purification of the oligonucleotides were also performed by a *Merck-Hitachi HPL-Chromatogram (Darmstadt, Germany)* configured with an *D-7000* interface, *L7420* UV-Vis detector, *L-7150* pump and *L-7350* column oven. The sample to be purified was injected manually *via rheodyne*. For LCMS and HPLC-ESI-MS/MS, an *Agilent Technologies (Waldbronn, Germany) 1100 series HPLC* was employed, configured with a quaternary pump, vacuum degasser, autosampler, column thermostat, and UV-detector (variable wavelength). A variety of columns were utilized depending upon purposes. For DNA purification, preferentially a *Nucleosil 100-7 C18 Macherey-Nagel* column (250*10 mm) was explored. Analytical separations were performed with a series of different columns: reverse phase *Nucleosil 100-5 C18 (250*4)* and *120-3 C18 (250*4 mm)* columns were used from

Macherey-Nagel; ion exchange *Nucleogel SAX* (1000-8) from *Macherey-Nagel* was explored extensively for UV-induced damage studies. A highly efficient *Uptisphere 3 HDO C18* (150*2.1 mm) was used for LCMS analysis.

The buffers were prepared from quality *puriss. p.a* or *purum* reagents and solvents, purchased preferentially from *Fluka*. *Purum* solvents were distilled prior to use. The commercially available reagents were used without further purification.

Mass Spectroscopy (MS): The MS service was generously obtained from the *Department of Chemistry, Philipps University Marburg*; *AG Marahiel (Department of Chemistry, Philipps University Marburg)* and *Department of Chemistry and Pharmacy, Ludwig-Maximilians University Munich*. The ESI-Mass Spectrometries were either from *Finnigan TSQ7000* (probe concentration ca 10^{-5} M in MeOH or MeCN, flow 25 μ L/min, N₂ spray) or *Finnigan MAT95*. ESI-MS/MS were measured with a *QStar Pulsar i (ESI-Q-q-TOF)* mass spectrometer from *Applied Biosystem, Darmstadt, Germany*. MALDI-TOF mass spectra were measured with a *Brucker Biflex III* instrument (Matrix: 2,4,6-Trihydroxyacetophenon (0.5 M in EtOH)/Diammoniumcitrate (0.1 M in water) in 1:1 vol. ratio or 3-Hydroxypicolinic acid (0.5 M) in acetonitrile/water mixture in 1:1 vol. ratio). Probes were measured either with normal mode (both positive and negative) or reflective mode (negative) with 19 kV acceleration voltage. Irradiated DNA probes were desalted prior to measurement, through *MF-MilliporeTM* membrane filter (pore size 0.025 μ m). The mass signals were assigned by their *m/z* values.

Capillary Electrophoresis: A *P/ACETM MDQ* DNA system from *Beckman Coulter* was employed for analytical separation of oligo nucleotides. Separations were performed on the basis of *mass/size (m/z)* of the oligos. A 21 cm long, fused-silica capillary was used for analysis. The stationary phase was a highly viscous polyacrylamide gel, purchased from *Beckman Coulter* and was prepared with double distilled water. Tris-Borate-EDTA buffer also from *Beckman Coulter*, served as the mobile phase. The buffer contained 7 M urea, to suffice the DNA double strand denaturation. DNA probes were injected into the capillary by immersing the two ends of the capillary (function as electrodes) into sample vial for over 2 sec. with 10 kV injection voltage and were measured at a constant separation voltage of 9 kV for a period of 45 min. The detector was either a dual wavelength *laser induced fluorescence (LIF)* detector (488 nm argon ion laser module) or a *UV-VIS* detector.

Some of the other equipments used in this study are listed in below in table 5.2.

Table 5.2: Equipments used for DNA-damage and repair studies.

<i>Equipment</i>	<i>Manufacturer</i>
Autoclave	Systemec (Wettenberg)
Speed vac	Savant (Zürich)
Centrifugate	Heraeus AG
Rotovapor	Heidolph
Thermomixer comfort	Eppendorf

Oligonucleotides

The chemically available oligos were purchased from *Metabion* or *MWG-Biotech AG* (Germany). Oligos were further purified by HPLC and characterized by MADI-TOF. The RNA's and DNA-RNA mixed oligos were purchased from *IBA* (Germany) and were used without further purification.

5.1.2. Materials and Reagents

Solvents and Chemicals: All used solvents and chemicals were of analytical grade (*p.a*) and were purchased from *Fluka* (Deisenhofen), *Sigma* (München), *Roth* (Karlsruhe), *Acros* (Belgium) and *Merck* (Darmstadt). Solvents were distilled prior to use and dried when needed following established protocols. Distillations were performed using rotovapor from *Büchi*. Dry solvents for DNA synthesis were further dried over molecular sieve (4 Å) prior to use. A list of materials used is shown in Table 5.3.

Table 5.3: List of important materials used for this study.

<i>Materials</i>	<i>Manufacturer</i>
Quartz cuvettes	Helma (Mülheim)
Pipettes	Eppendorf, ABimed (France)
DNA CPG-cartridges	Glen Research
Eppendorf cups	VWR (Darmstadt)
PCR tubes	VWR (Darmstadt)
Membrane filters	Millipore
Sep-pak ^R C-18 cartridges	Waters Millipore
syringe filters (0.45 µm and 0.2 µm)	Whatman, Macherey-Nagel
HPLC vial	VWR

Enzymes for DNA digestion

The commercial enzymes used for oligonucleotide digestion is depicted in Figure 5.4.

Table 5.4: List of the commercial enzymes used in this study

Nuclease P1 (from penicillium citrinum)	Roche Diagnostic GmbH
Phosphodiesterase I (from snake venom)	USB
Phosphodiesterase II (from calf spleen)	CalBioChem
Alkaline Phosphatase (CIP)	BioLabs

5.2. *Methods*

5.2.1. *DNA damage study*

5.2.1.1. *Purification of oligos*

All purchased DNA-hairpins were further purified by reversed-phase HPL-chromatography. About 1 mL of concentrated DNA was injected manually into the HPLC *via rheodyne*. Peaks were detected by absorption at 260 nm. The following protocol was used for purification:

VP 250/10 Nucleosil 100-7 C18 column from *Macherey-Nagel*

Buffer A: 0.1 M Triethylammoniumacetate in H₂O

Buffer B: 0.1 M Triethylammoniumacetate in H₂O/ 80% Acetonitrile

Flow: 5 mL /min

Gradient: 0-45% B in 35 min

5.2.1.2. **Characterization of oligos**

The purified DNA was dissolved in about 1 mL double-distilled water in an eppendorf cup. DNA was characterized by its m/z value obtained from *MALDI-TOF*. Two kinds of matrices were used for the measurement:

2,4,6-Trihydroxyacetophenon (0.5 M in EtOH)/Diammoniumcitrate (0.1 M in water) in 1:1 vol. ratio

3-Hydroxypicolinic acid (0.5 M) in acetonitrile/water (1:1 vol. ratio)

A 1:1 mixture (by volume) of a DNA-probe (1-10 pmol/ μL) and the matrix was prepared. About 0.5 μL was pipetted onto the target which was subsequently allowed to dry at room temperature to obtain solid crystal. *MALDI-TOF* was measured either in normal mode (positive or negative) or reflector mode (negative) with 19 KV acceleration voltage.

5.2.1.3. **Concentration and melting point determination**

With a fraction of the DNA stock solution, optical density (OD) was measured at 260 nm. The probe solution, taken in a UV-cuvette, was heated to 85 °C inside UV-spectrometer and OD_{260} was measured compared to a reference cuvette filled only with double-distilled water. Concentration of the DNA stock solution was then determined applying *Lamberts-Beer's* equation:

$$A_{260} = \log I/I_0 = c \cdot \epsilon_{260} \cdot d$$

$$\epsilon_{260} = \sum_i \epsilon_i$$

where A_{260} is the absorbance of the probe at 260 nm which is determined from the intensity of the transmitted light (I) compared to the intensity of the emerging light (I_0), c is the concentration of the probe DNA, ϵ_{260} is the algebraic sum of extinction-coefficients of the individual nucleosides at 260 nm and d is the path-length of the light through the sample.

A 3 μM DNA solution was prepared in 150 mM NaCl/10 mM Tris-HCl buffer (pH 7.4) for melting point (T_m) determination. The solution (900 μL) was taken in a UV-cuvette with a thin layer of silicon-oil on top of it, to prevent evaporation. Absorptions (A_{260} , A_{280} , A_{320}) were measured, at a constant temperature gradient of 0.5 $^{\circ}\text{C}/\text{min}$ starting from 5 $^{\circ}\text{C}$ to 95 $^{\circ}\text{C}$. T_m was computed from a plot of absorptions against temperature in *Origin*^R.

5.2.1.4. Hybridization of oligos

Oligonucleotides, which preferentially adopt a tertiary, undefined structure in their normal state, were hybridized with their counter-strands (for hairpins, self hybridization), prior to any experiment, to obtain a well defined duplex structure. Oligonucleotide solutions, prepared in 150 mM NaCl/10 mM Tris-HCl (pH 7.4) buffer in eppendorf cups (1.5-2 mL), were heated to 85 $^{\circ}\text{C}$ in a *Test Tube Thermostat (TCR100, Roth)* containing pure water for a duration of 5-7 min. Turning off the power supply allowed slow cooling of the blocks to room temperature and subsequent annealing of the oligos.

Hybridizations were also performed inside PCR instrument by heating the probes (taken in PCR tubes) to 90 °C and subsequent cooling to 4 °C with a temperature gradient of 0.5 °C/min.

5.2.1.5. Irradiation of hairpins

All irradiations were performed at 254 nm (± 10 nm) inside a fluorimeter (150 W Xe-lamp). All oligonucleotide solutions were prepared at the same concentration (0.2 μ M) in a buffer containing 150 mM NaCl/10 mM Tris-HCl; pH = 7.4. About 200 μ L of each solution was taken in a 2 mm fluorescence cuvette and was irradiated for duration of 20-30 min at a constant temperature of 10 °C. A constant flow of nitrogen always kept the probe chamber free from oxygen/moisture in order to avoid any oxidation of DNA by external agents. After irradiation, 20 μ L of solution was injected into the HPLC for damage formation analysis.

Irradiation of DNA probe for enzymatic digestion was performed with a 254 nm hand lamp (2*15 W) from *Vilbert Lourmat (France)*, having an energy fluence rate of 7 mW/cm². DNA, RNA and/or DNA-RNA mixed hairpins (20 μ M) was irradiated for 14-15 min in a dark room at 10 °C, to produce enough damage for MS/MS analysis.

5.2.1.6. Desalting oligos by Sep-pak C18

The duplex oligonucleotide hairpins were desalted after irradiation through *sep-pak C18* column. The procedure involved the following steps.

Step 1: The column was activated by purging it with 10 mL Acetonitrile over 1 min.

Step 2: Column was then slowly equilibrated with 10-15 mL of double distilled H₂O over a period of 2 min.

Step 3: The remaining H₂O was pushed out of the column by purging air through it.

Step 4: DNA (less than 1 mL) was then injected onto the column by a syringe with a flow of about 1 mL /min

Step 5: Column was washed with 3-4 mL of double distilled H₂O with a flow of about 2 mL /min to get rid of all the salts present with DNA sample.

Step 6: Column was made dry by pumping air (about 2 mL) through it.

Step 7: Finally DNA was eluted using 4-5 mL of 80:20 Acetonitrile/water for a period of 3 min.

5.2.1.7. HPLC detection of DNA-damage

The lesion containing oligonucleotides, after irradiation, were separated and identified from their undamaged counterpart by means of analytical HPLC. A new methodology employing *Nucleogel-SAX-column* was established for the damage-separation.

All analyses were performed at room temperature (25 °C) using HPL-chromatography associated with a fluorescence detector (L-7480). A *Nucleogel-SAX (1000-8)* column, purchased from *Macherey-Nagel* was utilized for the separation. The following protocol was used.

Buffer A: 0.2 M NaCl/0.01 M NaOH in H₂O, pH = 13

Buffer B: 1.0 M NaCl/0.01 M NaOH in H₂O; pH = 13

Flow rate: 0.7 mL/min

Gradient: 0-75% B in 25 min and then to 85% B in 35 min.

20 µL of a sample was injected into the HPLC through an autosampler (L-7200). The fluorescence detector was set at an excitation-wavelength of 495 nm, which is the absorption maximum of 6-FAM. Consequently, emission spectrum was measured at 520 nm.

Detection of damage formation for very short, single-stranded oligonucleotides (4-6 nucleobases long) was achieved by reversed-phase (C18) column using a very flat gradient. The slight polarity difference between a dinucleotide and a photodimer could be detected by *120-3 C18* column only for very short oligonucleotides. The separation conditions were as follows:

VP 250/4 *Nucleosil 120-3 C18* column from *Macherey-Nagel*

Buffer A: 0.1 M Triethylammoniumacetate in H₂O

Buffer B: 0.1 M Triethylammoniumacetate in H₂O/80% Acetonitrile

Flow: 0.6 mL/min

Gradient: 0 to 30% B in 90 min

5.2.1.8. Determination of conformations of the hairpins

The conformations of the DNA, RNA and DNA/RNA mixed hairpins were determined using CD spectrometry. The probe (3 μM , 900 μL), taken from the UV-spectrometer after the T_m measurement, was used CD analysis at 25 $^{\circ}\text{C}$.

5.2.1.9. Enzymatic digestion

In order to characterize the photoproducts formed upon UVC irradiation, oligonucleotide hairpin was fully digested into the individual nucleobases by action of a set of enzymes. In addition to four canonical nucleobases, the irradiated hairpin also produced dinucleotide photoproducts upon enzymatic digestion. The hairpin (20 μM), after irradiation for 15 min by 254 nm hand lamp and subsequent desalting, was treated for complete enzymatic-digestion. A 100 μL (20 μM) solution of the oligonucleotide was taken in an Eppendorf cup. The digestion was performed in two steps at different pH conditions. The buffers used were:

Buffer A: 300 mM ammonium acetate, 100 mM CaCl_2 and 1 mM ZnSO_4 ; pH = 5.7

Buffer B: 500 mM Tris-HCl, 1 mM EDTA; pH = 8.0

Step 1: 10 μL of buffer A was added to the probe solution followed by addition of nuclease P1 (penicillium citrinum): 20 units
and phosphodiesterase II (calf spleen): 0.5 units

The solution was incubated at 37 °C for about 3 hrs in a thermomixer.

Step 2: to the resulting solution from *step 1*, 12 µL of buffer B was added to raise the pH to approximately 8.0 followed by successive addition of alkaline phosphatase (calf intestine) 10 units and phosphodiesterase I (snake venom) 0.1 unit

The solution was further incubated for a period of 2-3 hrs at 37 °C. The solution thus obtained was added to 6 µL of hydrochloric acid (0.1 N) to bring the pH down to approximately 7.0. The solution was then centrifuged at 3000 g for about 5 min to precipitate the excess enzymes. The supernatant aqueous phase was collected and transferred to another Eppendorf cup for storage at -80 °C. A 30 µL solution was transferred into HPLC injection vial for damage analysis. Samples were analyzed by HPLC-MS/MS system to characterize dinucleotide-monophosphate photoproducts. As a control, a parallel digestion was always performed with the corresponding unirradiated oligonucleotide.

5.2.1.10. HPLC-MS/MS analysis

The individual nucleosides and the lesion dinucleotides, after enzymatic digestion were identified by HPLC coupled to a mass spectrometer. A highly efficient *Uptisphere 3 HDO* column (150*2.1 mm) was utilized for separation of the nucleosides. The following conditions were used for the separation.

Buffer A: 2 mM Triethylammonia/Acetic acid in H₂O

Buffer B: 2 mM Triethylammonia/Acetic acid in 80% Acetonitrile/ 20% H₂O

Gradient: A mixed gradient was used with 0-3% B in 12 min and up to 20% B in 30 min.

Flow rate: A very low flow rate of 0.2 mL/min was used in order to facilitate detection of individual masses.

The UV detector was set at 210 nm, since most of the dinucleotide photoproducts absorb at this wavelength. A sample volume of 30 μ L of 20 μ M concentration was injected. The components coming apart from HPLC were allowed to pass through a Qstar i pulser mass spectrometer (*Applied Biosciences*) at a maximum flow rate of 200 μ L/min where they were ionized and were subsequently measured by ESI-MS. The characterization of the photoproducts was performed with a quadrupole. Here an ion of a particular m/z value was selected depending on its frequency and was passed through the quadrupole on a stable flight path where it gets fragmented and was identified by its characteristic fragmentation pattern.

The polarity was always set to the negative ion mode with ion-spray voltage of -4000 V. Ion source gas¹ was set to 40, curtain gas to 25. Other measuring parameters were as follows: DP1 -60V, FP -225V, DP2 -10V.

The TOF range was chosen from 150 amu to 600 amu for both MS and MS/MS measurements. For ESI-MS a standard CAD-gas value of 3 was used, while it was increased to 7 for MS/MS analysis. For better signal intensities, the product ion scans (MS/MS) were performed in the 'Enhance All' modes with a value of -34 V for the collision energy (CE), while the first quadrupole (Q1) was fixed during these experiments to the mass of the ions of interest.

5.2.2. DNA repair

5.2.2.1. Synthesis of oligonucleotides

The oligonucleotides containing lesions were synthesized with a *Perseptive Biosystems' Expedite™ 8900* automated DNA synthesizer (Figure 5.1). Synthesis was performed on a controlled pore glass (CPG) supported cassette (cartridge). The cassette usually contained the 3'-nucleoside attached to CPG support. Synthesis was usually carried out automatically by sequential addition of β -cyanoethyl phosphoramidite monomers from 3' to 5' direction. The monomers and most of the other reagents were prepared with 10 ppm acetonitril (*p.a*) and were left overnight on pre dried molecular sieves (4Å) in dark. The following reagents were used during synthesis in 1.3 μ mol scale.

Phosphoramidite A, T, G, C: 0.10 M in 10 ppm MeCN

Modified Phosphoramidites: 0.15 M in 10 ppm MeCN

Detritylation: 3% Dichloroacetic acid in Dichloromethane (DCM)

Activator: Turbotetrazole (0.15 M) with 0.45 M tetrazole in THF

Capping (Cap A): Pac-anhydride (0.53 M), 2,6-Lutidin (11.1%) in 30 ppm MeCN

Capping (Cap B): N-Methylimidazol (16%) in 30 ppm MeCN

Washing: Dichloromethane, 30 ppm Acetonitril (MeCN)

Oxidation: Iodine (0.01 M) in 2,6-Lutidin/acetonitrile/H₂O 0.6:6.5:3



Figure 5.1: Depiction of a *Perseptive Biosystems' Expedite™ 8900* automated DNA synthesizer used in this study for automated DNA-synthesis.

After installing the reagents, the channels were filled up with fluids by priming each reagent following the procedure in the manual. All syntheses were performed with 'DMT-on' mode. The coupling time for usual phosphoramidites was 1 min and that of the modified phosphoramidites was chosen as 5 min. The advancement of the synthesis was monitored with a 'trityl viewer' on the basis of UV absorbance of the outgoing trityl group produced during detritylation.

5.2.2.2. **Deprotection of the oligonucleotide**

After the DNA synthesis is over, the cartridge was taken out of the synthesizer, transferred into an eppendorf (2 mL) cup and the DNA was cleaved from the solid support. The following protocol was employed for the deprotection.

DNA Cartridge: 1 μ mol

Ammonia (30% in H₂O, *p.a*): 0.9 mL

Ethanol (*p.a*): 0.3 mL

Temperature: 55 °C

Time: 12 hrs

Incubation speed: 1000 rpm

Deprotection of the oligonucleotide from the solid CPG-support and the cleavage of the phosphoramidite-protecting groups could be performed at room temperature in 4 hr. But for modified phosphoramidites such as *cis-syn* CPD-silyl-thymidine dimer or 6-FAM, an extended period of 12-14 hrs was used at elevated temperature, as shown above.

After deprotection, ammonia was evaporated in a *speed vac*, sample was diluted with double distilled water (0.5 mL) and the glass beads were filtered 'off' through a Whatman 0.2 μ m syringe filter. The solution was then concentrated in a *speed vac*, and finally a solution of 1 mL was made and stored at -80 °C.

5.2.2.3. **Purification of oligonucleotides**

The deprotected DNA was purified from the unsuccessfully coupled sequences by reversed-phase HPLC as described earlier in this section. For hairpin DNAs, purification were performed at an elevated column temperature of 50 °C.

VP 250/10 *Nucleosil 100-7 C18* column from *Macherey-Nagel*

Buffer A: 0.1 M Triethylammoniumacetate in H₂O

Buffer B: 0.1 M Triethylammoniumacetate in H₂O/80% acetonitrile

Flow: 5 mL/min

Gradient: 0-45% B in 35 min

Fractions were collected in 10 mL eppendorf tubes, followed by evaporation of the solvent and finally transferred into 2 mL eppendorf cups. The identity of the desired DNA was confirmed by MALDI-TOF measurement. Finally a stock solution of 1 mM was made and was stored at -80 °C for further studies.

5.2.2.4. **Repair studies with the purified *A. nidulans* photolyase**

Repair measurements were performed using a fluorescence spectrometer (*JASCO-FP-750*). An assay solution (100 µL) containing photoreactivation buffer (NaCl: 150 mM, Tris: 10 mM), DTT (10 mM) and *A. nidulans* enzyme (0.15 µM) was prepared. The solution, taken in a cuvette, was sealed with a rubber-septum and was set free from oxygen by purging nitrogen-gas slowly through the sample for about 2 min. The complete reduction and activation of the FAD-containing *A.*

nidulans was performed by shining white-light onto the solution for about 1 min, followed by addition of the substrate molecular beacon **21** (0.2 μM). For the catalytic study, the assay solution was irradiated by white-light and the fluorescence intensity (excitation: 495 nm, emission: 520 nm) was measured time to time. The experiment was performed at 27 °C. The dark control was carried out simultaneously using a similar cuvette and identical conditions. Irradiation in the absence of photolyase was also performed under similar conditions. The analysis of the repair reaction by HPLC was performed with an assay solution (200 μL) containing molecular beacon **21** (4 μM), buffer (NaCl: 150 mM, Tris: 10 mM), DTT (10 mM) and *A. nidulans* photolyase (0.2 μM). The solution was again irradiated by white light. 10 μL samples were taken out after defined time intervals. To these samples was added 20 μL of an acetic acid (20%) solution to stop any further repair. HPLC analysis was performed using the following conditions:

VP 250/4 *Nucleosil 120-3 C18* column from *Macherey-Nagel*

Buffer A: 0.1 M Triethylammoniumacetate in H_2O , pH 7.0

Buffer B: 0.1 M Triethylammoniumacetate in $\text{H}_2\text{O}/80\%$ acetonitrile, pH 7.0

Flow: 0.7 mL/min

Gradient: 0-45% B in 35 min

5.2.2.5. Repair studies with the purified *A. thaliana* photolyase:

Repair experiment was carried out as described above. The assay solution (100 μL) contained the molecular beacon **21** (0.2 μM), photoreactivation buffer (see above) and *A. thaliana* photolyase in a concentration of 1.2 μM . The

photoreactivation of the enzyme was commenced by irradiating the assay solution under white-light for a short time. All irradiations were carried out with a 366 nm lamp (energy fluence rate 44 Wm⁻²) at 27 °C. The dark control was performed simultaneously but the assay solution was kept in the dark. Total protein extracts were prepared from rosette leaves of 21-day-old *A. thaliana* wild-type (ecotype Landsberg erecta) and photolyase mutant *uvr2-1* plants essentially as described previously.

5.2.2.6. Repair study with cell extracts:

Repair experiments were carried out as described above. The assay solution (100 µL) contained the molecular beacon **21** (0.2 µM), photoreactivation buffer (see above) and cell extracts in a final concentration of 0.7 µg per µL. All irradiations were carried out with a 366 nm lamp (44 Wm⁻²) at 27 °C. As a background control, another assay solution was kept in the dark.

6. Abbreviations

EtOH	Ethanol
MeOH	Methanol
THF	Tetrahydrofuran
MeCN	Acetonitrile
DCM	Dichloromethane
EDTA	Ethylenediaminetetraacetate
6-FAM	6-Fluorescein
THA	2,4,6-Trihydroxyacetophenone monohydrate
NEt ₃	Triethylamine
AcOH	Acetic acid
TFA	Trifluoroacetic acid
Pac-anhydride	Phenylloxyacetic anhydride
Tetrazol	5-(4-Nitrophenyl)-Tetrazol
NMR	Magnetic Resonance
min	Minute
MS	Mass Spectrometry
UV	Ultra-violet
CD	Circular Dichroism
Vol.	Volume
Min	Minute
hr	Hour
μM	Micro-molar
μL	Micro-liter
L	Liter
Oligo	Oligonucleotide

Tris Tris-(hydroxymethyl)-aminomethane hydrochloride

7. Literature

- [1] F. S. Rowland and M. J. Molina, *Rev. Geophys. Space Phys.* **1975**, *13*, 1-35, Chlorofluoromethanes in the Environment.
- [2] F. S. Rowland, *Nobel Lecture* **1995**, Nobel Lecture in Chemistry.
- [3] M. Prather, P. Midgley, F. S. Rowland and R. Stolarski, *Nature* **1996**, *381*, 551-554, The Ozone Layer: The Road Not Taken.
- [4] A. R. Ravishankara, G. Hancock, M. Kawasaki and Y. Matsumi, *Science* **1998**, *280*, 60-61, Photochemistry of Ozone: Surprises and Recent Lessons.
- [5] O. B. Toon and R. P. Turco, *Scientific American* **1991**, *264*, 68-74, Polar Stratospheric Clouds and Ozone Depletion.
- [6] H. Johnston, *Science* **1971**, *173*, 517-525, Reduction of Stratospheric Ozone by Nitrogen Oxide Catalysts from Supersonic Transport Exhaust.
- [7] M. J. Molina and F. S. Rowland, *Nature* **1974**, *249*, 810-812, Stratospheric Sink for Chlorofluoromethanes: Chloride Atom-Catalysed Destruction of Ozone.
- [8] D. T. Shindell, D. Rind and P. Lonergan, *Nature* **1998**, *392*, 589-592, Increased Polar Stratospheric Ozone Losses and Delayed Eventual Recovery Owing to Increasing Greenhouse-Gas Concentrations.
- [9] H. Slaper, G. J. M. Velders, J. S. Daniel, F. R. deGruijl and J. C. van der Leun, *Nature* **1996**, *384*, 256-258, Estimates of Ozone Depletion and Skin Cancer Incidence to Examine the Vienna Convention Achievements.
- [10] J. W. Elkins, *Nature* **1993**, *364*, 780-783, Decrease in the Growth Rates of Atmospheric Chlorofluorocarbons 11 and 12.
- [11] J. B. Kerr and C. T. McElroy, *Science* **1993**, *262*, 1032-1034, Evidence for Large Upward Trends of Ultraviolet-B Radiation Linked to Ozone Depletion.

- [12] F. S. Rowland and M. J. Molina, *Chem. & Eng. News* **1994**, 72, 8-13, Ozone Depletion: 20 Years after the Alarm.
- [13] P. J. Crutzen, *Geophys. Res. Lett.* **1974**, 1, 205-208, Estimates of Possible Future Ozone Reduction from Continued Use of Chlorofluoromethanes.
- [14] P. J. Crutzen, *Q.J.R. Meteorol. Soc.* **1970**, 96, 320-325, The Influence of Nitrogen Oxides on the Atmospheric Ozone Content.
- [15] P. J. Crutzen, *Nobel Lecture* **1995**, My Life with O₂, NO_x and other YZO_xs.
- [16] *Scientific Assessment of Ozone Depletion: 1994 (Rep. 37, World Meteorological Organization, Geneva, 1995)* Scientific Assessment of Ozone Depletion: 1994 (Rep. 37, World Meteorological Organization, Geneva, 1995).
- [17] S. B. Fels, J. D. Mahlman, M. D. Schwarzkopf and R. W. Sinclair, *J. Atmos. Sci.* **1980**, 37, 2265-2297, Stratospheric Sensitivity to Perturbations in Ozone and Carbon Dioxide: Radiative and Dynamical Response.
- [18] D. Rind, R. Suozzo, N. K. Balachandran and M. J. Prather, *J. Atmos. Sci.* **1990**, 47, 475-494, Climate Change and the Middle Atmosphere. Part I: The Doubled CO₂ Climate.
- [19] J. F. Mahfouf, D. Cariolle, J.-F. Royer, J.-F. Geleyn and B. Timbal, *Clim. Dyn.* **1994**, 9, 345-362, Response of the Meteo-France Climate Model to Changes in CO₂ and Sea Surface Temperature.
- [20] R. Müller, P. J. Crutzen, J.-U. Grooss, C. Brühl, J. M. Russell III, H. Gernandt, D. S. Mckenna and A. Tuck, *Nature* **1997**, 389, 709-712, Severe Chemical Ozone Loss in the Arctic During the Winter of 1995-96.
- [21] R. L. McKenzie, *Global Ozone Research and Monitoring Project WMO Rep. 37 Chapter 9 (WMO, Geneva, 1995)*
- [22] R. Stolarski, R. Bojkov, L. Bishop, C. Zerefos, J. Staehelin and J. Zawodny, *Science* **1992**, 256, 342-349, Measured Trends in Stratospheric Ozone.

- [23] F. S. Rowland, *Angew. Chem.* **1996**, *35*, 1786-1798, Stratospheric Ozone Depletion by Chlorofluorocarbons (Nobel Lecture).
- [24] F. R. De Gruijl and P. D. Forbes, *BioEssays* **1995**, *17*, 651-660, UV-Induced Skin Cancer in a Hairless Mouse Model.
- [25] H. Slaper, A. A. Schothorst and J. C. van der Leun, *Photodermatol.* **1986**, *3*, 271-283, Risk Evaluation of UVB Therapy for Psoriasis: Comparison of Calculated Risk for UVB Therapy and Observed Risk in PUVA-Treated Patients.
- [26] F. R. De Gruijl and J. C. van der Leun, *Health Phys.* **1994**, *67*, 319-325, Estimate of the Wavelength Dependency of Ultraviolet Carcinogenesis in Humans and Its Relevance to the Risk Assessment of a Stratospheric Ozone Depletion.
- [27] K. H. Kraemer, *Proc. Natl. Acad. Sci. USA* **1997**, *94*, 11-14, Sunlight and Skin Cancer: Another Link Revealed.
- [28] I. E. Kochevar and D. A. Dunn, *Bioorganic Photochemistry, Vol. 1*, Wiley, New York, **1990**.
- [29] R. B. Setlow, *Proc. Natl. Acad. Sci. USA* **1974**, *81*, 3363-3366, The Wavelengths in Sunlight Effective in Producing Skin Cancer: A Theoretical Analysis.
- [30] J. Jagger, *Solar UV Actions on Living Cells*, Preager: New York, **1985**.
- [31] H. N. Ananthaswamy and W. E. Pierceall, *Photochem. Photobiol.* **1990**, *52*, 1119-1136, Molecular Mechanisms of Ultraviolet Radiation Carcinogenesis.
- [32] J.-S. Taylor, *Acc. Chem. Res.* **1994**, *27*, 76-82, Unraveling the Molecular Pathway from Sunlight to Skin Cancer.

- [33] H. S. Black, F. R. de Gruijl, P. D. Forbes, J. E. Cleaver, H. N. Ananthaswamy, E. C. de Fabo, S. E. Ullrich and R. M. Tyrrell, *J. Photochem. Photobiol. B: Biol.* **1997**, *40*, 29-47, Photocarcinogenesis: An Overview.
- [34] *Sun Safety*: <http://www.pp.okstate.edu/ehs/MODULES/sun/uvindex.htm>.
- [35] S. A. Ackerman and J. A. Knox, *UV Radiation and Skin Cancer*: http://profhorn.aos.wisc.edu/wxwise/AckermanKnox/chap2/uv_radiation.html.
- [36] J.-S. Taylor, *Pure Appl. Chem.* **1995**, *67*, 183-190, DNA, Sunlight and Skin-Cancer.
- [37] J.-S. Taylor, *J. Chem. Educ.* **1990**, *67*, 835-841, DNA, Sunlight and Skin Cancer.
- [38] C. O. Doudney, in *Photochemistry and Photobiology of Nucleic Acids, Vol. II* (Ed.: S. Y. Wang), Academic Press, New York, **1976**, pp. 309-374.
- [39] J. Cadet and P. Vigny, in *Bioorganic Photochemistry, Vol. 1* (Ed.: H. Morrison), Wiley, New York, **1990**, pp. 1-272.
- [40] T. Douki and J. Cadet, in *Interface between Chemistry and Biochemistry* (Eds.: P. Jollés and H. Jörnvall), Birkhäuser Verlag, Basel, **1995**, pp. 173-197.
- [41] M. G. Friedel, M. Cichon and T. Carell, in *Organic Photochemistry and Photobiology* (Eds.: W. Horspool and F. Lenci), CRC Press, New York, **2004**, pp. 141/1-141/15.
- [42] J. Cadet, M. Berger, T. Douki, B. Morin, S. Raoul, J.-L. Ravanat and S. Spinelli, *Biol. Chem.* **1997**, *378*, 1275-1285, Effects of UV and Visible Radiation on DNA -Final Base Damage.
- [43] H. T. Nguyen and K. W. Minton, *J. Mol. Biol.* **1988**, *200*, 681-693, Ultraviolet-Induced Dimerization of Non-Adjacent Pyrimidines. A Potential Mechanism for the Targeted -1 Frameshift Mutation.

- [44] T. Douki, G. Laporte and J. Cadet, *Nucleic Acids Res.* **2003**, *31*, 3134-3142, Inter-Strand Photoproducts Are Produced in High Yield within A-DNA Exposed to UVC Radiation.
- [45] J. T. Millard, S. Raucher and P. B. Hopkins, *J. Am. Chem. Soc.* **1990**, *112*, 2459-2460, Mechlorethamine Cross-Links Deoxyguanine Residues at 5'-GNC Sequences in Duplex DNA Fragments.
- [46] H. T. Nguyen and K. W. Minton, *J. Mol. Biol.* **1989**, *210*, 869-874, Extensive Photodimerization of Non-Adjacent Pyrimidines.
- [47] P. A. Todd and B. W. Glickman, *Proc. Natl. Acad. Sci. USA* **1982**, *79*, 4123-4127, Mutational Specificity of UV Light in *E. Coli* : Indication for a Role of DNA Secondary Structure.
- [48] L. M. Kundu, U. Linne, M. Marahiel and T. Carell, *Chem. Euro. J.* **2004**, *10*, 5697-5705, RNA Is More UV Resistant Than DNA: The Formation of UV-Induced DNA Lesions Is Strongly Sequence and Conformation Dependent.
- [49] T. Douki and J. Cadet, *Biochemistry* **2001**, *40*, 2495-2501, Individual Determination of the Yield of the Main UV-Induced Dimeric Pyrimidine Photoproducts in DNA Suggests a High Mutagenicity of CC-photolesions.
- [50] T. Douki and J. Cadet, *Biochemistry* **1994**, *33*, 11942-11950, Formation of Cyclobutane Dimers and (6-4) Photoproducts Upon Far-UV Photolysis of 5-Methylcytosine-Containing Dinucleoside Monophosphates.
- [51] T. Douki, T. Zaluzniak and J. Cadet, *Photochem. Photobiol.* **1997**, *66*, 171-179, Far-UV-Induced Dimeric Photoproducts in Short Oligonucleotides: Sequence Effects.
- [52] C. A. Smith, M. Wang, N. Jiang, L. Che, X. Zhao and J.-S. Taylor, *Biochemistry* **1996**, *35*, 4146-4154, Mutation Spectra of M13 Vectors Containing Site-Specific *cis-syn*, *trans-syn* I, (6-4), and Dewar Pyrimidone

- Photoproducts of Thymidylyl-(3'-5')-Thymidine in *Escherichia coli* under SOS Conditions.
- [53] J.-S. Taylor, D. S. Garrett and M. J. Wang, *Biopolymers* **1988**, *27*, 1571-1593, Models for the Solution Structure of the (6-4) Photoproduct of Thymidylyl-(3'→5')-Thymidine Derived *via* a Distance- and Angle-Constrained Conformation Search Procedure.
- [54] T. Douki, L. Voituriez and J. Cadet, *Photochem. Photobiol.* **1991**, *53*, 293-297, Characterization of the (6-4) Photoproduct of 2'-Deoxycytidylyl-(3'→5')-Thymidine and of Its Dewar Valence Isomer.
- [55] T. A. Slieman and W. L. Nicholson, *Appl. Environ. Microbiol.* **2000**, *66*, 199-205, Artificial and Solar UV Radiation Induces Strand Breaks and Cyclobutane Pyrimidine Dimers in *Bacillus subtilis* Spore DNA.
- [56] B. Setlow, K. J. Tautvydas and P. Setlow, *Appl. Environ. Microbiol.* **1998**, *64*, 1958-1962, Small, Acid-Soluble Spore Proteins of the α/β Type Do Not Protect the DNA in *Bacillus subtilis* Spores against Base Alkylation.
- [57] J. E. Donnellan and R. B. Setlow, *Science* **1965**, *149*, 308-310, Thymine Photoproducts but Not Thymine Dimers Found in Ultraviolet-Irradiated Bacterial Spores.
- [58] A. J. Varghese, *Biochem. Biophys. Res. Comm.* **1970**, *38*, 484-490, 5-Thyminylyl-5,6-Dihydrothymine from DNA Irradiated with Ultraviolet Light.
- [59] P. Setlow, *Environ. Mol. Mutagen.* **2001**, *38*, 97-104, Resistance of Spores of *Bacillus* Species to Ultraviolet Light.
- [60] E. Cabrera-Juárez and J. K. Setlow, *Arch. Biochem. Biophys.* **1977**, *475*, 315-322, Formation of a Thymine Photoproduct in Transforming DNA by near-Ultraviolet Irradiation.

- [61] S. C. Mohr, N. V. H. A. Sokolov, C. He and P. Setlow, *Proc. Natl. Acad. Sci. USA* **1991**, *88*, 77-81, Binding of Small Acid-Soluble Spore Proteins from *Bacillus subtilis* Changes the Conformation of DNA from B to A.
- [62] J. M. Berg, J. L. Tymoczko and L. Stryer, *Biochemistry (5th Edition)*, Freeman, New York, **2002**.
- [63] J. D. Watson and F. H. Crick, *Nature* **1953**, *171*, 737-738, A Structure for Deoxyribose Nucleic Acid.
- [64] H. G. Khorana, *Nobel Lecture 1968*, Nucleic Acid Synthesis in the Study of the Genetic Code.
- [65] E. Ohtsuka, M. W. Moon and H. G. Khorana, *J. Am. Chem. Soc.* **1965**, *87*, 2956, Studies on Polynucleotides. XLIII. The Synthesis of Deoxyribopolynucleotides Containing Repeating Dinucleotide Sequences.
- [66] R. Dawkins, *The Selfish Genes*, Oxford University Press, Oxford, **1999**.
- [67] B. A. J. Ponder, *Nature* **2001**, *411*, 336-341, Cancer Genetics.
- [68] A. P. Breen and J. A. Murphy, *Free Radic. Biol. Med.* **1995**, *18*, 1033-1077, Reactions of Oxyl Radicals with DNA.
- [69] P. Hasty, J. Campisi, J. Hoeijmakers, H. van Steeg and J. Vijk, *Science* **2003**, *299*, 1355-1359, Aging and the Genome Maintenance: Lessons from the Mouse?
- [70] G. W. Hsu, M. Ober, T. Carell and L. S. Beese, *Nature* **2004**, *431*, 217-221, Error-Prone Replication of Oxidatively Damaged DNA by a High-Fidelity DNA Polymerase.
- [71] B. B. Zhou and S. J. Elledge, *Nature* **2000**, *408*, 433-439, The DNA Damage Response: Putting Checkpoints in Perspective.
- [72] O. D. Schärer, *Angew. Chem. Int. Ed.* **2003**, *42*, 2946-2974, Chemistry and Biology of DNA Repair.

- [73] C. Coulondre and J. H. Miller, *J. Mol. Biol.* **1977**, *117*, 577-606, Genetic Studies of the Lac Repressor IV. Mutagenic Specificity in the *lacI* Gene of *Escherichia coli*.
- [74] D. E. Brash, J. A. Rudolph, J. A. Simon, A. Lin, G. J. McKenna, H. P. Baden, A. J. Halperin and J. Pontén, *Proc. Natl. Acad. Sci. USA* **1991**, *88*, 10124-10128, A Role for Sunlight in Skin Cancer: UV-Induced *P53* Mutations in Squamous Cell Carcinoma.
- [75] D. Fix and R. Bockrath, *Mol. Gen. Genet.* **1981**, *182*, 7-11, Thermal Resistance to Photoreactivation of Specific Mutations Potentiated in *E. coli* B/r *ung* by Ultraviolet Light.
- [76] J.-S. Taylor and S. Nadji, *Tetrahedron* **1991**, *47*, 2579-2590, Unraveling the Origin of the Major Mutations Induced by Ultraviolet Light, the C→T Transition at dTpdC Sites. A DNA Synthesis Building Block for the *cis-syn* Cyclobutane Dimer of dTpdU.
- [77] N. Jiang and J.-S. Taylor, *Biochemistry* **1993**, *32*, 472-481, *In Vivo* Evidence That UV-Induced C→T Mutations at Dipyrimidine Sites Could Result from the Replicative Bypass of *cis-syn* Cyclobutane Dimers or Their Deamination Products.
- [78] A. Ziegler, D. J. Leffell, S. Kunala, H. W. Sharma, M. Gailani, J. A. Simon, A. J. Halperin, H. P. Baden, P. E. Shapiro, A. E. Bale and D. E. Brash, *Proc. Natl. Acad. Sci. USA* **1993**, *90*, 4216-4220, Mutation Hotspots Due to Sunlight in the *P53* Gene of Non-Melanoma Skin Cancers.
- [79] J.-S. Taylor and C. L. O'Day, *Biochemistry* **1990**, *29*, 1624-1632, *cis-syn* Thymine Dimers Are Not Absolute Blocks to Replication by DNA Polymerase I of *Escherichia coli in vitro*.
- [80] S. K. Banerjee, R. B. Christensen, C. W. Lawrence and J. E. LeClerc, *Proc. Natl. Acad. Sci. USA* **1988**, *85*, 8141-8145, Frequency and Spectrum of

- Mutations Produced by a Single *cis-syn* Thymine-Thymine Cyclobutane Dimer in a Single-Stranded Vector.
- [81] J.-S. Taylor, D. S. Garrett, I. R. Brockie, D. L. Svoboda and J. Tesler, *Biochemistry* **1990**, *29*, 8858-8866, 1H-NMR Assignment and Melting Temperature Study of *cis-syn* and *trans-syn* Thymine Dimer Containing Duplexes of d(CGTATTATGC)_xd(GCATAATACG).
- [82] J.-K. Kim and B. S. Choi, *Eur. J. Biochem.* **1995**, *228*, 849-854, The Solution Structure of DNA Duplex-Decamer Containing the (6-4) Photoproduct of Thymidylyl(3'→5')Thymidine by NMR and Relaxation Matrix Refinement.
- [83] Y. Fujiwara and S. Iwai, *Biochemistry* **1997**, *36*, 11050-11050, Thermodynamic Studies of the Hybridization Properties of Photolesions in DNA.
- [84] Y. Jing, J. F.-L. Kao and J.-S. Taylor, *Nucleic Acids Res.* **1998**, *26*, 3845-3853, Thermodynamic and Base-Pairing Studies of Matches and Mismatched DNA Dodecamer Duplexes Containing *cis-syn*, (6-4) and Dewar Photoproducts of TT.
- [85] J. S. Taylor, D. S. Garrett and M. P. Cohrs, *Biochemistry* **1988**, *27*, 7206-7215, Solution-State Structure of the Dewar Pyrimidinone Photoproduct of Thymidylyl-(3'→5')-Thymidine.
- [86] C.-I. Wang and J.-S. Taylor, *Chem. Res. Toxicol.* **1993**, *6*, 519-523, The *trans-syn*-I Thymine Dimer Bends DNA by ~22° and Unwinds DNA by ~15°.
- [87] J. Kemmink, R. Boelens, T. Koning, G. A. van der Marel, J. H. van Boom and R. Kaptein, *Nucleic Acids Res.* **1987**, *15*, 4645-4653, 1H NMR Study of the Exchangeable Protons of the Duplex d(GCGT=TGCG)d(CGCAACGC) Containing a Thymine Dimer.

- [88] C. L. O'Day, P. J. Burgers and J.-S. Taylor, *Nucleic Acids Res.* **1992**, *20*, 5403-5406, PCNA-Induced DNA Synthesis Past *cis-syn* and *trans-syn-I* Thymine Dimers by Calf Thymus DNA Polymerase Delta *in vitro*.
- [89] D. L. Mitchell and R. S. Nairn, *Photochem. Photobiol.* **1989**, *49*, 805-819, The Biology of the (6-4) Photoproduct.
- [90] D. L. Svoboda, C. A. Smith, J. S. Taylor and A. Sancar, *J. Biol. Chem.* **1993**, *268*, 10694-10700, Effect of Sequence, Adduct Type, and Opposing Lesions on the Binding and Repair of Ultraviolet Photodamage by DNA Photolyase and (a)BC Exinuclease.
- [91] J. T. Reardon, A. F. Nichols, S. Keeney, C. A. Smith, J.-S. Taylor, S. Linn and A. Sancar, *J. Biol. Chem.* **1993**, *268*, 21301-21308, Comparative Analysis of Binding of Human Damaged DNA-Binding Protein (XPE) and *Escherichia coli* Damage Recognition Protein (UvrA) to the Major Ultraviolet Photoproducts: T[C,S]T, T[T,S]T, T[6-4]T, and T[Dewar]T.
- [92] E. C. Friedberg, G. C. Walker and W. Siede, *DNA Repair and Mutagenesis*, ASM Press, Washington, D.C., **1995**.
- [93] T. Lindahl and R. D. Wood, *Science* **1999**, *286*, 1897-1905, Quality Control by DNA Repair.
- [94] A. Sancar, *Annu. Rev. Biochem.* **1996**, *65*, 43-81, DNA Excision Repair.
- [95] R. D. Wood, *J. Biol. Chem.* **1997**, *272*, 23465-23468, Nucleotide Excision Repair in Mammalian Cells.
- [96] A. Sancar, *J. Biol. Chem.* **1995**, *270*, 15915-15918, Excision Repair in Mammalian Cells.
- [97] T. Lindahl, *Nature* **1993**, *362*, 709-715, Instability and Decay of the Primary Structure of DNA.
- [98] A. Sancar, *Biochemistry* **1994**, *33*, 2-9, Structure and Function of DNA Photolyase.

- [99] T. Carell, L. T. Burgdorf, L. M. Kundu and M. Cichon, *Curr. Opin. Chem. Biol.* **2001**, *5*, 491-498, The Mechanism of Action of DNA Photolyases.
- [100] D. L. Wulff and C. S. Rupert, *Biochem. Biophys. Res. Commun.* **1962**, *7*, 237-240, Disappearance of Thymine Photodimer in Ultraviolet Irradiated DNA Upon Treatment with a Photoreactivating Enzyme from Baker's Yeast.
- [101] A. Sancar, *Chem. Rev.* **2003**, *103*, 2203-2238, Structure and Function of DNA Photolyase and Cryptochrome Blue-Light Photoreceptors.
- [102] G. B. Sancar, *Mutat. Res.* **1990**, *236*, 147-160, DNA Photolyase: Physical Properties, Action Mechanism, and Roles in Dark Repair.
- [103] S.-T. Kim and A. Sancar, *Photochem. Photobiol.* **1993**, *57*, 895-904, Photochemistry, Photophysics, and Mechanism of Pyrimidine Dimer Repair by DNA Photolyases.
- [104] G. B. Sancar and A. Sancar, *Trends in Biochem. Sci.* **1987**, *12*, 259-261, Structure and Function of DNA Photolyases.
- [105] C. S. Rupert, S. H. Goodgal and R. M. Herriott, *J. Gen. Physiol.* **1958**, *41*, 451-471, Photoreactivation *in vitro* of Ultraviolet Inactivated Hemophilus Influenzae Transforming Factor.
- [106] G. B. Sancar, M. S. Jorns, G. Payne, D. J. Fluke, C. S. Rupert and A. Sancar, *J. Biol. Chem.* **1987**, *262*, 492-498, Action Mechanism of Escherichia-coli DNA Photolyase 3. Photolysis of the Enzyme-Substrate Complex and the Absolute Action Spectrum.
- [107] G. B. Sancar, F. W. Smith, R. Reid, G. Payne, M. Levy and A. Sancar, *J. Biol. Chem.* **1987**, *262*, 478-485, Action Mechanism of Escherichia-coli DNA Photolyase 1. Formation of the Enzyme-Substrate Complex.
- [108] M. S. Jorns, E. T. Baldwin, G. B. Sancar and A. Sancar, *J. Biol. Chem.* **1987**, *262*, 486-491, Action Mechanism of *Escherichia-coli* DNA Photolyase 2. Role of the Chromophores in Catalysis.

- [109] G. Payne and A. Sancar, *Biochemistry* **1990**, *29*, 7715-7727, Absolute Action Spectrum of E-FADH₂ and E-FADH₂-MTHF Form of Escherichia coli DNA Photolyase.
- [110] A. Sancar and G. B. Sancar, *J. Mol. Biol.* **1984**, *172*, 223-227, Escherichia coli DNA Photolyase Is a Flavoprotein.
- [111] T. Tamada, K. Kitadokoro, Y. Higuchi, K. Inaka, A. Yasui, P. E. de Ruiter and A. P. M. Eker, *Nat. Struct. Biol.* **1997**, *4*, 887-891, Crystal Structure of DNA Photolyase from *Anacystis nidulans*.
- [112] H.-W. Park, S.-T. Kim, A. Sancar and J. Deisenhofer, *Science* **1995**, *268*, 1866-1872, Crystal Structure of DNA Photolyase from Escherichia coli.
- [113] A. Sancar, F. W. Smith and G. B. Sancar, *J. Biol. Chem.* **1984**, *259*, 6028-6032, Purification of *Escherichia coli* DNA Photolyase.
- [114] B. J. van de Breg and G. B. Sancar, *J. Biol. Chem.* **1998**, *273*, 20276-20284, Evidence for Dinucleotide Flipping by DNA Photolyase.
- [115] R. J. Roberts, *Cell* **1995**, *82*, 9-12, On Base Flipping.
- [116] S. D. Bruner, D. P. G. Norman and G. L. Verdine, *Nature* **2000**, *403*, 859-866, Structural Basis for Recognition and Repair of the Endogenous Mutagen 8-Oxoguanine in DNA.
- [117] R. S. Lloyd and X. Cheng, *Curr. Op. Chem. Biol.* **1998**, *4*, 139-151, Mechanistic Link between DNA Methyltransferases and DNA Repair Enzymes by Base Flipping.
- [118] J. van Noort, F. Orsini, A. Eker, C. Wyman, B. de Grooth and J. Greve, *Nucleic Acids Res.* **1999**, *27*, 3875-3880, DNA Bending by Photolyase in Specific and Non-Specific Complexes Studied by Atomic Force Microscopy.
- [119] S. J. T. van Noort, K. O. van der Werf, A. P. M. Eker, C. Wyman, B. de Grooth, N. F. van Hulst and J. Greve, *Biophys. J.* **1998**, *74*, 2840, Direct

- Visualization of Dynamic Protein-DNA Interactions with a Dedicated Atomic Force Microscope.
- [120] H. Komori, R. Masui, S. Kuramitsu, S. Yokoyama, T. Shibata, Y. Inoue and K. Miki, *Proc. Natl. Acad. Sci. USA* **2001**, *98*, 13560-16565, Crystal Structure of Thermostable DNA Photolyase: Pyrimidine-Dimer Recognition Mechanism.
- [121] J. Deisenhofer, *Mutation Res.* **2000**, *460*, 143-149, DNA Photolyases and Cryptochromes.
- [122] D. B. Sanders and O. Wiest, *J. Am. Chem. Soc.* **1999**, *121*, 5127-5134, A Model for the Enzyme-Substrate Complex of DNA-Photolyase and Photodamaged DNA.
- [123] J. Antony, D. M. Medvedev and A. A. Stuchebrukhov, *J. Am. Chem. Soc.* **2000**, *122*, 1057-1065, Theoretical Study of Electron Transfer between the Photolyase Catalytic Cofactor FADH⁻ and DNA Thymine Dimer.
- [124] S. Weber, G. Richter, E. Schleicher, A. Bacher, K. Möbius and C. W. M. Kay, *Biophys. J.* **2001**, *81*, 1195-1204, Substrate Binding to DNA Photolyase Studied by Electron Paramagnetic Resonance Spectroscopy.
- [125] T. Carell and R. Epple, *Eur. J. Org. Chem.* **1998**, 1245-1258, Repair of UV Light Induced DNA Lesions: A Comparative Study with Model Compounds.
- [126] R. Epple, E.-U. Wallenborn and T. Carell, *J. Am. Chem. Soc.* **1997**, *119*, 7440-7451, Investigation of Flavin-Containing DNA-Repair Model Compounds.
- [127] N. J. Saettel and O. Wiest, *J. Am. Chem. Soc.* **2001**, *123*, 2693-2694, DFT Study of the [2+2] Cycloreversion of Uracil Dimer Anion Radical: Water Matters.

- [128] R. Epple and T. Carell, *Angew. Chem. Int. Ed.* **1998**, *37*, 938-941, Flavin and Deazaflavin Containing Model Compounds Mimic the Energy-Transfer Step in Type II DNA-Photolyases.
- [129] R. Epple and T. Carell, *J. Am. Chem. Soc.* **1999**, *121*, 7318-7329, Efficient Light-Dependent DNA Repair Requires a Large Cofactor Separation.
- [130] C. Aubert, P. Mathis, A. P. M. Eker and K. Brettel, *Proc. Natl. Acad. Sci. U.S.A.* **1999**, *96*, 5423-5427, Intraprotein Electron Transfer between Tyrosine and Tryptophan in DNA Photolyase from *Anacystis nidulans*.
- [131] C. Aubert, K. Brettel, P. Mathis, A. P. M. Eker and A. Boussac, *J. Am. Chem. Soc.* **1999**, *121*, 8659-8660, EPR Detection of the Transient Tyrosyl Radical in DNA Photolyase from *Anacystis nidulans*.
- [132] C. Aubert, M. H. Vos, P. Mathis, A. P. M. Eker and K. Brettel, *Nature* **2000**, *405*, 586-590, Intraprotein Radical Transfer During Photoreactivation of DNA Photolyase.
- [133] S.-T. Kim, P. F. Heelis and A. Sancar, *Meth. Enzymol.* **1995**, *258*, 319-343, Role of Tryptophans in Substrate Binding and Catalysis by DNA Photolyase.
- [134] A. Sancar, *Science* **1996**, *272*, 48-49, No "End of History" for Photolyases.
- [135] D. M. Popovic, A. Zmiric, S. D. Zaric and E.-W. Knapp, *J. Am. Chem. Soc.* **2002**, *124*, 3775-3782, Energetic of Radical Transfer in DNA Photolyase.
- [136] A. Mees, T. Klar, P. Gnau, U. Hennecke, A. P. M. Eker, T. Carell and L.-O. Essen, *Science* **2004**, *306*, 1789-1793, Crystal Structure of a Photolyase-DNA Complex with a CPD-Like DNA Lesion after *in situ* Repair.
- [137] I. Husain, J. Griffith and A. Sancar, *Proc. Natl. Acad. Sci. USA* **1988**, *85*, 2558-2562, Thymine Dimers Bend DNA.

- [138] H. J. Park, K. Zhang, Y. Ren, S. Nadji, N. Sinha, J.-S. Taylor and C. H. Kang, *Proc. Natl. Acad. Sci. USA* **2002**, *99*, 15965-15970, Crystal Structure of a DNA Decamer Containing a *cis-syn* Thymine Dimer.
- [139] T. Todo, H. Takemori, H. Ryo, M. Ihara, T. Matsunaga, O. Nikaido, K. Sato and T. Nomura, *Nature* **1993**, *361*, 371-374, A New Photoreactivating Enzyme That Specifically Repairs Ultraviolet Light-Induced (6-4) Photoproducts.
- [140] S. Weber, C. W. M. Kay, H. Mögling, K. Möbius, K. Hitomi and T. Todo, *Proc. Natl. Acad. Sci. U.S.A.* **2002**, *99*, 1319-1322, Photoactivation of the Flavin Cofactor in *Xenopus laevis* (6-4) Photolyase: Observation of a Transient Tyrosyl Radical by Time-Resolved Electron Paramagnetic Resonance.
- [141] S.-T. Kim, K. Malhotra, C. A. Smith, J.-S. Taylor and A. Sancar, *J. Biol. Chem.* **1994**, *269*, 8535-8540, Characterization of a (6-4) Photoproduct DNA Photolyase.
- [142] G. Prakash and D. E. Falvey, *J. Am. Chem. Soc.* **1995**, *117*, 11375-11376, Model Studies of the (6-4) Photoproduct DNA Photolyase: Synthesis and Photosensitized Splitting of a Thymine-5,6-Oxetane.
- [143] A. Joseph, G. Prakash and D. E. Falvey, *J. Am. Chem. Soc.* **2000**, *122*, 11219-11225, Model Studies of the (6-4) Photoproduct Photolyase Enzyme: Laser Flash Photolysis Experiments Confirm Radical Ion Intermediates in the Sensitized Repair of Thymine Oxetane Adducts.
- [144] J. R. Epstein, A. P. K. Leung, K.-H. Lee and D. R. Walt, *Biosensors and Bioelectronics* **2003**, *18*, 541-546, High-Density, Microsphere-Based Fiber Optic DNA Microarrays.

- [145] J. P. Renault, A. Bernard, D. Juncker, B. Michel, H. R. Bosshard and E. Delamarche, *Angew. Chem. Int. Ed* **2002**, *41*, 2320-2323, Fabricating Microarrays of Functional Proteins Using Affinity Contact Printing.
- [146] M. Schena, R. A. Heller, T. P. Theriault, K. Konrad, E. Lachmeier and R. W. Davis, *Trends Biotechnol.* **1998**, *16*, 301-306, Microarrays: Biotechnology's Discovery Platform for Functional Genomics.
- [147] J. Wang, *Chem. Euro. J.* **1999**, *5*, 1681-1685, Towards Genoelectronic: Electrochemical Biosensing of DNA Hybridization.
- [148] S. Tyagi and F. R. Kramer, *Nature Biotechnology* **1996**, *14*, 303-308, Molecular Beacons: Probes That Fluoresce Upon Hybridization.
- [149] X. Fang, J. J. Li, J. Perlete, W. Tan and W. Wang, *Anal. Chem.* **2000**, *747 A - 753 A*, Molecular Beacons: Novel Fluorescent Probes.
- [150] G. Leone, H. Schijndel, B. Gemen, F. R. Kramer and C. D. Schoen, *Nucleic Acids Res.* **1998**, *26*, 2150-2155, Molecular Beacon Probes Combine with Amplification by NASBA Enable Homogeneous, Real-Time Detection of RNA.
- [151] B. A. J. Giesendorf, J. A. M. Vet, S. Tyagi, E. J. M. G. Mensink, F. J. M. Trijbels and H. J. Blom, *Clin. Chem.* **1998**, *44*, 482-486, Molecular Beacons: A New Approach for Semiautomated Mutation Analysis.
- [152] A. G. Frutos, S. Pal, M. Quesada and J. Lahiri, *J. Am. Chem. Soc.* **2002**, *124*, 2396-2397, Method for the Detection of Single-Base Mismatches Using Bimolecular Beacons.
- [153] H. Wang, J. Li, H. Liu, Q. Liu, Q. Mei, Y. Wang, J. Zhu, N. He and Z. Lu, *Nucleic Acids Res.* **2002**, *30*, e61, Label-Free Hybridization Detection of a Single Nucleotide Mismatch by Immobilization of Molecular Beacons on an Agarose Film.

- [154] D. L. Sokol, X. Zhang, P. Lu and A. M. Gewirtz, *Proc. Natl. Acad. Sci. USA* **1998**, *95*, 11538-11543, Real Time Detection of DNA-RNA Hybridization in Living Cells.
- [155] L. G. Kostrikis, S. Tyagi, M. M. Mhlanga, D. D. Ho and F. R. Kramer, *Science* **1998**, *279*, 1228-1229, Spectral Genotyping of Human Allels.
- [156] X. Liu, W. Farmerie, S. Schuster and W. Tan, *Anal. Biochem.* **2000**, *283*, 56-63, Molecular Beacons for DNA Biosensors with Micrometer to Submicrometer Dimensions.
- [157] L. M. Kundu, L. T. Burgdorf, O. Kleiner, A. Batschauer and T. Carell, *ChemBioChem* **2002**, *3*, 1053-1060, Cleavable Substrate Containing Molecular Beacon for the Quantification of DNA-Photolyase Activity.
- [158] T. Antony and V. Subramaniam, *J. Biomol. Struct. Dyn.* **2001**, *19*, 497-504, Molecular Beacons: Nucleic Acid Hybridization and Emerging Applications.
- [159] T. Drake and W. Tan, *Appl. Spec.* **2004**, *58*, 269-280, Molecular Beacon DNA Probes and Their Bioanalytical Applications.
- [160] D. P. Bratu, B. J. Cha, M. M. Mhlanga, F. R. Kramer and S. Tyagi, *Proc. Natl. Acad. Sci. USA* **2003**, *100*, 13308-13313, Visualizing the Distribution and Transport of mRNAs in Living Cells.
- [161] N. Nitin, P. Santangelo, G. Kim, S. Nie and G. Bao, *Nucleic Acids Res.* **2004**, *32*, e58, Peptide-Linked Molecular Beacons for Efficient Delivery and Rapid mRNA Detection in Living Cells.
- [162] J. R. Lakowicz, *Principles of Fluorescence Spectroscopy*, 2nd ed., Kluwer Academic/Plenum Publishers, New York, **1999**.
- [163] G. Bonnet, S. Tyagi, A. Libchaber and F. R. Kramer, *Proc. Natl. Acad. Sci. USA* **1999**, *96*, 6171-6176, Thermodynamic Basis for the Enhanced Specificity of Structured DNA Probes.

- [164] X. Fang, X. Liu, S. Schuster and W. Tan, *J. Am. Chem. Soc.* **1999**, *121*, 2921-2922, Designing a Novel Molecular Beacon for Surface- Immobilized DNA Hybridization Studies.
- [165] S. L. Beaucage, *Curr. Med. Chem.* **2001**, *8*, 1213-1244, Strategies in the Preparation of DNA Oligonucleotide Arrays for Diagnostic Applications.
- [166] B. Dubertret, M. Calame and A. J. Libchaber, *Nat. Biotechnol.* **2001**, *19*, 365-370, Single Mismatch Detection Using Gold-Quenched Fluorescent Oligonucleotides.
- [167] J. J. Li, X. Fang, S. M. Schuster and W. Tan, *Angew. Chem.* **2000**, *112*, 1091-1094, Molecular Beacons: A Novel Approach to Detect Protein-DNA Interactions.
- [168] R. Bar-Ziv and A. Libchaber, *Proc. Natl. Acad. Sci. USA* **2001**, *98*, 9068-9073, Effects of DNA Sequence and Structure on Binding of RecA to Single Stranded DNA.
- [169] S. Tyagi, D. P. Bratu and F. R. Kramer, *Nature Biotechnology* **1998**, *16*, 49-53, Multicolor Molecular Beacons for Allele Discrimination.
- [170] S. A. Marras, F. R. Kramer and S. Tyagi, *Nucleic Acids Res.* **2002**, *30*, e122, Efficiencies of Fluorescence Resonance Energy Transfer and Contact - Mediated Quenching in Oligonucleotide Probes.
- [171] T. Förster, *Discuss. Faraday Soc.* **1959**, *27*, 7-17, (Energietransfer).
- [172] S. Tyagi, *Designing Molecular Beacons*: http://molecular-beacons.com/PA_design.html.
- [173] J. R. Grunwell, J. L. Glass, T. D. Lacoste, A. A. Deniz, D. S. Chemla and P. G. Schultz, *J. Am. Chem. Soc.* **2001**, *123*, 4295-4303, Monitoring the Conformational Fluctuations of DNA Hairpins Using Single-Pair Fluorescence Resonance Energy Transfer.

- [174] M. I. Wallace, L. Ying, S. Balasubramanian and D. Klenermann, *Proc. Natl. Acad. Sci. USA* **2001**, *98*, 5584-5589, Non-Arrhenius Kinetics for the Loop Closer of a DNA Hairpin.
- [175] X. Fang and W. Tan, *Anal. Chem.* **1999**, *71*, 3101-3105, Imaging Single Fluorescent Molecules at the Interface of an Optical Fiber Probe by Evanescent Wave Excitation.
- [176] J. Li, R. Geyer and W. Tan, *Nucleic Acids Res.* **2000**, *28*, e52, Using Molecular Beacons as Sensitive Fluorescence Assay for Enzymatic Cleavage of Single Stranded DNA.
- [177] X. Fang, J. J. Li and W. Tan, *Anal. Chem.* **2000**, *72*, 3280-3285, Using Molecular Beacons to Probe Molecular Interactions between Lactate Dehydrogenase and Single-Stranded DNA.
- [178] J. B. Biggins, J. R. Prudent, D. J. Marshall, M. Ruppen and J. S. Thorson, *Proc. Natl. Acad. Sci. USA* **2000**, *97*, 13537-13542, A Continuous Assay for DNA Cleavage: The Application of "Break Lights" to Eneidyne, Iron-Dependent Agents, and Nucleases.
- [179] S. Hashimoto, B. Wang and S. M. Hecht, *J. Am. Chem. Soc.* **2001**, *123*, 7437-7438, Kinetics of DNA Cleavage by Fe(II)-Bleomycins.
- [180] S. A. E. Marras, F. R. Kramer and S. Tyagi, *Methods Mol. Biol.* **2003**, *212*, 111-128, Genotyping SNPs with Molecular Beacons.
- [181] D. R. Hodgson, C. A. Foy, M. Partridge, S. Pateromichelakis and N. J. Gibson, *Mol. Med.* **2002**, *8*, 227-237, Development of a Facile Fluorescent Assay for the Detection of 80 Mutations within the P53 Gene.
- [182] K. E. Pierce, J. E. Rice, J. A. Sanchez, C. Brenner and L. J. Wangh, *Mol. Hum. Reprod.* **2000**, *6*, 1155-1164, Real-Time PCR Using Molecular Beacons for Accurate Detection of the Y Chromosome in Single Human Blastomeres.

- [183] K. Abravaya, J. Huff, R. Marshall, B. Merchant, C. Mullen, G. Schneider and J. Robinson, *Clinical Chemistry* **2003**, *41*, 468-474, Molecular Beacons as Diagnostic Tools : Technology and Applications.
- [184] H. H. El-Hajj, S. A. E. Marras, S. Tyagi, F. R. Kramer and D. Alland, *J. Clin. Microbiol.* **2001**, *39*, 4131-4137, Detection of Rifampin Resistance in Mycobacterium Tuberculosis in a Single Tube with Molecular Beacons.
- [185] F. R. Kramer, *Introduction to Molecular Beacons*: <http://molecular-beacons.com/Introduction.html>.
- [186] J. A. M. Vet, A. R. Majithia, S. A. E. Marras, S. Tyagi, S. Dube, B. J. Poiesz and F. R. Kramer, *Proc. Natl. Acad. Sci. U.S.A.* **1999**, *96*, 6394-6399, Multiplex Detection of Four Pathogenic Retroviruses Using Molecular Beacons.
- [187] T. Matsuo, *Biochim. Biophys. Acta.* **1998**, *1379*, 178-184, *In Situ* Visualization of Messenger RNA for Basic Fibroblast Growth Factor in Living Cells.
- [188] P. Santangelo, B. Nix, A. Tsourkas and G. Bao, *Nucleic Acids Res.* **2004**, *32*, e57, Dual FRET Molecular Beacons for mRNA Detection in Living Cells.
- [189] J. Cadet, T. Douki, D. Gasparutto, M. Gromova, J.-P. Pouget, J.-L. Ravanat, A. Romieu and S. Sauvaigo, *Nucl. Instr. and Meth. in Phys. Res. B* **1999**, *151*, 1-7, Radiation-Induced Damage to DNA : Mechanistic Aspect and Measurement of Base Lesions.
- [190] T. Douki, M. Court, S. Sauvaigo, F. Odin and J. Cadet, *J. Biol. Chem.* **2000**, *275*, 11678-11685, Formation of the Main UV-Induced Thymine Dimeric Lesions within Isolated and Cellular DNA as Measured by High Performance Liquid Chromatography-Tandem Mass Spectrometry.
- [191] T. Douki, G. Vadesne-Bauer and J. Cadet, *Photochem. Photobiol. Sci.* **2002**, *1*, 565-569, Formation of 2' -Deoxyuridine Hydrates Upon Exposure of

- Nucleotides to Gamma Radiation and UVC-Induced of Isolated and Cellular DNA.
- [192] A. M. Soto, B. I. Kankia, P. Dande, B. Gold and L. A. Marky, *Nucleic Acids Res.* **2001**, *29*, 3638-3645, Incorporation of a Cationic Aminopropyl Chain in DNA Hairpins: Thermodynamics and Hydration.
- [193] C. Behrens and T. Carell, *Chem. Comm.* **2003**, 1632-1633, Excess Electron Transfer in Flavin-Capped, Thymine Dimer-Containing DNA Hairpins.
- [194] L. A. Marky and K. J. Breslauer, *Biopolymers* **1987**, *26*, 1601-1620, Calculating Thermodynamic Data for Transitions of Any Molecularity from Equilibrium Melting Curves.
- [195] D. G. Vassylyev, T. Kashiwagi, Y. Mikami, M. Ariyoshi, S. Iwai, E. Ohtsuka and K. Morikawa, *Cell* **1995**, *83*, 773-782, Atomic Model of a Pyrimidine Dimer Excision Repair Enzyme Complexed with a DNA Substrate: Structural Basis for Damaged DNA Recognition.
- [196] J. H. Miller, *J. Mol. Biol.* **1985**, *182*, 45-68, Mutagenic Specificity of Ultraviolet Light.
- [197] R. D. Wood, T. R. Skopek and F. Hutchinson, *J. Mol. Biol.* **1984**, *173*, 273-291, Changes in DNA Base Sequence Induced by Targeted Mutagenesis of Lambda Phage by Ultraviolet Light.
- [198] J. E. LeClerc, J. R. Christensen, P. V. T. R. B. Christensen and C. W. Lawrence, *J. Mol. Biol.* **1988**, *203*, 619-633, Ultraviolet Light Induces Different Spectra of lacI Sequence Changes in Vegetative and Conjugating Cells of Escherichia coli.
- [199] S.-T. Kim and A. Sancar, *Photochem. Photobiol.* **1995**, *61*, 171-174, Photo Repair of Nonadjacent Pyrimidine Dimers by DNA Photolyase.
- [200] D. E. Brash and W. A. Haseltine, *Nature* **1982**, *298*, 189-192, UV-Induced Mutation Hotspots Occur at DNA Damage Hotspots.

- [201] G. M. Blackburn and R. J. H. Davis, *J. Chem. Soc. (C)* **1966**, 2239-2244, The Structure of Thymine Photo-Dimers.
- [202] G. M. Blackburn, *Tetrahedron Lett.* **1966**, 37, 4471-4475, The Structure of Uracil Photo-Dimer.
- [203] B. Witkop, *Photochem. Photobiol.* **1968**, 7, 813-827, Mechanisms of Photoreductions and Hydrogenolysis of Pyrimidine Nucleosides and Their Photodimers.
- [204] T. Douki and J. Cadet, *Photochem. Photobiol. Sci* **2003**, 2, 433-436, Formation of the Spore Photoproduct and other Dimeric Lesions between Adjacent Pyrimidines in UVC-Irradiated Dry DNA.
- [205] T. Douki, M. Court and J. Cadet, *J. Photochem. Photobiol. B: Biol.* **2000**, 54, 145-154, Electrospray-Mass Spectrometry Characterization and Measurement of Far-UV-Induced Thymine Photoproducts.
- [206] X. Zhao, S. Nadji, J. F.-L. Kao and J.-S. Taylor, *Nucleic Acids Res.* **1996**, 24, 1554-1560, The Structure of d(TpA), the Major Photoproduct of Thymidylyl-(3'→5')-Deoxyadenosine.
- [207] F.-T. Liu and N. C. Yang, *Biochemistry* **1978**, 17, 4865-4876, Photochemistry of Cytosine Derivatives. 1. Photochemistry of Thymidylyl-(3'→5')-Deoxycytidine.
- [208] M. H. Patrick and D. M. Gray, *Photochem. Photobiol.* **1976**, 24, 507-513, Independence of Photoproduct Formation on DNA Conformation.
- [209] D. L. Mitchell, J. Jen and J. E. Cleaver, *Nucleic Acids Res.* **1992**, 20, 225-229, Sequence Specificity of Cyclobutane Pyrimidine Dimers in DNA Treated with Solar (Ultraviolet B) Radiation.
- [210] J.-H. Yoon, C.-S. Lee, T. R. O'Connor, A. Yasui and G. P. Pfeifer, *J. Mol. Biol.* **2000**, 299, 681-693, The DNA Damage Spectrum Produced by Simulated Sunlight.

- [211] K. Ito and S. Kawanishi, *Methods Enzymol.* **2000**, *319*, 417-427, Sequence Specificity of Ultraviolet a-Induced DNA Damage in the Presence of Photosensitizer.
- [212] R. E. Rycyna, J. C. Wallace, M. Sharma and J. L. Alderfer, *Biochemistry* **1988**, *27*, 3152-3163, Ultraviolet Irradiation of Nucleic Acids: Formation, Purification, and Solution Conformational Analyses of Oligothymidylates Containing *cis-syn* Photodimers.
- [213] R. E. Rycyna and J. L. Alderfer, *Nucleic Acids Res.* **1985**, *13*, 5949-5963, UV Irradiation of Nucleic Acids: Formation, Purification and Solution Conformational Analysis of the "6-4 Lesion" of dTpdT.
- [214] W. L. Nicholson, B. Setlow and P. Setlow, *Proc. Natl. Acad. Sci. USA* **1990**, *88*, 8288-8292, Ultraviolet Irradiation of DNA Complexed with β -Type Small, Acid-Soluble Proteins from Spores of Bacillus or Clostridium Species Makes Spore Photoproduct but Not Thymine Dimers.
- [215] W. Saenger, *Principles of Nucleic Acid Structure*, Springer Verlag, Heidelberg, **1984**.
- [216] J. Butenandt, L. T. Burgdorf and T. Carell, *Angew. Chem. Int. Ed.* **1999**, *38*, 708-711, Base Flipping: Photodamaged DNA-RNA Duplexes Are Poor Substrates for Photoreactivating DNA-Rapair Enzymes.
- [217] W. C. Johnson Jr, *Determination of the Conformation of Nucleic Acids by Electronic Cd*, Plenum Press, New York, **1996**.
- [218] B. D. Wells and J. T. Yang, *Biochemistry* **1974**, *13*, 1317-1321, A Computer Probe of the Circular Dichroic Bands of Nucleic Acids in the Ultraviolet Region. II. Double-Stranded Ribonucleic Acid and Deoxyribonucleic Acid.
- [219] J.-L. Ravanat, T. Douki and J. Cadet, *J. Photochem. Photobiol. B: Biol.* **2001**, *63*, 88-102, Direct and Indirect Effects of UV Radiation on DNA and Its Components.

- [220] H. Gaillard, D. J. Fitzgerald, C. L. Smith, C. L. Peterson, T. J. Richmond and F. Thoma, *J. Biol. Chem.* **2003**, *278*, 17655-17663, Chromatin Remodeling Activities Act on UV-Damaged Nucleosomes and Modulate DNA Damage Accessibility to Photolyase.
- [221] R. E. Wellinger and F. Thoma, *EMBO J.* **1997**, *16*, 5056-5056, Nucleosome Structure and Positioning Modulate Nucleotide Excision Repair in the Non-Transcribed Strabd of an Active Gene.
- [222] K. Bloch, *Chem. Biol.* **1996**, *3*, 405-407, Some Biochemical Thoughts on the RNA World.
- [223] W. Gilbert, *Nature* **1986**, *319*, 618, The RNA World.
- [224] J. Butenandt, R. Epple, E.-U. Wallenborn, A. P. M. Eker, V. Gramlich and T. Carell, *Chem. Eur. J.* **2000**, *6*, 62-72, A Comparative Repair Study of Thymine- and Uracil-Photodimers with Model Compounds and a Photolyase Repair Enzymes.
- [225] H. Schöneborn, J. Bülle and G. von Kiederowski, *ChemBioChem* **2001**, *2*, 922-927, Kinetic Monitoring of Self-Replicating Systems through Measurement of Fluorescence Resonance Energy Transfer.
- [226] S. Nadji, C.-I. Wang and J.-S. Taylor, *J. Am. Chem. Soc.* **1992**, *114*, 9266-9269, Photochemically and Photoenzymatically Cleavable DNA.
- [227] R. J. Lewis and P. C. Hanawalt, *Nature* **1982**, *298*, 393-396,
- [228] D. A. Vivic, D. T. Odom, M. E. Nunez, D. A. Gianolio, L. W. McLaughlin and J. K. Barton, *J. Am. Chem. Soc.* **2000**, *122*, 8603-8611, Oxidative Repair of a Thymine Dimer in DNA from a Distance by a Covalently Linked Organic Intercalator.
- [229] S. L. Beaucage and M. H. Caruthers, *Tetrahedron Lett.* **1981**, *22*, 1859-1862, Deoxynucleoside Phosphoramidites: A New Class of Key Intermediates for Deoxypolynucleotide Synthesis.

- [230] M. H. Caruthers, *Science* **1985**, *230*, 281-285, Gene Synthesis Machines: DNA Chemistry and Its Uses.
- [231] S. L. Beaucage and R. Iyer, *Tetrahedron* **1992**, *48*, 2223-2311, Advances in the Synthesis of Oligonucleotides by the Phosphoramidite Approach.
- [232] K. Malhotra, S.-T. Kim, C. Walsh and A. Sancar, *J. Biol. Chem.* **1992**, *267*, 15406-15411, Roles of FAD and 8-Hydroxy-5-Deazaflavin Chromophores in Photoreactivation by *Anacystis nidulans* DNA Photolyases.
- [233] S.-T. Kim, P. F. Heelis and A. Sancar, *Biochemistry* **1992**, *31*, 11244-11248, Energy Transfer (Deazaflavin-FADH₂) and Electron Transfer (FADH₂→T=T) in *Anacystis nidulans* Photolyase.
- [234] O. Kleiner, J. Butenandt, T. Carell and A. Batschauer, *Eur. J. Biochem.* **1999**, *264*, 161-167, Class-II DNA Photolyase from *Arabidopsis thaliana* Contains FAD as Cofactor.
- [235] N. L. Anderson and N. G. Anderson, *Electrophoresis* **1998**, *19*, 1853-1861, Proteome and Proteomics: New Technologies, New Concepts and New Words.
- [236] A. Pandey and M. Mann, *Nature* **2000**, *405*, 837-846, Proteomics to Study Genes and Genomes.
- [237] D. Figeys, A. Ducret, J. R. Yates III and R. Aebersold, *Nat. Biotechnol.* **1996**, *14*, 1579-1683, Protein Identification by Solid Phase Microextraction-Capillary Zone Electrophoresis-Microelectrospray-Tandem Mass Spectrometry.
- [238] Y. Liu, M. P. Patricelli and B. F. Cravatt, *Proc. Natl. Acad. Sci. U.S.A.* **1999**, *96*, 14694-14699, Activity-Based Protein Profiling: The Serine Hydrolases.
- [239] G. C. Adam, B. F. Cravatt and E. J. Sørensen, *Chemistry & Biology* **2001**, *8*, 81-95, Profiling the Specific Reactivity of the Proteome with Non-Directed Activity-Based Probes.

- [240] N. Winssinger, J. L. Harris, B. J. Backes and P. G. Schultz, *Angew. Chem. Int. Ed.* **2001**, *40*, 3152-3155, From Split-Pool Libraries to Spatially Addressable Microarrays and Its Application to Functional Proteomic Profiling.
- [241] W. Adam, A. Kurz and C. R. Saha-Möller, *Chem. Res. Toxicol.* **2000**, *13*, 1199-1207, Peroxidase-Catalyzed Oxidative Damage of DNA and 2'-Deoxyguanosine by Model Compounds of Lipid Hydroperoxides: Involvement of Peroxy Radicals.

RESUME

Name LAL MOHAN KUNDU

E-Mail lmkundu77@yahoo.com

Nationality Indian

Sex Male

Marital Status Single

Date of Birth 27.10.1977

Place of Birth Hooghly, West Bengal, India

Language skill Fluent in English, Bengali, Hindi;
some knowledge of German

Academic Records

Jan. 2003-Feb. 2005 Continuation of doctoral thesis with Prof.
Dr. T. Carell in Ludwig-Maximilians-
University Munich; Germany

Sept. 2000-Dec. 2003	Doctoral thesis with Prof. Dr. T. Carell in Philipps-University Marburg; Germany
1998-2000	Master of Science (M. Sc., Class I) in Chemistry; Indian Institute of Technology (IIT); Kharagpur; India
Dec. 2000-May 2000	Master thesis in organic chemistry with Dr. D. Mal, Indian Institute of Technology (IIT); Kharagpur; India
1995-1998	Bachelor of Science (B. Sc.) in Chemistry (Honors, Class II); University of Calcutta; India
1993-1995	Higher Secondary (10+2) education in Science (1 st Division); West Bengal Board of Higher Secondary Education; India
1983-1993	Secondary Education (10 th standard, 1 st Division); West Bengal Board of Secondary Education; India

Awards

Invited talk from Bruker Daltonic GmbH, 2004

Title: *"Identification and characterization of DNA lesions using HPLC coupled mass spectrometric methods"*

Graduate Aptitude Test in Engineering (Chemistry); Year 2000

Percentile: 98.58; All India Rank: 29 out of 2110

Merit Cum Means Scholarship (IIT Kharagpur, India) 1998-2000.

Prize in Seminar Lecture Competition in Chemistry (college level) 1997; 1998

List of Publications

- 1) **Kundu, L.M.**; Linne, U.; Marahiel, M; Carell, T.
"RNA is more UV resistant than DNA. The formation of UV-induced DNA lesions is strongly sequence and conformation dependent"
Chem. Euro. J. **2004**, *10*, 5697-5705

- 2) **Kundu, L.M.**; Burgdorf, L.T.; Kleiner, O.; Batschauer, A.; Carell, T.
"Cleavable Substrate Containing Molecular Beacons for the Quantification of DNA-Photolyase Activity"
ChemBioChem **2002**, *3*, 1053-1060.

- 3) Carell, T.; Burgdorf, L.T.; **Kundu, L.M.**; Cichon, M.
"The Mechanism of Action of DNA Photolyases"
Curr. Opin. Chem. Biol. **2001**, *5*, 491-498.

Poster Presentations:

- 4) **Kundu, L.M.**; Burgdorf, L.T.; Carell, T.
"A Novel Lesion Containing Assay for DNA- Repair"
Fifth International Symposium on Functional pi-Electron Systems
Ulm; Germany; May 29-June 3; 2002

5) **Kundu, L.M.; Burgdorf, L.T.; Carell, T.**

“Modified DNA Lesions and DNA Repair”

Conformational Control of Biomolecular Function

VW-Research Symposium

Lübeck, Germany ; 2001